THE ANNALS
OF "VALAHIA" UNIVERSITY

SUMMARY

A. PHYSICS SECTION

B. CHEMISTRY SECTION

C. MATHEMATICS SECTION

A. PHYSICS SECTION

THE STUDY OF SPECTROSCOPIC AND OPTICAL PROPERTIES OF VEGETATION IN RELATION WITH PHOTOSYNTHESIS

SIMONA LARISA APOSTOL

Valahia University, Physics Department, 24 Bd Unirii,0200 Targoviste

Abstract: In this paper we analyzed the optical and spectroscopical properties of vegetation that can be used for the monitoring of the photosynthetic activity in plants. The study present the spectroscopical properties of the main pigment involved in photrosynthesis, the chlorophyll, at different levels of organization from isolated molecule to complex assembly in a leaf, after a short remind of photosynthesis.

1. Introduction

The studies of optical and spectroscopic properties of vegetation make possible today the monitoring of the physiological state of plants and the efficiency of photosynthesis, especially by measurements of chlorophyll fluorescence. It has several advantages: no-invasive and no-destructive techniques, rapidity and simplicity of measurements, the availability at distance by the use of lasers.

Despite the enormous progresses maked the last decenies in the study of photosynthesis by chl fluorescence, fundamental studies are still needed; often they are correlated with applied studies in order to understand mechanisms and to assign molecular origins of the spectral signatures related to different physiological stresses that affect the functioning of plant photosynthesis.

2. How Photosynthesis works ?
2.1. What is Photosynthesis ?

Photosynthesis is the process by which living organisms (plant or bacteria) convert the energy of light into chemical energy of organic molecules. In plant, the solar energy is used to oxidize H_2O with the simultaneous production of O_2 and reduction of CO_2 to organic compounds as sugar:

$$CO_2 + 2H_2O + \text{light energy} \longrightarrow$$
$$(-CH_2O-) + O_2 + H_2O$$
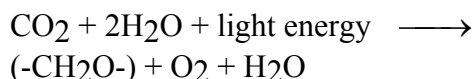
The chlorophyll (chl) is the molecule that play an essential role in the capture and conversion of light energy.

2.2. Photosystems Organization and functioning

In plants there are two Photosystems called PSI and PSII, working in series, that realize the photochemical act. Each photosystem is composed of various protein subunits, with which are associated specific pigments. PSI contains a reaction center with P700 - a special dimer of chla absorbing at wavelength longer than 690 nm. Similarly, PSII is composed of various protein subunits, chl*a* molecules and a reaction center containing P680. This photosystem interact with two light harvesting complexes - a tightly bound one and a slightly larger peripheral one, containing chl*a,* and chl*b* [1].

2.3. Photochemical act and Electron flow

The photochemical reaction of photosynthesis involves the removal of an electron from an excited state of the special chlorophyll that acts as an excitation trap. This electron is then transferred by a series of molecules and lead to ultimately to the reduction of NADP. The oxidized Chl trap, which has lost an electron can accept another from the water, leading to O_2 evolution.

3. Optical and spectroscopic properties of photosynthetic material at different levels of organisation

3.1 Photosynthetic Pigments

Several types of pigments harvest the energy of light (chlorophyll*a* and *b*, carotenoids, xantophylles for plants). Only special form of chl*a* form reaction centers. All other pigments are therefore accessory pigments forming groups arranged to extend the size of light-capturing units trap acting as antennae for capturing photons which donate excitation to reaction centers.

Pigments absorb in different part of the spectrum and in combination enable an organism to absorb light of different wavelengths over a wide range of visible solar spectrum. This is of great ecological importance for organisms, which may exploit a greater energy supply or grow in different radiation environment.
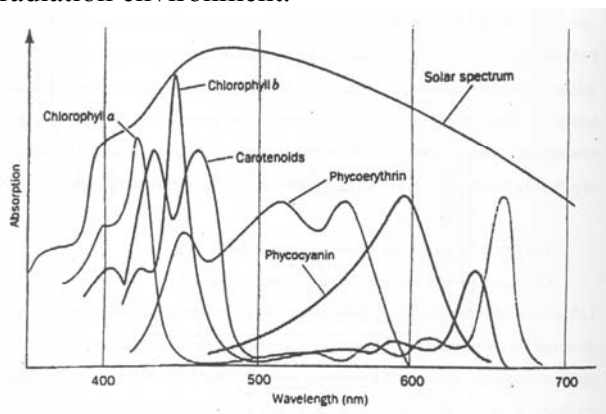

Figure 1. Absorbtion spectra of various photosynthetic pigments compared to solar spectrum

Chlorophyll is the most abundant pigment in the leaf and appear green due to their absorbtion of blue and red light. Chemically, chlorophyll are clorin macrocycles with four-fold symmetry, derived from porphyrin .

Absorbtion spectra
Measured in organic solvents after extraction from the plant chl*a* absorbs most strongly at 430 nm (Soret band) and 660nm, and chl*b* at 450 and 640 nm (see Figure 2). The absorbtion maxima shift with the solvent.
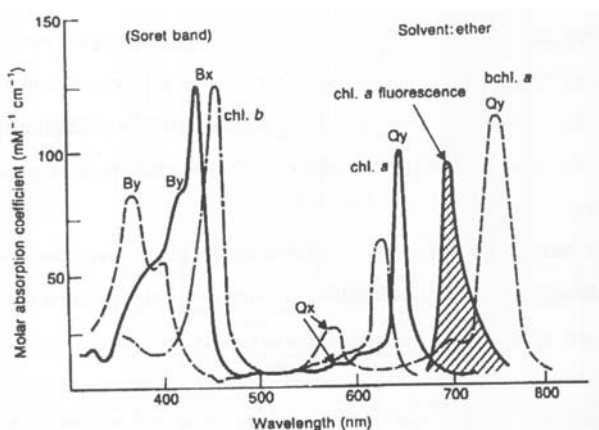
Figure 2. Absorbtion and fluorescence emission spectra from chlorophyll in ether
Aggregation of chl also cause a shift; crystalline chl*a* has its long wave absorbtion maximum at 740 nm. Chlorophyll is a very efficient pigment with a cross-section

absorbing area per molecule of $3,8*10^{-16}$ cm^2. Chl*a* has a molar extinction coefficient of $1,2*10^5$ M^{-1}cm^{-1} at 430 nm [4] .

Fluorescence
Electrons in the higher levels of the first singlet decay by radiationless transition to the lower levels and if not used in photochemistry or transferred to other molecules, decay to the singlet ground state by emission of fluorescence. In chl*a* of the thylakoids fluorescence is emitted at a peak of 685 nm. It shows the accumulation of excitation energy in the antennae and is inversely related to the use of electrons; it indicate the state of electron transport and biochemical processes relative to energy capture.

3.2. Photosystems
The photosynthetic pigments, except carotenoids, when extracted from the photosynthetic membranes with polar organic solvents, emit fluorescence with high quantum yields and characteristic spectra. But not all pigments in the pigment-protein complexes fluoresce. In LHC for example, the transfer of excitation from chl*b* to chl*a* is so efficient that fluorescence is emmited from chl*a* only. Also the transfer of energy from LHCII to RCII is so efficient that the fluorescence of LHCII can hardly be observed.

At low temperature PSI, PSII and LHC can be distinguished by their characteristic fluorescence bands. The emission spectrum consist of three bands: F685, F695 atributed to PSII and F735 attributed to PSI [6].

3.3. Leaves
3.3.1. Absorbtion spectra
In leaves, the high light scattering of the tissues increases the light path through the pigment containing cells, and even radiation of wavelengths between 500 and 600 nm, poorly absorbed by the chlorophylls is efficiently absorbed and utilized.
A dramatic self-absorbtion effect is often observed in leaves in which densely pigmented chloroplasts are concentrated in small volumes; the fluorescence spectrum of leaves also differs from that of chloroplasts isolated from them [7]. Thus, detailed study of absorbtion and fluorescence spectra requires fragmentation of the leaf in chloroplast, thylakoid or even into small membrane

fragments, so that the absorbtion within them becames low enough that appreciable distorsions are not produced .

The leaf epiderm represents an efficient filter for the UV radiations that are more energetic and may damage photosynthetic apparatus.

3.3.2. Transmitance and reflectance

A leaf absorb typicaly about 80% of the incident PAR (photosynthtic active radiation 400-700 nm). The rest 20% is transmitted and reflected with a local maximum in the green region of the spectrum. The transmitance and reflectance increases dramaticaly at longer wavelength in the FR region of the spectrum where there is no significant absorbtion by the leaf (see Fig. 3). The optical properties of a leaf depend on chlorophyll concentration and stage of development and also plant species [8].
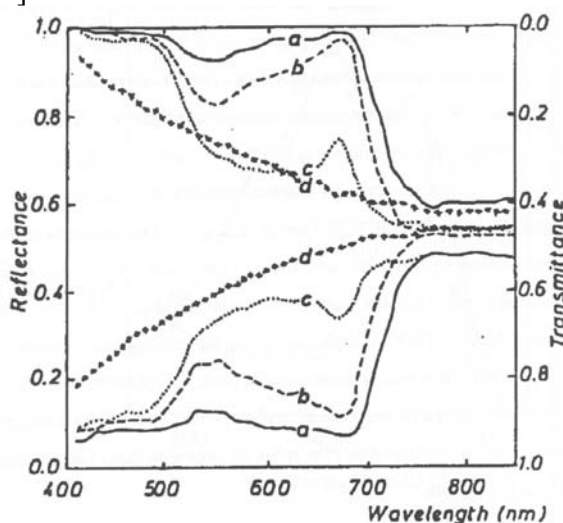
Figure 3. Reflectance and Transmission Spectra from leaves of deacreasing Chl concentration (from a to d)

3.3.3. Fluorescence emission

Under near-UV radiation, fluorescence emission from a leaf, as well as from intact chloroplast, can mainly be observed in the red and blue domains of the visible spectrum (Fig. 4). The well known red fluorescence is due to the chlorophyll but the origin of the blue fluorescence is still a subject in study.

Experimental results show that the blue fluorescence signal depends on the type of vegetation, and that blue and red fluorescence should be considered simultaneously because they contain complementary information and are highly specific of a type of vegetation. By using the UV-laser-induced fluorescence in plants it is possible to asses at distance the health of vegetation [9].
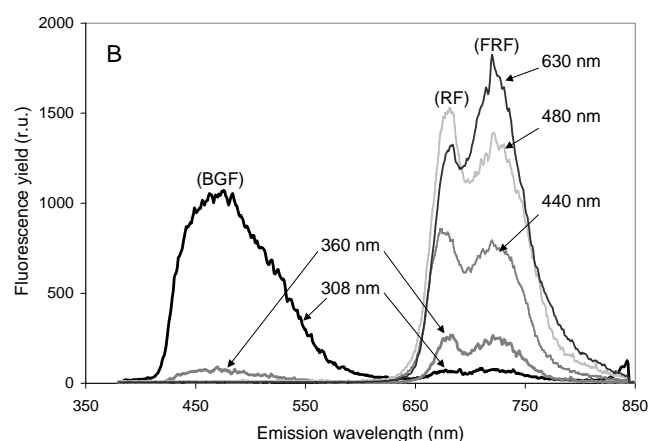
Figure 4. Fluorescence emission spectra from corn leaf after UV and VIS excitations

The blue-green fluorescence
It was shown that BGF emission spectrum depends on plant type [10] and anatomy [11, 12] and also on environmental factors like water stress [13] or nutrient concentration in soil [14].

All these findings make BGF to become a new potential signature for remote sensing of plant [9] comparable to red fluorescence. Unlike the red fluorescence, BGF is a sum of emissions by several fluorophores distributed in different compartments of the leaf and the plant cell.

Many studies were performed in order to analyze the molecular origin of BGF, for example [11]; [15]; [16]. The principals candidates were divided in two classes: 1) aromatic compounds located in vacuole and cell walls of epidermis and 2) cofactors of the metabolism: pyridine and flavine nucleotides which are directly related to the redox state in the plant cell [16]. The fluorescence of pyridine nucleotide could be complementary to the red, chlorophyll, fluorescence, but its detectability in intact leaves was questioned.

The red chlorophyll fluorescence
After the absorbtion of light, a part of the excitation energy of chlorophyll is lost by radiationless de-excitation and most is used to drive the "chemical" reactions of photosynthesis (ATP synthesis, NADP reduction, etc.). Some energy is also dissipated as fluorescence. There is a competition between the different ways of deactivation of excited states of chlorophyll.

Fluorescence derive from the lower more persistent S1 level rather then S2 level which decays in about 10^{-13} s. For this reason chlorophyll fluorescence is red (see Fig 1), regardless of the quality of the exciting light. It is slightly shifted to longer wavelength than the red absorption peak (Stokes shift) .

In vivo, most emission at normal temperatures is from chl*a* of PSII [19]; PSI only produce significant fluorescence at low temperatures (77K). The specificity of the red fluorescence coming from chlorophyll *in vivo* is the variable fluorescence under actinic light conditions. This parameter is a very sensitive indicator of the energy status of the photosynthetic system, indicating how the multiple processes of energy absorption and utilization interact.

a) Fluorescence yield and lifetime

The rate of decay of the excited state depends on radiationless transitions, excitation transfer, fluorescence and photochemistry. The associated rate constants for these processes are respectively Kd, Kt, Kf and Kp so that the overall rate constant is K=Kd+Kt+Kf+Kp. Singlet excited states are relatively short lived, that of chlorophyll in an organic solvent being about 5.10^{-9} s. The fluorescence quantum yield, defined as the number of emitted quanta divided by the number of absorbed quanta, is expressed by the relation:

$$Øf=Kf/(Kd+Kt+Kf+Kp*P) \quad (1)$$

P being the fraction of PSII reaction centers that can perform photochemical conversion.

The rate of fluorescence emission, F, is proportional to the light absorbed (I), to the fraction of the energy reaching PSII (b), with the chl *a* concentration and quantum yield (Øf);

$$F=I*b *(chl\ PSII)* Øf \quad (2)$$

Chlorophyll *a* solution emits about 30% of the light absorbed as fluorescence but *in vivo* its yield is much lower (see table I).

Table I: Typical utilization of absorbed quanta by photosystem II when electron transport is optimal or blocked (Rosema et al. 1991).

Mecanism	Electron transport	
	optimal	blocked
Photosynthesis	84	0
Heat	14	88
Fluorescence	2	12

Following the absorbtion of photons of a short light pulse, the initial number (No) of excited states decrease in time as:

$$-dN/dt=No*(Kd+Kt+Kf+Kp) \quad (3)$$

giving the time course of the excited states:

$$N(t)=No*\exp(t/\tau) \quad (4)$$

where the lifetime is defined by:

$$\tau=1/(Kd+Kt+Kf+Kp) \quad (5)$$

The fluorescence intensity is proportional to the number of excited states

$$F(t)=N(t)*Kf \quad (6)$$

The natural or intrinsec lifetime τ_0 is the lifetime when fluorescence is the only deacivation pathway; the fluorescence yield is related to these lifetimes by:

$$Øf=\tau/\tau_0 \quad (7)$$

In photosynthetic material the fluorescence decay is assumed to results from the superposition of several exponentially decaying processes and the mean lifetime can be calculated from the individual lifetimes τ_i and amplitudes Ai as :

$$\overline{\tau} = \frac{\sum_{i=1}^{N} A_i\tau_i^2}{\sum_{i=1}^{N} A_i\tau_i} \quad (8)$$

Analysis of picosecond fluorescence kinetics at room temperature suggest that there are three exponential components with lifetimes of about 0,1; 0,4 and 2 ns. The 0,1 ns component seems originate from PSI, and 0,4 and 2 ns from PSII. The 2ns component becomes dominant in the presence of DCMU suggesting that is emmited from RCII in which first quinone acceptor Q_A is reduced [7].

b) Yield changes

Changes in fluorescence yield is caused by various factors such as: quenching at the RC, quenching by stimulation of internal conversion, a change in exciton transfer and a change in absorbtion cross section of PSI and PSII. In contrast to PSII, the fluorescence of PSI doesn't change with the redox state [6].

Illumination of a dark-adapted leaf induces a typical chl*a* transient fluorescence (the Kautsky curve) from a minimum Fo to a maximum level Fm, of 5-6 times higher intensity.

3.3.4. Luminescence

Thermoluminescence

The states resulting from the charge separation in PSII can be stabilized at subzero temperatures. Then, by heating the sample at a constant rate, a relatively well-characterized "glow curve" with distinct peaks can be recorded (Fig.5). Each peak is generated when the appropriate thermal energy kT (k, Boltzman constant; T absolute temperature) is available from the ambient medium; this thermal energy should be related somehow to the activation energy of some step along the recombination path. Qualitative and quantitative information can be obtained. TL constitutes a kind of "fingerprint" of the system, which having been suitably pretreated or modified, is frozen in a particular configuration of states [30]. Although the method is not very complicated, only a few groups have used it extensively. However, it has produced a wealth of results in recent years, related mainly to the donor side and acceptor side of PSII.
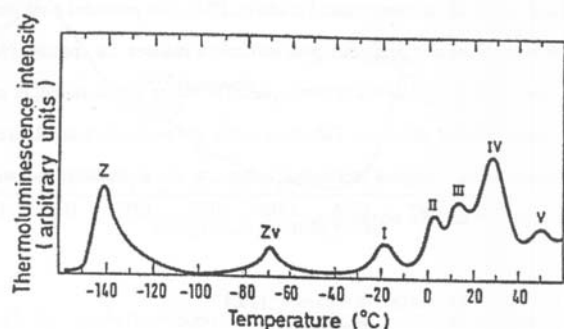
Figure 5. Thermoluminescence bands from a leaf

Phosphorescence

Even in vitro, phosphorescence data on Chl are scant. The quantum yield of phosphorescence is low (10^{-5} to 10^{-4}), the emission at long wavelengths (900-1000 nm), where the quantum efficiency of photomultipliers is low, and the experiments are marred by emission from the impurities, present even in the best purified preparation because of degradation of the pigments.

Phosphorescence data from leaves at 77°K are summarized in the following table:

Table II.

Material	Ex. λ (nm)	Em.λ (nm)	Life time (ms)	Assignment
Bean leaves	627 630-	870 920-	6,2 2,5-	ProtoChlorophyll(ide)
	647	970	3,3	idem
	678	1000	1,5	chlorophyllide
	668	960	1,7	chla
Maize leaves	640	980	1,9	chla
	690	995	1,4	chla

Excitation spectra at 77°K show that the phosphorescence arises mainly from pigments absorbing at about 670 nm. This suggest that the phosphorescence is due mainly to disagregated Chl [31].

4. References

1. Nobel, P. (1992) *Physicochemical and Environmental Plant Physiology*. ed. I. Academic Pess. San Diego, New York, Boston, London, Sydney, Tokyo, Toronto: Jovanovich, HB.
2. Fork, D. and Satoh, K. (1986) Annual Review of Plant Physiology, **37**: 335-361
3. Anderson, J. (1986) Annual Review of Plant Physiology, **37**: 93-136
4. Lawlor, D. (1993) *Photosynthesis: Molecular, Physiological and Environmental Processes*. 2nd ed. ed. L.S. Tehnical..
5. Goodwin, T. (1980) *The Biochemistry of the Carotenoids*. 2nd ed. Vol. 1. London: Chapman and Hall. pp.
6. Briantais, J., Vernotte, C., Krause, G. and Weis, E. (1986) *Chlorophyll a Fluorescence of Higher Plants: Chloroplasts and Leaves,* in *Light Emission by Plants and Bacteria,* (A. Govindgee, Fork, ed.) Academic Press, Inc.: pp. 540-587
7. Murata, N. and Satoh, K. (1986) *Absorbtion and Fluorescence Emission by Intact Cells, Chloroplasts and Chlorophyll-Protein Complexes,* in *Light Emission by Plants and Bacteria,* (A. Govindgee, Fork, ed.) Academic Press, Inc.: pp. 540-587
8. Baret, F., Andrieu, B. and Guyot, G. (1988) *A simple model for leaf optical properties in visible and near-infrared: applications to the analysis of spectral shift determinism,* in *Applications of Chlorophyll Fluorescence,* (H. Lichtenthaler, ed.) Kluwer Academic: Dordrecht, Boston, London, pp. 325-332
9. Moya, I., Guyot, G. and Goulas, Y. (1992) *Remotely sensed blue and red fluorescence emission for monitoring vegetation.* ISPRS J. Photogram. Remote Sens., **47**: 205-231
10. Chappelle, E.W., Wood, F.M., McMurtrey, J.E. and Newcomb, W.W. (1984)

Laser-induced fluorescence of green plants. 1: A technique for the remote detection of plant stress and species differentiation. Applied Optics, 23: 134-138

11.   Lang, M., Stober, F. and Lichtenthaler, H.K. (1991) *Fluorescence emisson spectra of plant leaves and plant constituents.* Radiat Environ Biophys, **30**: 333-347

12.   Lang, M., Siffel, P., Braunova, Z. and Lichtenthaler, H.K. (1992) Bot Acta, **105**(6): 435-440

13.   Theisen, A.F. (1988) *Fluorescence changes of a drying marple leaf observed in the visible and near-infrared,* in *Applications of Chlorophyll Fluorescence in Photosynthesis Research, Stress Physiology, Hydrobiology and Remote Sensing,* (H.K. Lichtenthaler, ed.) Kluwer Academic Publisher: Dordrecht, pp. 197-201

14.   Chappelle, E.W., McMurtrey, J.E. and Kim, M.S. (1991) *Identification of the pigment responsible for the blue fluorescence band in the laser induced fluorescence (LIF) spectra of green plants, and the potential use of the band in remotely estimating rates of photosynthesis.* Remote Sens. Environ., **36**: 213-218

15.   Broglia, M. (1993) Appl Opt, **32**(3): 334-338

16.   Cerovic, Z.G., Bergher, M., Goulas, Y., Tosti, S. and Moya, I. (1993) Photosynth Res, **36**(3): 193-204

17.   Duysens, L.N.M. and Kronenberg, G.H.M. (1957) *The fluorescence spectrum of the complex of reduced phosphopyridine nucleotide and alcohol dehydrogenase from yeast.* Biochim. Biphys. Acta., **26**: 437-438

18.   Müller, F. (1991) *Chemistry and Biochemistry of Flavoenzymes.* Vol. I. Boca Raton, Ann Arbor, Boston: CRC Press. pp.

19.   Duysens, L.N.M. and Sweers, H.E. (1963) *Mechanism of the two photochemical reactions in algae as studied by means of fluorescence,* in *Studies on microalgae and phosynthetic bacteria,* (J.S.o. Physiol., ed.) Univ of Tokyo Press: Tokyo, pp. 353-372

20.   Neubauer, C. and Schreiber, U. (1987) *The polyphasic rise of chlorophyll fluorescence upon onset of strong continuous illumination: I. Saturation characteristics and partial control by the Photosystem II acceptor side.* Z. Naturforsch., **42c**: 1246-1254

21.   Briantais, J.-M., Dacosta, J., Goulas, Y., Ducruet, J.-M. and Moya, I. (1996) *Heat-stress induces in leaves an increase of the minimum level of clorophyll fluorescence, F_o: A time resolved analysis.* Photosynth. Res., **46**: 189-196

22.   Genty, B., Briantais, J. and Baker, N. (1989) Biochim Biophys Acta, **990**: 87-92

23.   Horton, P. (1996) *Non-photochemical quenching of chlorophyll fluorescence,* in *Light as Energy Source and Information Carrier in Plant Physiology,* (R. Jennings, *et al.,* eds.) Plenum Press: New York and London, pp. 99-112

24.   Schreiber, U., Schliwa, U. and Bilger, W. (1986) *Continuous recording of photochemical and non-pnotochemical chlorophyll fluorescence quenching with a new type of modulation fluorimeter.* Photosynth. Res., **10**: 51-62

25.   Allen, J.F. (1992) *Protein phosphorylation in regulation of photosynthesis.* Biochim. Biophys. Acta, **1098**: 275-335

26.   Horton, P. and Hagen, A. (1988) Biochim Biophys Acta, **932**: 107-115

27.   Timmerhaus, M. and Weis, E. (1990) *,* in *Current Research in Photosynthesis,* (M. Baltscheffsky, ed.) Kluwer Acad.: Netherlands, pp. 771-774

28.   Öquist, G., Chow, W.S. and Anderson, J.M. (1992) *Photoinhibition of photosynthesis represent a mechanism for long-term regulation of photosystem II.* Planta, **186**: 450-460

29.   Jursinic, P. (1986) *Delayed Fluorescence: Current Concepts and Status,* in *Light Emission by Plants and Bacteria,* (A. Govindgee, Fork, ed.) Academic Press, Inc.: pp. 291-328

30.   Lavorel, J., Breton, J. and Lutz, M. (1986) *Methodological Principles of Measurements of Light Emitted by Photosynthetic Systems,* in *Light Emission by Plants and Bacteria,* (A. Govindgee, Fork, ed.) Academic Press, Inc.: pp. 58-98

31.   Hoff, A. (1986) *Triplets: Phosphorescence and Magnetic Resonance,* in *Light Emission by Plants and Bacteria,* (A. Govindgee, Fork, ed.) Academic Press, Inc.: pp. 226-267

LEAVES TREES ANALYSIS BY ATOMIC ABSORPTION SPECTROMETRY

ANCA BANCUTA[1], ION V. POPESCU[1], CLAUDIA STIHI[1]
GABRIELA BUSUIOC[2], MARIUS BELC[3]

[1] Valahia University of Targoviste, Science Faculty, Physics Department, No.2 Carol I Street, Targoviste, Romania
[2] Valahia University of Targoviste, Biology Department, No.2 Carol I Street, Targoviste, Romania
[3] Ovidius University of Constanta, Romania

Abstract: *The aim of this work is to determine the elemental composition of tree leaves using Atomic Absorption Spectrophotometry (AAS) method. Biological samples are interesting from many aspects of environmental monitoring. By analyzing tree leaves conclusions can be drown regarding the metal loading in the environmental growth medium.*

So that, starting from assumption that the pollution factors from environmental medium can modify the normal concentration of elements, we decided to control the presence of toxic elements and the deviation from normal state of elements in leaves of different trees from areas situated at the same distance of pollution source.

Using AAS spectrophotometer SHIMADZU we identified and determined the concentration of: Cd, Co, Cu, Zn, Mn, Cr, Fe, Se with an instrumental error less than 1% for most of the elements analyzed.

1. Introduction

Atomic Absorption Spectrophotometry (AAS) is a destructive technique used for elemental analysis of different samples from different domains. We use AAS method to determine the concentration of: Cd, Co, Cu, Zn, Mn, Cr, Fe, Se in the different leaves of trees collected in different period at 2 Km distance from pollution source – Special Steel Complex, Targoviste, Romania.

2. EXPERIMENTAL

The AAS (Atomic Absorption Spectrophotometry) spectrophotometer (figure 1) use by us is a SHIMADZU spectrophotometer [1, 2] with hollow cathode lamp (HCL). The atomic spectrometry uses absorption of light of intrinsic wavelength by atoms contains in a sample. The HCL gives of light characteristic to the elemental wavelength being measured. Thus, the light absorbed measure the atomic density. The atomic density determines the absorption rate and the Lambert-Beer's law give the value of absorbance from each element of the samples.
The formula of Lambert-Beer's law is:

$$I = I_0 \times e^{k \cdot l \cdot c} \quad \text{or} \quad -\log\frac{I}{I_0} = k \cdot l \cdot c, \text{ where } -\log\frac{I}{I_0}$$

value is absorbance, formula, which indicates that absorbance, is proportional to atomic density.

Atomic absorption spectrometry determines the sample by using the fact that the sample concentrations are proportional to light absorbance's in the atomization stage.

Using the calibration curve – absorbance and concentration – when the absorbance of an unknown sample is obtained, the concentration of the element can be obtained.

The principle mentioned above can be applied to light absorption of "Free atoms". A "Free atom" means an atom not combined with other atoms. However, elements in the sample to be analyzed are not in the free state, and are combined with other elements invariably to make a so-called molecule.

Absorption cannot be done on samples in the molecule state, because molecules do not absorb light. The combination must be cut off by some means to free the atoms. This is called atomization.

The most popular method of atomization is dissociation by heat-samples is heated to a high temperature so that molecules are converted into free atoms. This method is classified into the flame method, in which a chemical flame is used as the heat source; and a flameless

method, in which a very small electric furnace is used.

Sample for AAS experiments (table 1) was prepared in the following manner [2,3]: leaves of trees, collected of approximately in some position, have been washed and simply air-dried at a temperature of 105^0 C in a clean box

.

preventing further contamination. The dried leaves have been grained and after powdering, 0.25-g powder leaves have been digested in 8-ml acid nitric and 10-ml peroxide. The filtrated solution was diluted with water at 50-ml solution.
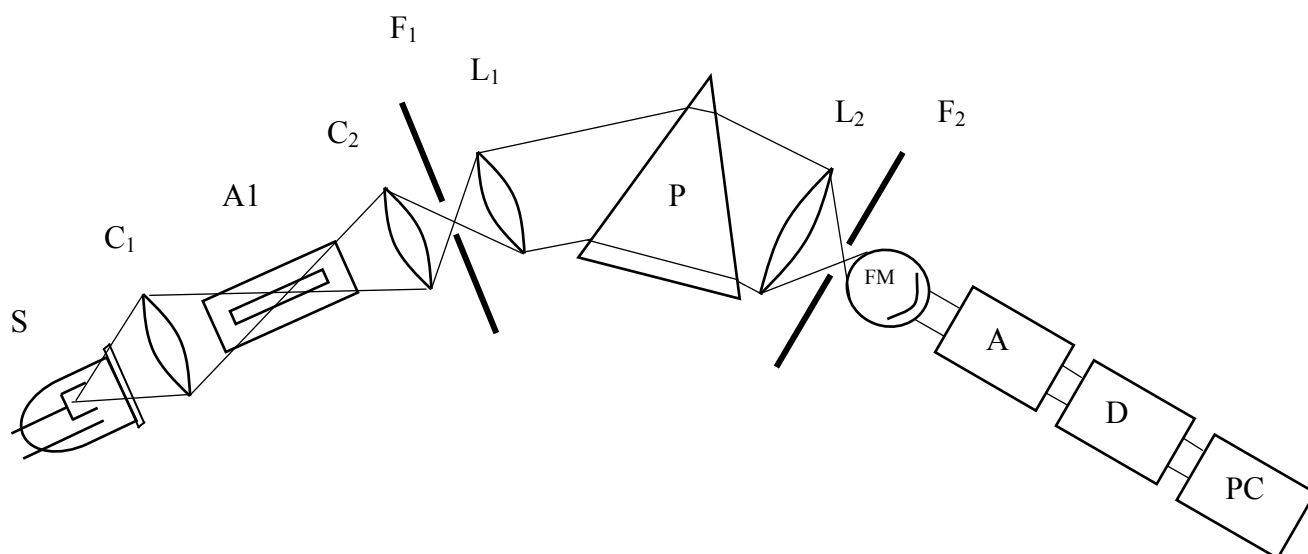
Figure 1: Instrumentation for Atomic Absorption Spectrophotometry [3, 4]
S - source of characteristic monochromatic radiation of the analyzed elements (hallow cathode lamp); C1, C2 – condensor lens; A1 – burner with flame when the solution sample is nebulised; F1, F2 – input and output slits; L1, L2 – collimators lens; P – monochromator prism; FM - photomultiplier; A – amplifier; D – detector; PC – personal computer for data acquisition

3. Results and discussion

Using AAS method we identified and determined analyzed samples the concentration of: Cd, Co, Cu, Zn, Mn, Cr, Fe, Se with an instrumental error less than 1% for most of the elements analyzed.

Experimental results obtained by AAS method are presented in tables 2.

The variation of elements concentration for different type of sample is presented in figure 2.

Table 1. Sample type in AAS experiments

Sample title	Sample type	The period of collection
A1	Leaves of plum tree	July 2001
A2	Leaves of plum tree	September 2001
B1	Leaves of mulberry tree	July 2001
B2	Leaves of mulberry tree	September 2001
C1	Leaves of lime tree	July 2001
C2	Leaves of lime tree	September 2001
D1	Leaves of cherry tree	July 2001
D2	Leaves of cherry tree	September 2001

Table 2. **The concentration (ppm) of elements in samples obtained using AAS method**

Sample title	Cr	Mn	Fe	Co	Cu	Zn	Se	Cd
A1	0.212	0.029	0.103	0	0	0.005	0.901	0.003
A2	0.167	0.513	1.766	0.006	0.142	0.098	3.575	0
B1	0.276	0.486	2.274	0	0.046	0.242	3.471	0.018
B2	0.054	0.854	0	0	0.141	0.348	1.773	0
C1	0.321	0.879	2.907	0.177	0.057	0.142	4.701	0.003
C2	0.063	1.421	1.534	0.023	0.022	0.195	1.999	0.006
D1	0	0.266	1.785	0	0.104	0.167	2.391	0
D2	0.141	0.567	2.216	0.026	0.079	0.168	3.134	0
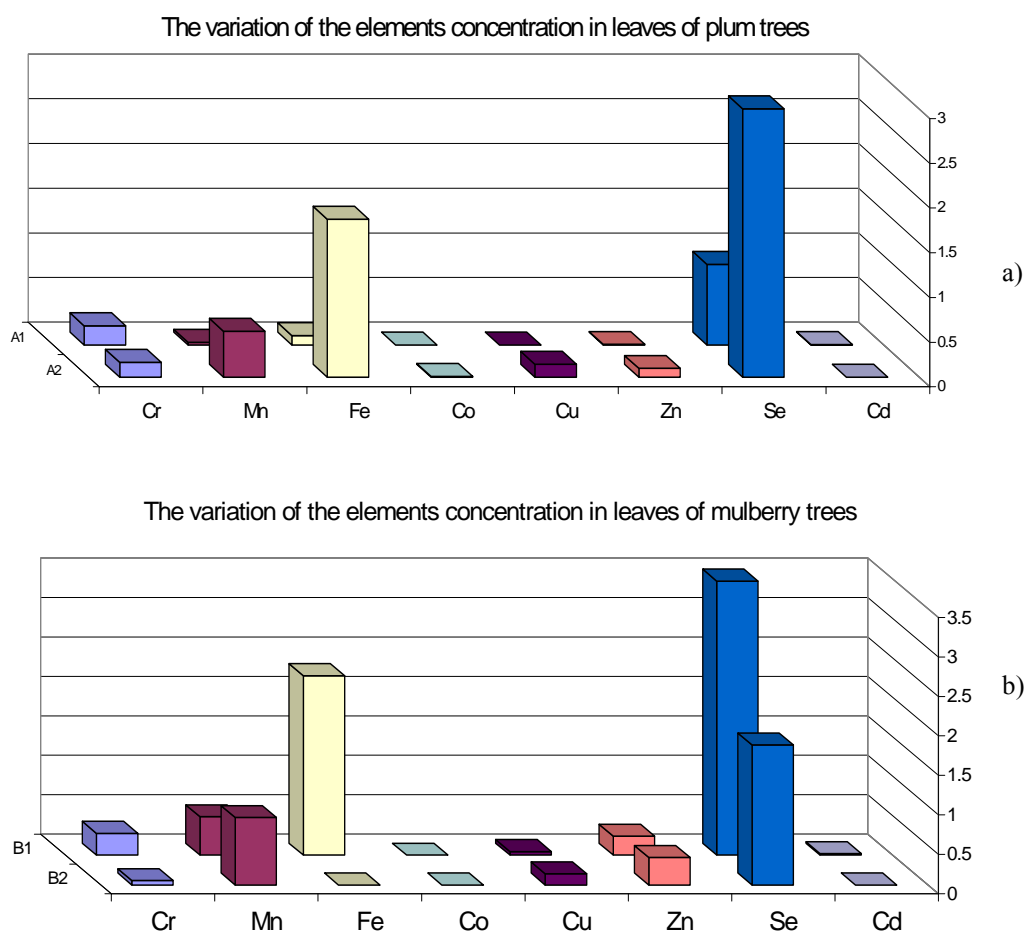
Figure 2. The variation of elements concentration for different type of samples: a) leaves of plum tree; b) leaves of mulberry tree

The variation of the elements concentration in leaves of lime trees

The variation of the elements concentration in leaves of cherry trees
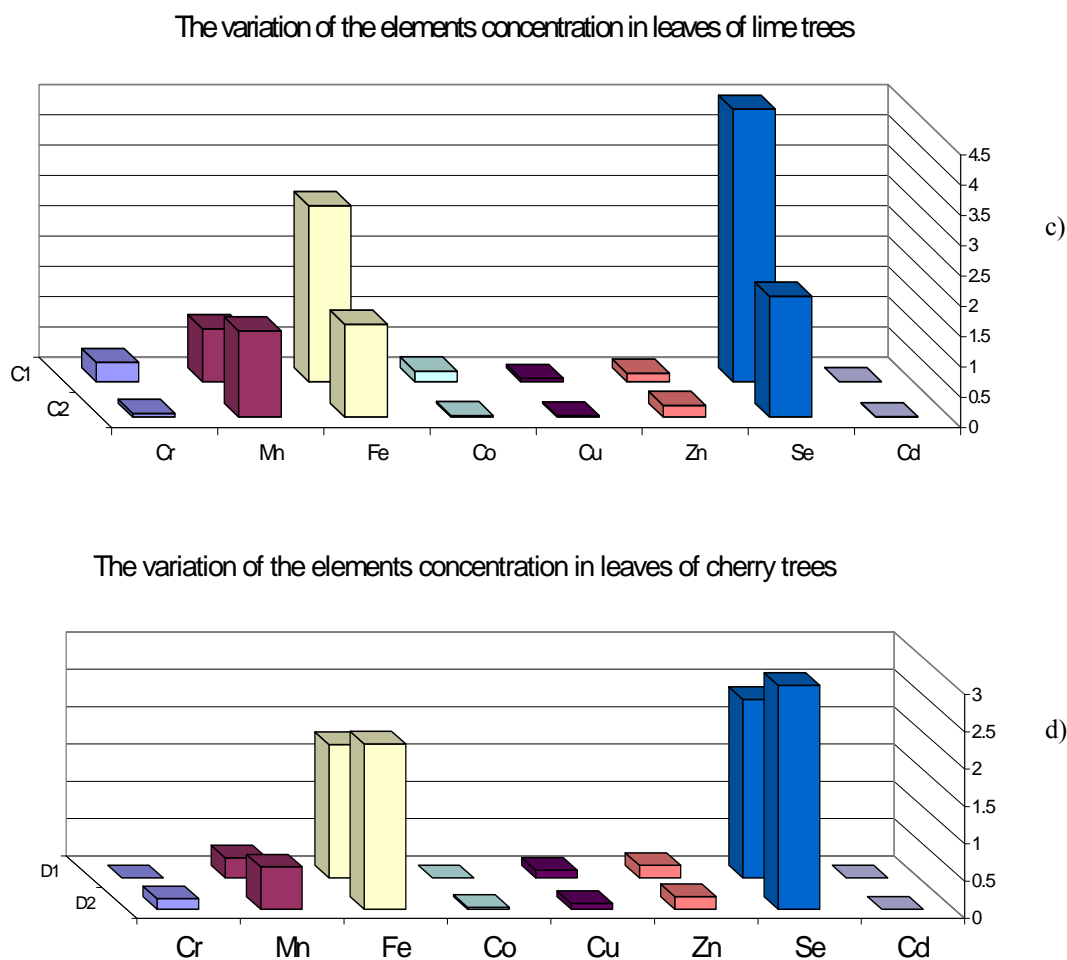
Figure 2. The variation of elements concentration for different type of samples:
c) leaves of lime tree; d) leaves of cherry tree.

We can state that:
- In leaves of plum tree the Mn and Cd concentrations are greater in September than July and the other concentration are lower in July than September.
- In leaves of mulberry tree the Mn, Cu and Zn concentrations are greater in September than July and the other concentration are lower in July than September.
- In leaves of lime tree the Mn, Zn and Cd concentrations are greater in September than July and the other concentration are lower in July than September.
- In leaves of cherry tree the Cr, Mn, Fe, Co and Se concentrations are greater in September than July and the other

concentration are lower in July than September.

So, we observe that the Mn concentration is high for all the species trees and the other elements an aleatory variation in concentration.

4. Conclusions

The uses of AAS techniques give the possibility to determine the elemental composition of plants with a great sensibility. We identified and determined the concentration of heavy and toxic elements Cd, Co, Cu, Cr, Se and Zn, which can put in evidence the presence of these elements in environmental medium, together with mineral elements Fe, Mn. This study demonstrates the potential of AAS method in environmental

biomonitoring, and also we can say that the leaves of trees can be used as an indicator for pollution.

The results of this work were use in the following biological and environmental research activities.

5. References

[1] Shimadzu Corporation, Atomic Absorption Spectrophotometry cookbook.

[2] Haswell, S.J.,1991. Atomic Absorption Spectrometry; Theory, Design and Applications. Elsevier, Amsterdam.

[3] Claudia Stihi, I.V. Popescu,V. Ciupina, Anca Bancuta, Gabriela Busuioc, V. Stihi, G. Dima, M. Belc, Gh. Vlaicu, Inductively Coupled Plasma-Optical Emission Spectroscopy (ICP-OES) And Atomic Absorption Spectrophotometry (AAS) In Environmental Analysis, Rom. J. of Physics vol.48, No.1-4, 295-299, (2003)

[4] I. V. Popescu, V. Ciupina, Claudia Stihi, Anca Bancuta, M. Belc, Gabriela Busuioc, T.Badica, Gh. Vlaicu , Trace elements analysis by PIXE (Particle Induced X-Ray Excitation) and AAS (Atomic Absorbtion Spectrometry) from environmental samples), Rom. J. of Physics vol.48,No.1-4, 283-287,(2003)

FROM MICRO TO NANO-TECHNOLOGIES

OANA CATALINA BUTE

*Physics Department, Science Faculty , Valahia University of Targoviste, **oanab@valahia.ro***

Abstract: The aim of this article is to present the tendency to use more and more precise technologies, namely going from microtechnologies (which are able to handle details at the scale of microns), to nanotechnologies (which go down to the dimension scale of atoms and molecule).

1.Definition of the domain.

1.1 Microsystem. Microtechnologies.

By definition, a microsystem must detect, process and evaluate external signals, must make decisions based on the obtained information, and finally must convert the decisions into corresponding actuator commands/1/. A microsystem doesn't represent a miniaturised version of the bigger system because by scalling down, the phenomena are different and the system must be re-engineered or constructed on a completely different principles.

In Europe, there is a clear distinction between microelectronics and the so-called "microsystem technologies"(MST). In our conception, microtechnologies include both microelectronics and MST/2/. Many new process and technologies used for Microsystems are derived from microelectronic technology which is dedicated to fabricate complex electronic circuits constructed from electron devices.

Microtechnologies are structuring the macroscopic materials at the micrometer level. In general, they are able to fabricate physical structures, which are activated by various forms of energy. Microsensors and microactuators are typical examples.

A complete system, which can interact with the external world, can be also fabricated. This is possible by integration in one component of various components performing completely different tasks .We can speak about MEMS (Micro-Electro-Mechanical Systems), BIO-MEMS and MEOMS (Micro-Electro-Opto Mechanical Systems).

1.2. Nanoscience and nanotechnologies.

Nanoscience and nanotechnologies are related to physical structures and features in the range of nanometers and the corresponding specific phenomena. In a broad definition, nanotechnology includes all technologies associated with either the "top-down" approach of sculpting the desired structure from a macroscopic piece of material, or the "bottom-up" approach of building a nanostucture atom by atom and molecule by molecule/3/. Development of nanotechology have been spurred by refinement of tools to see the nanoworld, such as more sophisticated electron microscopy and scanning tunneling microscopy. By 1990, scientists at IBM had managed to position individual xenon atoms on a nickel surface to spell out the company logo, using scanning tunneling microscopy probes, as a demonstration of the extraordinary new technology being developed/5/.

On the other hand, the development of nanotechnologies has created a great interest in the worlds of materials and life sciences. The nanostuctured materials have a huge potential. They allow creation of completely new materials with desired properties. About these nanomaterials we will discuss in the next chapter.

2.The future of nanomaterials and nanobiotechnologies.

Nanoparticles, nanospheres and other nanostructured materials are products of the current interest in nanomaterials. While they may not yet have revolutionized our daily life, nanomaterials are set to become key components in future high technologies market/4/.

2.1. Range of nanomaterials.

Over the past decade, nanomaterials have been the subject of enormous interest. Nanomaterials can be metals, ceramics, polymeric materials, or composites materials. Their defining characteristic is a very small feature size in the range of 1-100 nanometers (nm). The unit of nanometer derives its prefix from a Greek word meaning dwarf or extremely small/5/. One spans 3-5 atoms lined up in a row. By comparision the diameter of a human hair is about 5 orders of magnitude larger than a nanoscale particle.

Nanomaterials have actually been produced and used by humans for hundreds of years –the beautiful ruby red color of some glass is due to gold nanoparticles trapped in the glass matrix. The decorative glaze known as luster, found on some medieval pottery, contains metallic spherical nanoparticles dispersed in a complex way in the glaze, which give rise to its special optical properties. The techniques used to produce these materials were considered trade secrets at the time, and are not wholly understood even now.

The bottom-up synthetic approach has been used by chemists to initiate developments of three major kinds of nanomaterilas with applications in very different fields.

The first are *nanoparticles* which are developed on a very small scale. These are particles(spheres or tubes) designed with dimensions less than 100 nm and they are used in fields like electronics or cosmetic industries. On a larger scale, there are the so- called *surface-structured nanomaterials* and *volume-structured nanomaterials.*

Surface-structured nanomaterials get their name from the fact they are coted with a 100 nm thick layer. They are typically used in the textile industry or for data storage. Finally, *volume-stuctured nanomaterials* are characterised by the fact that one of their components (for example, grain, particle, charge) is smaller than 100 nm. They are typically used in the automobile or packaging industries.
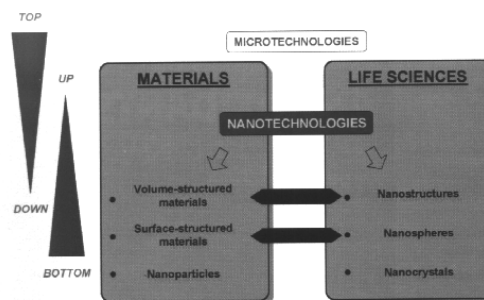
Figure1.The organization of nanomaterials in the fields of materials sciences and life sciences/4/.

2.2 Applications of nanomaterials.

The variety of nanomaterials is great, and their range of properties and possible applications appear to be enormous, from extraordinarily tiny electronic devices to biomedical uses. In this order we can speak about nanoparticles, which are today marketed as dry powders or liquid/ paste dispersions to which some additives can be added to obtain stable and homogeneous media/4/. The principal nanometric powders available today are the metallic oxide powders and nano-clays:silica, alumina, titanium oxide.
A new category of nanoparticles is carbon-nanotubes. They are tiny tubes about 10,000 times thinner than a human hair-consist of rolled up sheets of carbon hexagons. They have the potential for use as minuscule wires or in ultrasmall electronic devices. To build those devices, science-men must be able to manipulate nanotubes in a controlled way. IBM researchers using an atomic force microscope (AFM), an instrument whose tip can apply accurately measured forces to atoms and molecules, have recently devised a means of changing a nanotube's position, shape, orientation, as well as cutting it.
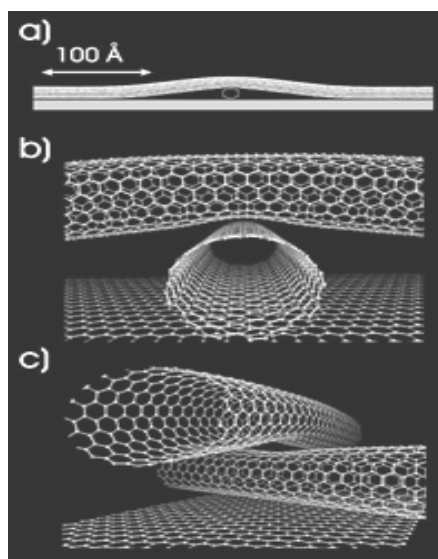
Figure2. Carbon nanotube: 1-50 nm in diameter; 10-100 micrometers long.

There are two categories of surface-structured materials, which are commercially available today. The first concerns materials with high magneto-resistance that are used in the reading heads of large capacity computer hard disks and the second category are nanocapsules that contain an active ingredient. In this application, a protective coating of nanometer dimensions of active products covers the active ingredients. Nanocapsules may present new possibilities for drug delivery, gene therapy, and medical diagnostics.

Volume-structured materials includes nanocomposites, nanoporous or nanocrystallised materials. Of this group, nanocomposites are the products used most at the industrial level.

There are several varieties of polymeric nanocomposites, but the most commercially advanced are those that involve dispersion of small amounts of nanoparticles in a polymer matrix. In this way it is possible to improve certain physico-chemical properties of the matrix polymer. For example, adding such small amounts as 2% by volume of silicate nanoparticles to a polyimide resin increases the strength by 100% /5/.

3. Biomimetics

Some materials, structures and subsystems are now inspired from the living organisms. The technical systems may become much more efficient in this way. The Japanese scientists who are attempting to construct microrobots take the same biomimetic approach, in simulating the "mechanical" construction of the insect body/2/. We have also to consider new methods of fabrication such as self-assembly, auto-organisation and self-repair/3/.

The use of biomimetics and the design of novel matrices will be used in organ reconstruction and to decrease the body's rejection of implants/4/.

4. References

1.Sergej Fatikow; Ulrich Rembold; " Microtechnologies of systems and robotics";
2.CAS'98 Proccedings, volume 1, p (3-12);
3.CAS'2000 Proccedings, volume 2, p (399-402);
4.Arnaud Paris; Vicent Pessey , "The future of nanomterials and nanobiotechnologies";
5.Kathleen Hickman;" Nanomaterials: It's a small, small world".

FROM NANOSTRUCTURED MATERIALS TO FUTURE ELECTRON DEVICE

V.CIMPOCA

Department of Physics, The Valahia University of Targoviste, 0200 Targoviste, Romania

Tel./Fax. +40-45-620611, cimpoca@valahia.ro

Abstract: *In this paper we present a brief introduction to the nanostructure science and technology and its impact to the future electronic and photonic devices. Among new methods of controlled synthesis and in-situ characterisation for nanoparticles and nanocoating, a strong emphasis is focused on the self-assembly organisation as a paradigm change for the preparation of quantum wires, quantum dots, dislocations, loops and carbon nanotubes structures. These self-assembled nanobuilding blocks used in the post silicon devices era will create high density and efficient functionalities in the next years.*

Key words: nanostructure, carbon nanotubes, quantum dot devices, single electron device

INTRODUCTION

In the last three decades the research and development in micro-electronics has continuously enlarged the computing power per silicon chip by reducing the geometrical dimensions of the integrated devices and increasing their complexity [1]. Nowadays, there is an intense study around the world to determine the exact point where the dimensional scaling becomes either physically unfeasible or financial impracticable. The limit seems to be related to the gate length of MOSFET transistors, which cannot be lowered below 100 nm due to short channel effects. Below 100 nm MOSFET's face a scaling limit when SiO_2 gate dielectric is used to high direct tunneling gate leakage currents. This unprecedented shrinkage of the volume needed per transistor was the driving force for the development of process equipment and high chemical and spatial resolution analytical characterisation tools. In the material research area, the same trend of miniaturisation has occurred.

This was motivated by the microelectronics requirements and also by the realisation that new properties will enable breakthrough in a multitude of technological important fields.

Within this framework, the nanostructure science and technology has been born as a broad and multidisciplinary area of research and development, which has been growing rapidly in the last few years. The paradigm of the new science is: novel performance through nanostructuring. This means that the synthesis and control of materials in nanometer dimensions can open the way to new material properties and devices. The explosive development of this new field is explained by the interdisciplinary activities involved in nanostructuring, where scientific interlinking has fuelled novel concepts and materials. The nanostructure science and technology is covering simultaneously the field of new materials and technological processes in conjunction with their application in future devices, including those ones from the post-silicon era. Within this paper we present a brief overview on the specific synthesis methods for the formation of nanostructured materials and their application to future electron nanodevices.

CONTROLLED SYNTHESIS AND ASSEMBLY OF NANOPARTICLES AND COATINGS

Controlled synthesis and assembly of materials at the nanoscale level is the starting point and the key to new functionalities.

Preliminary results of the research in nanostructured materials have increased the belief that the ability to control the nanoscale building blocks of the materials can result in enhanced properties at the macroscale level: increased hardness, magnetic coupling catalytic absorption or higher efficiency electronic or optic behaviour. The strategies of controlled synthesis for nanostructured materials can be classified in two groups, as "bottom-up" and "top-down" approaches.

Within the "bottom-up", initially, the nanostructured building blocks are formed and subsequently they are assembled into the final material. An example of "bottom-up" approach is the formation of powder components through the aerosol technique and their compaction into final material by physical and chemical annealing [2]. Sol-gel technology is also an example of "bottom-up" method for nanostructure coatings formation by wet chemical synthesis, where both building blocks formation and their assembly are integrated within one process.

The "top-down" approach, either starts from raw material and then "moulds" the functionality, or it begins with the formation of nanostructured building blocks by "ball-milling"-type techniques and, then they are subsequently assembled [3].

To met the requirements of nanostructuring, the physical (reactive sputtering, reactive evaporation, laser ablation) and chemical method (chemical vapour deposition, atomic layer epitaxy, molecular beam epitaxy) for nanocoating preparation have to be conducted to the their limit of in-situ control and defect-free standard. The "bottom-up" approach is expected to play an important role in the synthesis of new materials like nanoparticles chain (wires), nanometer fiber or tubes and self-assembled quantum dots, 2D and 3D nanostructures. Actually, chain aggregates of nanoparticles assembled in molecular or quantum wires are going to revolutionise computational devices and optoelectronics in terms of number of atoms per logic function and electro-optical efficiency [4]. In addition, the synthesis of single-crystal semiconductor nanofibres with diameters in the range of 3 to 15 nm, by vapour phase epitaxy and laser ablation vapour-liquid-solid techniques [5]

offers a considerable technological promise for optoelectronic device applications, such as p-n junction for light emission. A possible and effective way to generate nanofibers (or tubes) is based on the use of membrane-template technique [6], where nanochannels were generated in the membrane by electrochemical etching.

Self-assembly and "natural nanoscaled templates" specific to organic material synthesis have become a new paradigm and a deliberate strategy for nanostructured material synthesis. Self-assembly is a process in which, a big molecular structures is obtained from the organization of a large number of molecules or atoms into a given shape, typically through specific interactions of the molecules among themselves and with a template. Due to the important role of the chemical bonds in the self-assembly organization, the interaction of the different bonding mechanism is a matter of strong fundamental research all over the world [7]. In Fig. 1, it is presented the large variety of carbon nanotube structures with different wall configurations, including metal filled nanotubes. Within the family of the carbon materials, there are also included fullerenes (like endohedral fullerenes and metal coated fullerenes), carbon nanoparticles and porous carbon.
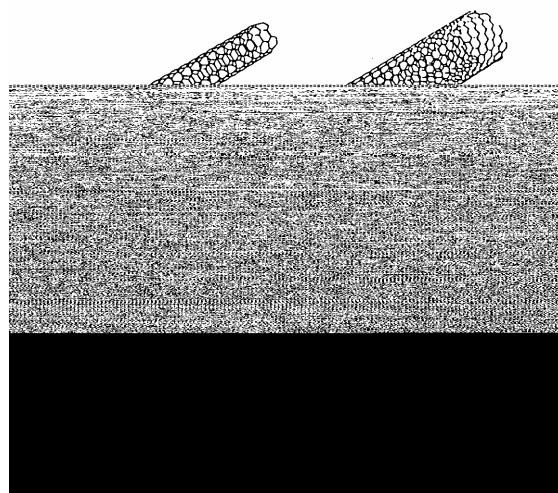

Fig.1 Examples of carbon nanotube structures with different wall configuration, including a metal-atom filled nanotube.

The carbon nanotubes have the interesting properties that its semiconductor or metallic behaviour depends on the form and the diameter of the nanotube.

Porous carbon is also an important material to be used as molecular sieve (or membrane) or as nanostraws for filtration. Self-assembled synthesis of carbon-based nanotubes and quantum dots exhibits a great potential in optical devices and self-assembled semiconductor quantum dots applied in future memories and semiconductor lasers.

The principles of self-assembly have been applied to the physical vapour deposition processes for the formation of arrays of semiconductor quantum dot. Thus, due to the inherent strain during epitaxial growth of lattice-mismatched materials and expected strain-induced transition from two-dimensional (layer stage) to three-dimensional (islanded) growth, an array of semiconductor quantum dots with a density of about 10^{11} cm^{-2} was formed [8]. The quantum dots diameters were in the range of 200-300 Å, and they varied by only about 7% from one to the other. Such semiconductor quantum dots were also obtained by the epitaxial growth of InAs thin layers on GaAs substrate). This new method of quantum dot fabrication is much beyond of the capabilities of standard high resolution lithographic and pattern transfer processes. This method has opened the way to the new generation of laser structures. The mechanical, optical and electronic transport properties of these new materials can be varied by controlling the diameter and the monodispersity of the primary particles, the crystalline structure and morphology, aggregate length, interfacial properties and material purity.

The success of the new methods for nanostructured material preparation can be obtained only by the contribution of high resolution, in-situ monitoring strategies. Here, we have to mention the role of reflection high energy electron diffraction (RHEED) on the understanding the nature of surface bonding. In addition, the powerful scanning probe technology, including scanning tunneling microscopy (STM) and atomic force microscopy (AFM) has brought an increased understanding of the surface morphology of the new nanomaterials. Recently, these material characterization methods have extended their application range and they

become the basis of material patterning, processing and manipulation at the nanometer scale [8]. Thus, in Fig. 2, it is shown the application of atomic force microscopy for "repairing" a metal path on the surface [9]. One can see how 50 nm gold particles are manipulated in the opened area between two interrupted paths, re-making thus their continuity [9]. This is a very good example of the "positive feed-back" between the synthesis technology and the material characterisation technology, sustaining each the development of the other, and both of them contributing to the evolution of future electron devices.
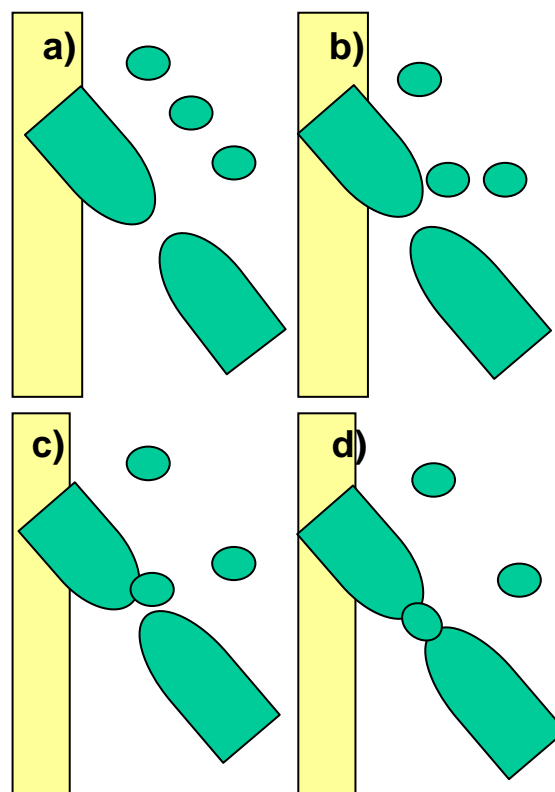

Fig.2. The tip of the AFM is used for manipulation of 50 nm gold particle into the gap between two Au/Ti electrodes.

FUTURE ELECTRON DEVICES

The recent efforts performed within the nanostructured science and technologies have created conditions for the investigation of new electronic devices with dimensions ranging from 0.1 to 50 nm, as described in the previous section.

In Fig. 3, we present the evolution of primary electronic devices, which are now intensively investigated in different laboratories, all over the world as a function of size. The materials that are considered at the laboratory level cover a broad range from charge clusters shaped by electric fields to metallic colloids and to single oligomer.
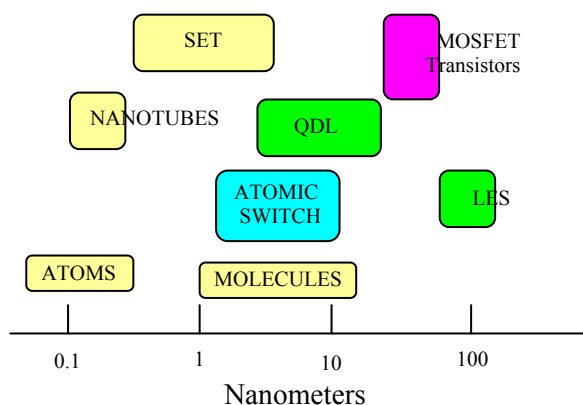

Fig.3.Evolution of primary electronic devices as function of size

STE – Single electron Transistors

LES – Light Emitting Silicon

QDL – Quantum Dots in Lasers

SINGLE ELECTRON TRANSITORS

The challenge in the field of semiconductor memory devices is the single electron transistor (SET), which opens to way to increase the capacity of data storage electronic circuits, may be to a level compatible to magnetic technology. The single-electron charging effect was discovered back to 1950's on granular metallic systems, but the theoretical model based on Coulomb gap appeared at the end of 1980's, when a nanoscale tunnel junction was built and measured [10]. Today, there are many technological approaches for the SET fabrication. They start from the conventional technologies based on semiconductor materials (GaAs, Si) and continue to more sophisticated directions like Si edge quantum wire approach and the self-organised quantum dot (SOQD), which are prepared on semiconductor (as it was described in the previous section). Recently, non-semiconductor materials have been used for the SET implementation.

Thus, a single molecule of benzene-1,4-dithiol was self-assembled from solution onto two electrodes of a mechanically controllable break junction [11]. The spacing between the electrodes is about 0.8 nm and I-V measurements at rom temperature showed a Coulomb gap of 0.7 V. Electronic transport in oligomers located between two electrodes is also studied. The single electron devices may be used in quantum cellular automata (QCA) for data storage. Each cell holds two electrons having two polarization configurations, which can represent the "0" and "1" states. These cells would interact via Coulomb forces with their neighbour ones, eliminating thus the need for the metal interconnections [12]. This might be a change in the paradigm of future electron-based memory devices. Another important change brought by the nanostructured materials may be in the field of the semiconductor lasers with large applications in compact disk players, laser printers and optical communication schemes.

QUANTUM DOTS IN LASERS

The quantum well based semiconductor laser was the first step in the paradigm change in this field, where "bulk" active layers were used for inversion of mobile charge population and its coupling to an optical field, which will finally stimulate an radiative emission. The refinements in the molecular beam epitaxy have allowed preparation of very thin and controlled-structure films making possible a good engineering of the spacing between energy levels in the band gap and finally, increasing the efficiency of lasers. Much greater improvements are now expected from the lasers with quantum dots active layers, with respect to quantum well laser generation. It is predicted that the QD lasers may be less temperature-dependent than the existing ones and that they will better withstand to higher temperature operation. In addition it is anticipated a reduction of threshold current for laser operation. The most important requirement for the success of the QD lasers with respect to quantum well and bulk lasers come from the necessity to get uniform size quantum dots.

The ideal behaviour of QD laser is obtained when all the quantum dots have the same size, in order to avoid smearing out of the density of states. Figure 4. illustrates one of the key concept in the AlGaAs/GaAs lasers operation. Stimulated recombination of electron-hole pairs takes place in the GaAs quantum well region (active layer), where the confinement of carriers and of the optical mode enhance the interaction between carriers and radiation.
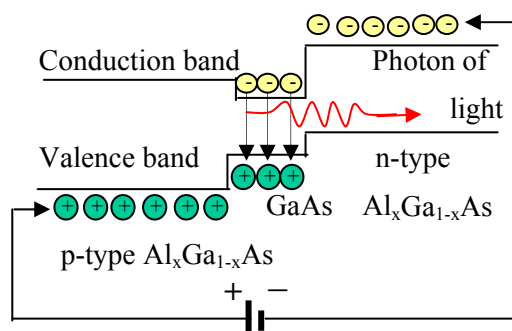

Fig.4. Schematic of a AlGaAs/GaAs laser

Figure 5 shown the change in the electronic density of states as a function of the dimensionally of the active layer.
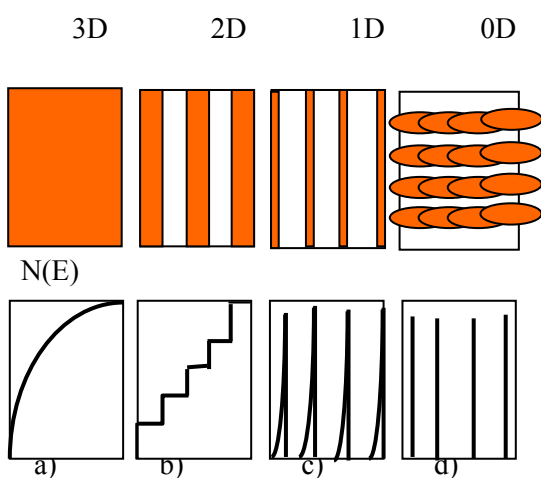

Fig.5. Density of electronic states as a function of structure size

a) Bulk Semiconductor; b) Quantum well

c) Quantum Wire and d) Quantum dot

Even if now, there are many unsolved technological problems related to QD uniform size distribution, which limit the optical efficiency of the present QD lasers (like in the earlier stages of quantum well lasers), the solution seems to be natural self-assembly of QD, which already proven high optical efficiency [13].

DEVICES BASED ON NANOTUBES

An important step to the post-silicon era of electron devices is made with the recent progresses in the nanocarbon-based electronic devices. The discovery of the self-assembled single wall nanotubes (SWNT) prepared by laser ablation of a graphite rod chemical vapour deposition [12] has increased the belief that high quality nano carbon tube can be industrially applied. The engineering of the electronic properties of the carbon nanotubes is performed by the control of the nanotube diameter and its chirality, and this was already proven by four-point probe conductivity measurements. It has been proven that the electric transport mechanism in carbon nanotubes is controlled by resonant tunneling and single-electron charging effects. The hole transport seems to be predominant in the electrical conductivity. Metallic nanotubes present a high field enhancement at their extremities due to their strongly polarisation behaviour in an electric field. This effect and others related to quantum confinement at the tip, make the nanotubes outstanding field emitting materials. It has been recently shown that the nanotubes emit electrons very efficiently when they are exposed to an electric field and irradiated by a laser to remove their cap [14]. This property has opened the gate to the future field-emission displays and microwave tubes. One of the last convincing applications of carbon nanotubes is the cathode ray tube (CRT) based on nanotube field emitter. The result is not industrially applicable for the moment, but it supports the efforts necessary to solve the present technological problems.

Therefore, all the above examples of future devices shows that the next years belongs to generation of self-aligned structures amplifying the material properties by self-organisation to an unprecedented level.

LIGHT EMITTING SILICON

Dislocation engineering enables Light-Emitting Silicon.

The introduction of dislocation loop array and associated strain fields prevent carrier diffusion and recombination in high quality silicon. The dislocation loops introduce a local strain field, witch modifies the band structure and provides spatial confinement of the charge carriers. The band gap of the silicon is raised on carrier diffusion is presented. The electrons are effectively blocked and forced to give up their energy as radiative emission, or electro-luminescence. The stress at the outside edge (1.2 A) of the interstitial dislocation loop is 25-50 GPa, witch will cause an increase in band gap energy at the edge of 0.3-0.85 eV.

Dislocation loops in mono-crystal of silicon are produce by ion implantation (boron, phosphorous or another implant species) so that to form the p-n junction can be achieved both and independently. In the figure 6 we reported a light-emitting silicon were made by implanting boron.
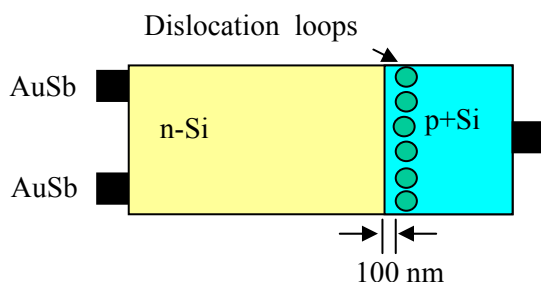

Fig.6. Light-Emitting Silicon

The dislocation loops has been observed in a planar region parallel with implanting surface, and around 100 nm from the p-n junction. These dislocations formed an array and are typically about 80-100 nm in diameter and are spaced about 10-20 nm apart. The strain field at the edge of the dislocation loop is high and it falls off around each loop approximately with the distance. The device operates as a conventional light-emitting diode under forward bias.

Therefore, all the above examples of future devices shows that the next years belongs to generation of self-aligned structures amplifying the material properties by self-organisation to an unprecedented level.

CONCLUSIONS

The nanostructure science and technology is reshaping the landscape of materials synthesis and characterisation and future devices taking the benefit of the unexpected enhancement of the electrical, optical, magnetic and mechanic properties of the self-organised nanostructured materials.

The controlled synthesis of nanoparticles and nanolayers is obtained by refinement of the existing chemical and physical methods and by adding in-situ monitoring techniques during the material formation in the earlier nanostructuring stages. A change of paradigm in the new material formation at the nanoscale comes from the bio-inspired technologies, where self-assembly method appears to be a solution to the future electron devices.

Self-assembled quantum dot technology seems to be the key to the quantum cellular automata based on single electron transistor, quantum dot lasers and high emission display based on carbon nanotubes, considered in this paper as outstanding examples of electron devices belonging to the post silicon generation of the third millennium

R E F E R E N C E S

1.H. Roher, *Jpn. J.Appl.Phys.*, 32, 1993, pp. 1335-1342.
2.M.K. Wu, R.S. Windeler, C.K. Steiner, T. Bors and S.K. Friedlander, *Aerosol Sci. Technol.*, 19, 1993, pp. 527-535.
3.C.C. Koch, *Annual Review of Mater. Sci.*, 19, 1989, pp.121-143.
4.E.E.D. Chidsey and R.W. Murray, *Science,* 231, 1986, pp.25-32.
5.K.M. Hiruma, M. Yazawa, T.Katsoyama, K. Ogawa, K. Haraguchi, M. Koguchi, and H. Kakibayashi, *J. Appl. Phys.*, 77(2), 1995, pp.476-485.
6.C.R. Martin, *Science*, 266, 1994, pp. 1961-1966.
7.M.S. Dresselhaus, G. Dresselhaus and P.Eklund, *Science of fullerenes and carbon nanotubes*, San Diego, Academic Press, 1996.
8.D. Leonard, M. Krishnamurthy, C.M. Reaves, S.P. Denbaars and P.M.Petroff, *Appl. Phys. Lett.*, 63, 1993, pp.3205-3205.

9.T. Juno, S.-B Carlsson, H. Xu, L. Montelius and L. Samuelson, *Appl. Phys.Lett.*, 72, 1998, pp. 548-550.

10.D.V. Averin and K.K. Likharev, "*Mesoscopic Phenomena in solids*, Amsderdam, Elsevier, 1991, Chapter 6.

11.M.A. Reed, C. Zhou, C.J. Muller, T.P. Burgin, and J.M. Tour, *Science*, 278, 1997, pp. 252-259.

12.C.S. Lent, P.D. Tougaw, W. Porod, and G.H. Bernstein, *Nanotechnology*, 4, 1993, pp.49-53.

13.D. Bimberg, N. Ledentsov, M. Grundmann, N. Kirstaedter, O. Schmidt, M. Mao, V.M.Ustinov, *Jap. Journal Appl. Phys.*, 35, 1996, pp.1311-1319.

14.A.G. Rinzler, J.H. Hafner, P. Nikolaev, L. Lou, S.G. Kim, D. Tomanek, P. Nordlander, D.T. Colbert and R.E. Smalley, *Science*, 269, 1995, pp.1550-1554.

RARE EARTH DOPED LiNbO₃ WAVEGUIDE AMPLIFIERS AND LASERS

SERGIU DINU[1], CALIN OROS[1], GABRIEL DIMA[1], GABRIELA DINU[2]
[1]"Valahia" State University of Targoviste
[2]"Petru Cercel" High School of Targoviste

Abstract*: Rare earth doping (above all Nd^{3+} and Er^{3+}) mainly of silica-based optical fibers has been applied to develop fiber optical amplifiers and lasers of excellent properties. Moreover, it can also be an attractive method to fabricate active devices on the planar substrates of integrated optics.*

1. Introduction

In particular, rare earth doping of LiNbO₃ will significantly increase the potential of this material allowing a monolithic integration of optical amplifiers, lasers, modulators and other active and passive devices on the same substrate.

2. Doping and waveguide fabrication techniques

Different methods can be used to fabricate rare earth doped LiNbO₃ optical waveguides and lasers.The most straightforward way is to start with wafers already doped in the bulk.But also a localized (photolithographically defined) doping of a surface layer of undoped substrates by implantation and indiffusion is possible, before waveguides are prepared by proton exchange or Ti-indiffusion. a)Doped crystal growth The growth of rare earth doped LiNbO₃ crystals, using the Czochralski technique, has been successfully by several groups. It seems that a MgO-codoping, which also reduces the susceptibility of LiNbO₃ to optical damage (optically induced changes of the index of refraction), facilitates a striation-free growth. Up to now, bulk crystals doped by Nd^{3+} and Er^{3+} have been grown from a melt containing 0,4-2 mol % Nd₂O₃ and 0,2-0,6 mol % Er₂O₃, respectively.

b) Implantation and indiffusion
Localized doping is possibile by a (masked) ion beam implantion of rare earth ions followed by thermal annealing. This has been successfully demonstrated by Buchal and Mohr; the usually used 200 KeV as implantation energy, resulting in a penetration

depth of the peak of the Gaussian ion distribution underneath the surface of about 400 A^0. The implanted dose typically was $10^{16}/cm^2$ leading to a nearly complete amorphization of the doped surface layer. Immediately after the implantation the samples were annealed in a oxygen atmosphere (typically during 1 h at 1030 ^{0}C) to restore the crystallinity of the LiNbO₃ matrix by an epitaxial regrowth of the surface layer and to get simultaneously a diffusion of the rare earth dopant deeper into the substrate till a typical waveguide depth of some um is reached.

c) Proton exchange and titanium indiffusion
Both fabrication techniques have been used to prepare optical strip waveguides in LiNbO₃ substrates, homogeneously doped during crystal growth with Nd (and MgO, to reduce the susceptibility to optical damage). It was shown that the presence of Nd (~0,2 at %) has only a negligible effect on the proton-lithium exchange rate. However, the Ti-diffused channels fabricated up to now with a somewhat larger cross-section had rather high losses (~1,6 dB/cm) due to a poor substrate quality. Erbium-doped waveguides have been fabricated by the Ti-diffusion technique only in surface-doped LiNbO₃ substrates. After the implantation of Er, followed by thermal annealing, the optical waveguides have been prepared in the usual way (e. g.by indiffusion of 6μm and 7 μm wide Ti stripes of 95 nm thickness at 1060^{0}C during 9h).

3) Neodymium doped devices

Nd-doped optical amplifiers (with a gain up to 7.5 db) and lasers (with a maximum output power of 14 mW) for the wavelength λ_s = 1,08 μm are the first rare earth doped

LiNbO$_3$ waveguide devices. They take advantage of the excellent properties of the Nd^{3+} ions with a four-energy level system responsible for the λ_s=1,08 μm emission. (figure 1)
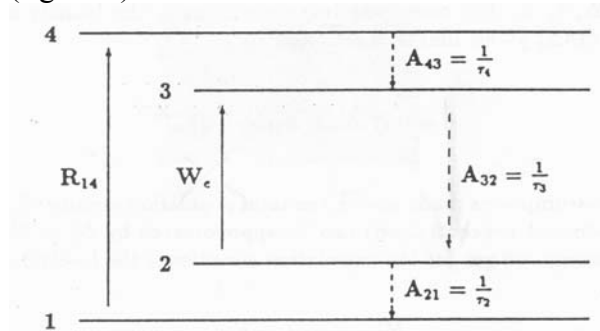

Figure 1: Simplified energy diagram of Nd:LiNbO$_3$ optical amplifier (and laser)

Gain evolution for various pump power levels (P$_p$(0)=0,1;5 mW) in a proton-exchanged Nd:MgO:LiNbO$_3$ channel guide in the low pump intensity limit compared with the theoretic results obtained by a numerical integration (solid lines)) is (figure 2):
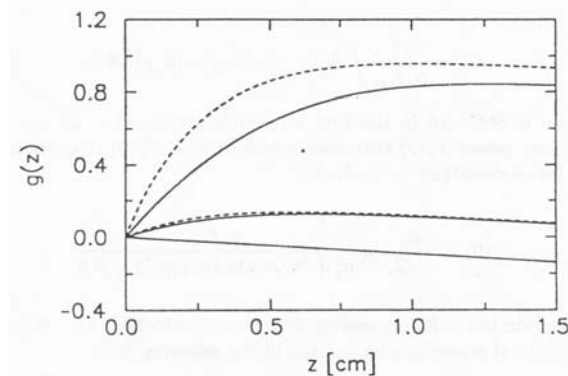

Figure 2: Gain evolution for various pump power levels

Small signal gain at λ =1,084 um of a 5,9 mm long channel guide amplifier as function of the coupled pump power (λ ~ 815nm) is shown in figure 3.

Lallier et al. operated a proton-exchanged channel guide in a Nd:MgO:LiNbO$_3$ substrate as an optical amplifier, pumped by a styryl 9M dye laser at λ ~815 nm. The French group used a Nd-doped waveguide laser as signal source for λ=1084nm and coupled about 1 μW into the 5,9 mm long amplifier. Fig. 3 shows the small signal gain as function of the coupled pump power with a maximum of 7,5 dB at 22 mW.
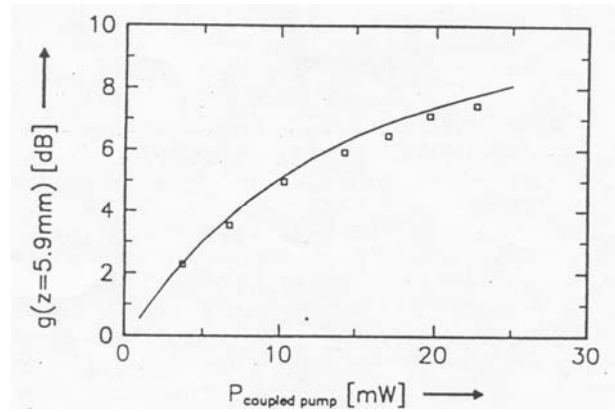
Figure 3: Small signal gain at as function of the coupled pump power

The efficient Nd-doped optical amplifier presented above allows to develop waveguide lasers by introducing the necessary optical feedback for the signal wave by appropriate mirrors or grating structures. Up to now, only dielectric mirrors, vacuum-deposited on the polished end faces of the amplifier waveguide, have been used to fabricate a laser. Lallier et al. succeeded in demonstrating the first Nd-doped waveguide laser in LiNbO$_3$. They prepared a proton exchanged channel guide in a X-cut Nd:MgO:LinbO$_3$ substrate doped with 0.22 at % Nd and 3 mol % MgO. By the combination of MgO-doping and proton exchange optical damage effects could be avoided allowing continuous wave (cw) operation of the laser in a single transverse mode. In the 12 mm long waveguide of effective pump area A$_{eff}$ = 35 μm^2 (width: 8.5 μm) 91 % of the coupled pump power (λ$_p$ = 0,814 μm) was absorbed. The fluorescence lifetime τ_3 = 109 μs and the stimulated cross-section σ^e_s = 1.7 × 10^{-19} cm^2 were found to be identical in the waveguide and in the bulk. From the mirror reflectivities of 90 % and the signal propagation loss a total loss L = 0.525 can be calculated resulting in a theoretical threshold pump power $P^{th}_{p,abs}$ = 1.34 mW. The figure favorably agrees with the measured threshold of 1.5 mW (figure 4). Also the calculated single end slope efficiency of 14 % with an emission wavelength λ$_s$=1.085 μm agrees well with the measured one of 13 %.
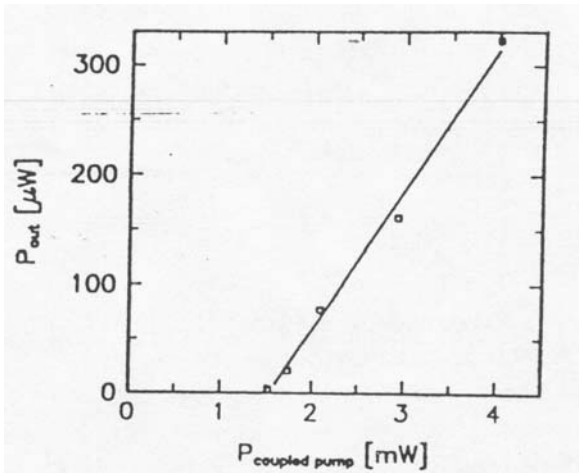
Figure 4: Power characteristics of the first Nd:MgO:LiNbO₃ waveguide laser with proton exchanged channel guide

Parallel to the Nd-doped waveguide lasers with proton exchanged channel, another version with Ti-diffused guide was developed by a German group. A Z-cut wafer of Nd:MgO:LiNbO₃, grown from a melt containing 0.34 mol % Nd_2O_3 and 5 mol % MgO, was used for the waveguide fabrication. The 6 μm wide channels of 0.8 cm length were monomode at both the pump (λ_p = 814.6 nm) and emission (λ_s = 1.084 μm) wavelengths.

The effective pump area A_{eff} = 36 μm² was comparable to or 3 times larger than that of the proton exchanged channels of the lasers reported above (figure 5).
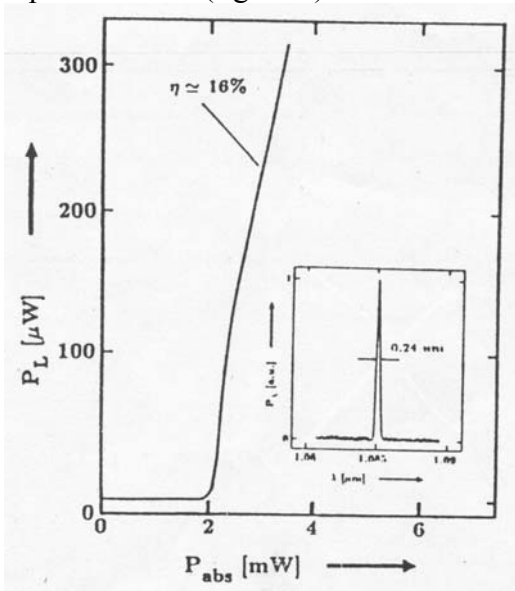
Figure 5: Power characteristics of Nd:MgO:LiNbO₃ wave guide laser with Ti-diffused channel guide

4. Erbium doped devices

Very recently, also Er-doped LiNbO₃ devices have been reported . As their well developed fiber optical counterparts they allow (broadband) amplification and lasing in the important wavelength range 1.5 μm ≤ λ_s ≤ 1.6 μm, preferred for future optical communication systems.

Erbium is substitutionally incorporated into the LiNbO₃ – lattice as Er^{3+} (probably replacing Li^+ and Nb^{5+} like Nd^{3+}).

To analyze signal amplification by stimulated emission in Er-doped LiNbO₃ – waveguides a simplified energy diagram is used neglecting the level splittings by the Stark-effect. If also excited state absorption is neglected, a three-level diagram is sufficient to model an amplifier for λ_s ≈ 1.53 μm radiation (figure 6).
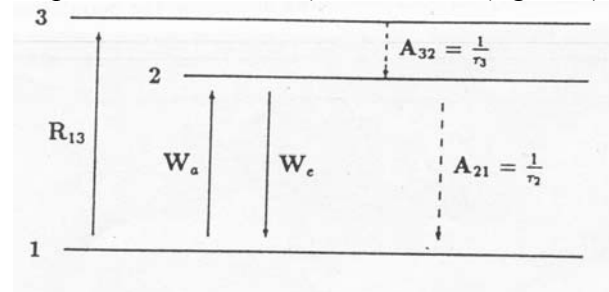
Figure 6: Simplified energy diagram of an Er:LiNbO₃ optical amplifier (and laser)
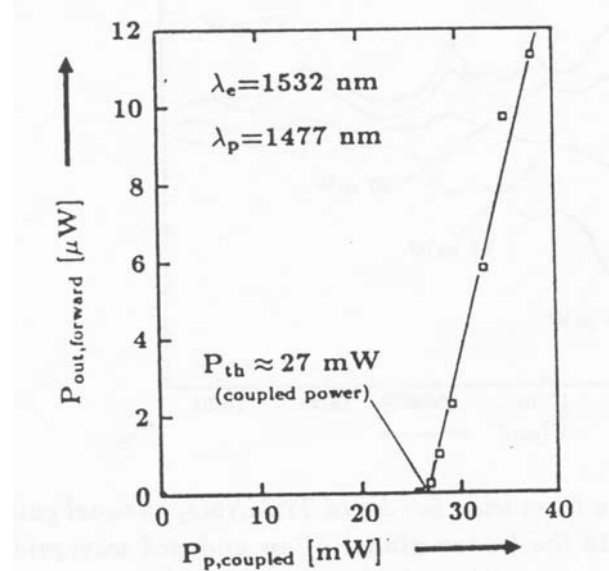
Figure 7: Output power in forward direction of an Er-doped Ti:LiNbO₃ waveguide laser in cw-operation versus coupled pump power

Figure 7 presents the power characteristics of a 10.5 mm long waveguide laser with a 7 μm wide Ti-diffused channel in the Er-doped

$LiNbO_3$ surface (Z-cut); the emission linewidth is 0.3 nm.

The laser has a dichroitic, dielectric rear mirror (vacuum-deposited on the polished end face) to give a high transmittance at λ_p=1.48 μm and a high reflectance at the laser wavelength λ_s = 1.53 μm simultaneously. The front mirror is a 35 nm thick Au-layer of about 0.5 % transmittance only.

5. Conclusions

The recent work on rare earth doped $LiNbO_3$ waveguide amplifiers and lasers was summarized. To analyse and to understand these devices in more detail, an appropriate theory of optical amplification in waveguides was developed; it gave results of fairly good agreement with the experimental data and will help to optimize amplifiers and lasers. It is likely, that in the near future not only improved (broadband) optical amplifiers and (tunable) lasers – eventually with mode-locking and Q-switching capability – will be developed, but also more complex integrated optical circuits with lasers and/or amplifiers on the same $LiNbO_3$ substrat.

References

1. Hassaun Jones-Bay, Blue microlaser technology focused on gas-laser applications, Laser focus world, vol. 36, no.1, 133-138, 2000
2. Gregg Sucha, Heinrich Endert, Femtosecond fiber lasers hit powed highs, Laser focus world, vol. 36, no.8, (133-136), 2000

SPECTROSCOPIC ANALYSIS FOR SOME PORPHYRINIC AGGREGATES

RODICA MARIANA ION[1,2], SIMONA APOSTOL[1]

[1]Valahia University, Targoviste, Targoviste
[2]Institute for Chemical Research - ICECHIM, Bucharest, Romania

Abstract: *The aggregation process of some porphyrins such as tetrakis(4-sulphonatophenyl) porphyrin (TSPP) and chlorophyll (ChL) are investigated by different spectral techniques: absorption, fluorescence, steady state and transient absorption spectroscopy, transmission and scanning microscopy. The excited states lifetimes and the aggregation process for two essential porphyrins, are discussed in this paper. The analysis of transient absorption kinetics revealed a decrease of the excited singlet state lifetime of TSPP from 5.0 ns (free porphyrin) to 1.6 ns (aggregated porphyrin). Excitation with 490 nm offer informations about the aggregates to the S2-exciton state. The decay of transient absorption anisotropy clearly shown that there is at least a fraction of porphyrin molecules which loss their mobility upon aggregation. Assuming that the intersystem crossing rate is not modified, the shortening of the singlet state lifetime will cause an important decrease of ϕ_T. For ChL excitation with 430 nm offer informations about the second singlet which decay to the first excited state in 10^{-12} s. In a solution of monomeric ChL there is little radiationless dissipation to the ground states but in aggregated ChL it dominates.*

1. Introduction

Aggregates of chromophores represent an interesting system for several reasons. Aggregation is a common phenomenon for molecules with a flat and extended π-electron system such as porphyrins, cyanines, xanthenes, etc [1-5]. Porphyrins can form a variety of structures from linear head-to-tail or J-aggregates to fractal aggregates grown under different regimes of aggregation, and can exhibit rich photophysical properties. Chlorophyll aggregates, as a natural porphyrin play an important role in nature by collecting light energy in the first steps of photosynthesis, which occur on the ultrafast time scale [6]. Photophysical properties of TSPP porphyrin, as a synthetic one have been studied extensively in vivo and in vitro with an application for photodynamic therapy of cancer [7-9].

The size and shape of TSPP aggregates in solution have been investigated extensively using spectroscopic and light scattering methods [5,7]. Aggregates can break into their constituent parts which can be monomers or smaller aggregates and this can probably be shown by the change of the relative peak positions. Also, interaction between intraaggregate substructures (monomers or smaller aggregates) can be probed by scanning electron microscopy (SEM). Images of solidification patterns can allow this information but they also can be complicated by a variety of additional processes occurring due to a complex nature of the solutions.

Fractal theory was developed in the last two decades in order to achieve a better characterization of different phenomena in physics, chemistry, biology, medicine and so on [10].

A direct method to determine fractal dimension is to analyze images obtained from scanning tunneling microscopy, scanning probe microscopy, transmission electron microscopy (TEM). TEM micrographs can provide high-resolution pictures of 3-dimensional objects.

The aim of this paper is to analyze TEM images in order to obtain fractal dimensions of 3-dimensional objects and to apply the method to some porphyrins. Also, it is reported some transient absorption studies of some porphyrins, the transient absorption and transient absorption anisotropy decays. Meanwhile, the interaction between intraaggregate substructures (monomers ans aggregates) can be probed by scanning electron microscopy (SEM) and transmission microscopy (TEM).

2. Materials and methods

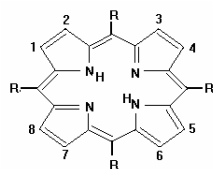H$_2$TSPP (Figure 1) has been prepared according to the literature [4]:

Fig.1 The structure of the
porphyrin molecule

R = SO$_3^-$

Figure 1. Structural formula of H$_2$TSPP .

Aggregates were prepared according to the procedure reported in [4] by adding an HCl and/or NaCl solution to a solution of meso-tetrakis(4-sulfonatophenyl)porphine tetrasodium salt (TSPP) (Aldrich), and used within a couple of days.

ChL was solved in 75 mM potassium phosphate buffer (pH 6.8) so that the final concentration of ChL was 4 μM. Aggregates form within 2 h of incubation in the dark at 4C.
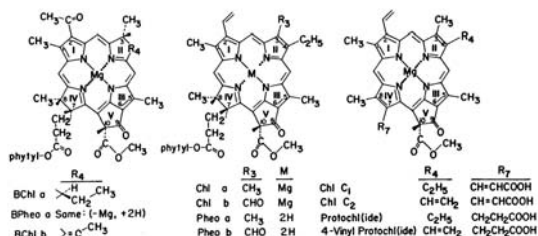
Figure 2. Structure of naturally occurring chlorophyll pigments.

Femtosecond transient absorption spectrometry measurements were performed using a setup described elsewhere [11]. Aggregates in solution were excited using ~130 fs pulses at a wavelength of 490 nm corresponding to the sharp S2-exciton peak on the ground state absorption spectrum. The temporal behavior of the recovery of the ground state of the aggregates was monitored at 706 nm.

SEM images were collected with a Hitachi S-2700 scanning electron microscope operating at 10 kV. Values of the fractal dimension, D$_f$, have been calculated using a box-counting technique where the minimum length of the box edge was equal to the size of the pixel, and the maximum length was taken as the 1/5 of the width of a fractal object.

Steady state absorption spectra have been measured with a Perkin-Elmer spectrophotometer Lambda 2S.

Transient absorption measurements in the nanosecond time range have been performed using an experimental set-up, elsewhere published [12].

Measurements of the mean fluorescence lifetime and fluorescence yield were also performed using a newly designed phase fluorimeter based on a laser-diode emitting at 635 nm (Philips CQL 840/D, Eindhoven, The Netherlands).

2. Results and discussion

a) Absorption measurements

(TSPP) is an anionic porphyrin, a very large disk-shape molecule which possess four negative charges the sulfonate groups from the four corners. In aqueous solutions, at neutral pH, the electronic absorption spectrum of TSPP is typical of free base porphyrins (D$_{2h}$ symmetry) and is characterized by an intense Soret band at arround 420 nm and four Q bands in the 500-700 nm range (the aetio-type spectrum).

Aggregation of TSPP can be activated by decreasing pH or increasing ionic strength of the solution, and it can be monitored using different positions of absorption peaks corresponding to different species, Fig.3.
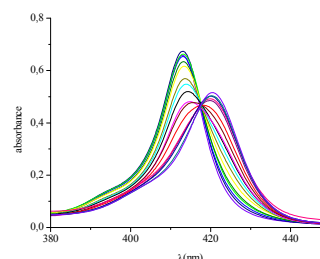
Figure 3. Evolution of absorption spectrum of a solution of 2.5x10^{-3} M H$_2$TSPP in upon addition of water

The J-aggregate is formed initially as a transparent colloidal solution which is then precipitated from the aqueous solution with time by exposure to light (after ionizing tratment of TSPP the light had a strong aggregation effect).

In acidic medium, new absorption bands (from 490, 707 nm) become dominant when the concentration of TSPP exceeds 10^{-5} M and they are attributed to the aggregated forms of TSPP, Table 1.

Table 1. The specific absorption bands of different TSPP forms

Porphyrinic forms	B band $\lambda/\varepsilon \times 10^3 (nm/M^{-1}.cm^{-1})$		Q bands $\lambda/\varepsilon \times 10^3 (nm/M^{-1}.cm^{-1})$
H_2TSPP^{-4}	412/355		515/130 551/4.5 579/1.9 33/1.01
$H_4{}^{+2}TSPP$	433/357		550/140 594/3 644/14
$H_4{}^{2+}TSPP^4$ J-aggregate	422	490	707
$H_4{}^{2+}TSPP^4$ H aggregate	401		517 552 593 650

Preliminary measurements of the size of H2TSPP indicate that $N \sim 10^4-10^5$ [15] and aggregate is roughly a hollow cylinder [16] with a radius corresponding to the radius TPP molecule (0.2 nm) and the length of the aggregate is 16 μM.

Fractal analysis of the images of the typical patterns found on a coverslip which were modified to the binary format was carried out using a box-counting method, and the following values of the fractal dimension were obtained: (i) Df = 1.44; (ii) Df = 1.50; (iii) Df = 1.71. These values characterize the geometry of the observed structures and reflect the complex phenomena which occurred during a crystallization process. From the analysis of the images it is noted that the situation is different from the case with the low porphyrin concentration.

b) Transient absorption measurements

Pumping in the Soret band populates the S_2 state of porphyrin. This state relaxes back on femtosecond time scale to the first excited singlet state S_1. This attribution is in good agreement with the value of 5.2 ns previously reported for the S_1 state lifetime of H2TSPP. The intermediate detected at the end of the decay of the S_1 state should be the triplet state T_1 because it is known that porphyrins have a high quantum yields for triplet state formation (ϕ_T).

The excitation wavelength of 490 nm was used to excite the aggregates to the S2-exciton state. This is seen as a sharp red-shifted relative to the monomer peak in the ground state absorption spectrum. The probe wavelength was chosen to be 706 nm corresponding to the dip in the transient difference absorption spectrum caused by the bleaching of the peak assigned to the S1-exciton state. Kinetics of the similar spectroscopic feature revealed relaxation dynamics of the hot S1-exciton state to the ground state for the case of linear TSPP J-aggregates. The first lifetime measured in the present study was on the order of 300 fs for all the cases, and was in agreement with the S2->S1 internal conversion kinetics.

c) TEM and SEM measurements

The second lifetime (0.9 - 8 ps) is ascribed to the process of intra aggregate vibrational energy redistribution for the cases (i) and (iii) because its typical value is ~ 1 ps but it is too long for the case (ii), $\tau_2 = 8$ ps, which corresponds to the largest value of fractal dimension. It is noticeable that the lifetimes for the cases of (i) and (iii) are closer to each other as well as the D_f values for these cases, and the increase in the lifetimes corresponds to the increase in D_f. This is reasonable since the increase in branching will lead to the increase in density of the vibrational states.

The third, large lifetime ($\tau_3 = 10-39$ ps) would be obvious to assign to the process of vibrational cooling, i.e. transfer of energy to surrounding solvent molecules. Again, lifetime values are in the reasonable range for the aggregates in the experimental condition (ii). This unusual behavior might be associated with the specificity of localized vibrational states of the self-similar fractals called fractons.

d) Chlorophyll Structure

Chlorophyll represent the principal class of pigments responsible for light absorption in photosynthesis ands are found in all photosynthetic organisms. It is, a tetrapyrrole having a relatively flat porphyrin head in the center of which a magnesium atom is coordinately bound. Mg divalent cation changes the electron distribution and produce powerful excited states. Attached to the head is a long chain phytol which acts like a "tail" about 2 nm in length containing 20 carbon atoms. This tail provides a non-polar region that helps bind the Chl molecules to Chl-

protein complexes, but it makes no appreciable contribution to the optical properties of Chl in the visible region. The association of Chl with proteins *in vivo* tunes the absorbtion of light over a wide range of wavelengths.

ChL self-assemble into a J-type aggregate [17] with a helical structure, the important factor responsible for this being ring-ring interactions. For the Chl a the red absorption is between 660 and 675 depending on solvent. Aggregation of Chl also causes a shift; crystalline chl a has its long wave absorption minimum at 740 nm. The maxima in the light absorption correspond to the different energy levels in the molecule The highest energy level is the second singlet, excited at 430 nm. The excited electrons make the transition in 10^{-12} s from the second to the first excited singlet state to which the electrons are excited by red light. The lifetime of the first singlet state is about $5x10^{-9}$ s before it decays to the singlet ground state. In a solution of monomeric Chl there is little radiationless dissipation to the ground states but in aggregated chlorophyll it dominates. The participation of the lowest vibrational sublevels of both the ground state and the lower excited states of Chl a can be appreciated by considering the minor band adjacent to the major red band. The shorter wavelength absorption band at 615 nm in ether – 14 kJ mol^{-1} higher in energy than the 662 nm bandncorrespond to a transition to the first excited vibrational sublevel of first excited singlet state S1.
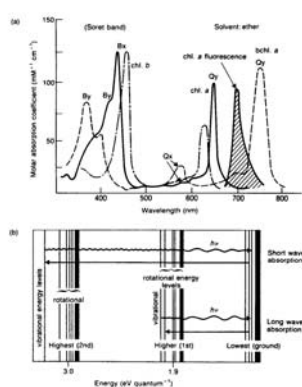
Figure 4.
Absorption spectra of chlorophylls a and b and bacteiochlorophyll a in ether showing principal electronic transitions in blue(Soret) and Red wavelengths

e) Chlorophyll fluorescence

Although Chl absorbs strongly in both the red and the blue, the fluorescence emission is essentially all in the red spectral region (see Figure 4). This is because the upper singlet state S2 of Chl excited by blue light is extremely unstable and goes very rapidly to lower singlet S1 by radiationless dissipation before any appreciable blue fluorescence can take place.

Electrons in the higher vibrational levels of the first excited singlet (called S1) decay also rapidly by radiationless transition to the lower levels and, if not used in photochemistry or transferred to other molecules, decay to the singlet ground state So, by emission of fluorescence of lower energy than the exciting light. Thus, a solution of Chl irradiated with blue light emits red fluorescence. The small band peaking at wavelength greater than 700 nm indicate electronic transition to excited vibrational sublevels of ground state.

In vivo Chl fluorescence shows the accumulation of excitation energy in the antenna and it is inversely related to the use of electrons; it indicates the state of electron transport and biochemical process relative to the energy capture. Chl a fluorescence is largely quenched by aggregation: in concentrated solutions and even in dilute solutions when by some means the molecules are associated into dimmers or higher aggregates (e.g. in the presence of dry nonpolar solvents Chl form nonfluorescent aggregates that dissociate by the addition of basic substances which ligate Mg, restoring Chl fluorescence; similar nonfluorescent aggregated forms of Chls are also produced when polar organic solutions are diluted by water).

There are always at least three options for the decay of the excited singlet state: fluorescence, in which the molecule returns to the ground state by emission of a quantum of light, internal conversion, in which the energy of the molecule is converted into vibrational energy of the ground state and intersystem crossing to the triplet excited states. For dilute Chla and b in solvent as ether or toluene, fluorescence and intersystem crossing account for at least 90 % of the singlet decay, for BChl a internal conversion account for at least half of the singlet state decay [13]. The study of Chl fluorescence quenching may bring useful

informations about molecules interactions. Others data such as the fluorescence lifetime in aerated and deoxygenated solutions τ_f, τ_f^0, could provide new and useful informations.

Table 2.
Fluorescence Lifetime (τ_f) and Quantum Yield (ϕ_f) for Chl solutions at room temperature, measured using SPF (single photon counting) and phase fluorimetry methods

Pigment	Solvent type	Concentration (M)	Degassed	τ_f (ns)	ϕ_f
Chl a	H	10^{-7}	Yes	6.44	0.35
		10^{-6}	No	6.54	
	P	10^{-7}	Yes	6.07	
		10^{-6}	No	5.1	0.3
Chl b	P	2×10^{-5}	No	3.6	0.11
	A		No	5.9	0.06
Chl	P	10^{-7}	Yes	6.1	
C1	P	10^{-7}	Yes	6.5	

4. Concluding remarks

Presently reported transient absorption measurements demonstrate that aggregation of TSPP significantly modifies the porphyrin photophysics. The transient absorption anisotropy measurements indicate that at least a fraction of aggregated porphyrins are considerably less mobile than the free porphyrins. This fraction losses probably some of its photosensitizing efficiency being less accessible by oxygen molecules.

The lifetime values are in the reasonable range for the aggregates in the experimental condition. This unusual behavior might be associated with the specificity of localized vibrational states of the self-similar fractals called fractons. Dynamic behavior of fractons is described by spectral dimension, ds, which is related to Df, and thus should also correlate with photophysical observations. It is of interest to determine the values of Df for all cases and will be the area of our future research.

Preliminary measurements of the size of H2TSPP indicate that the aggregate is roughly a hollow cyclinder with a radius corresponding to the radius TPP molecule (0.2 nm) and the length of the aggregate is 16 μM.

ChL self-assemble into a J-type aggregate with a helical structure, the important factor responsible for this being ring-ring interactions.

5. References

1. R.M.Ion, *J.Biomed.Optics, 4(1999), 319.*
2. K.Berg, J.C.Bommer, J.W.Winkelman, J.Moan, *Photochem.Photobiol., 52 (1990), 775.*
3. D.A.Dunn, V.H.Lin, I.E.Kochevar, Photochem.Photobiol.,53(1991), 47-56.
4. R.M.Ion, A.Planner, K.Wicktowicz, D.Frakowiak (1998) *Acta Biochimica Polonica, 45,3,833-845;*
5. R.M.Ion, M.Grigorescu, F.Scarlat, V.I.R.Niculescu, K.Gunaydin (2000) *J.Balkan Union Oncology 5(2),201-217*
6. Apostol, S. (2000). Utilisation de la fluorescence chlorophyllienne au suivi à distance de la végétation au niveau foliaire. *Thèse de doctorat.* Université Paris Sud, Orsay, France. No. 6233 pp. 1-97
7. M.L.Pascu, L.Danaila, R.M.Ion, A.Popescu, M.Pascu (2000) *Proc.SPIE, vol.4166,140;*
8. M.L.Pascu, L.Danaila, R.M.Ion, A.Popescu, M.Pascu (2000) *Proc.SPIE, Proc.SPIE, vol.4068,712;*
9. R.M.Ion (2000), *Current Topics on Biophysics, 24(1)30-42;*
10. R.M.Ion, Porfirinele si terapia fotodinamica a cancerului, *FMR Ed., Bucuresti, 2003 ISBN 973-8151-13-9;*
11. Near-infrared dyes for high technology applications, *Ed.S.Daehne, U.Resch-Genger, O.Wolfbeis, NATO ASI series, vol 3/52, 1998, pp. 87-114, Kluwer Academic Publishers, Dordrecht/Boston/ London, ISBN 0-7923-5101-0;*
12. D.Frackowiak, A.Planner, A.Waszkowiak, A.Boguta, H. Manikowski, RM.Ion, K. Wiktorowicz *J.Photochem.Photobiol., A:Chem., 141,101*(2001);
13. Apostol, S., Briantais, J.-M., Moise, N., Cerovic, Z.G., and Moya, I. (2001). *Photosynth. Res.* 67:215-227
14. Moise N. (2002), *These de Doctorat, Universite Paris Sud, Orsay France*
15. O.Ohno, Y.Kaizu, H.Kobayashi, *J.Chem.Phys., 99, 4128(1993);*

16. R.F.Pasternack, P.J.Collings, Resonance light scattering: a new technique for the studying chromophore aggregation, *Science, 269,935(1995);*

17. A.Scherz, V.Rosenbach-Belkin, JRE Fisher, *in Chlorophylls, H.Scheer Ed., CRC Press Boca Raton, 237(1991).*

Pb, Ar, Hg AND Cd INFLUENTION OF CATTLE METABOLISM

LAUR C. MANEA, IULIANA MANEA PREDA, GABRIEL D. DIMA, LAVINIA MOISE

"Valahia" University of Targoviste, Romania

Abstract: *In the west of Târgovişte exist the intense metallurgic activity, this reason make in the area the evident rush of motor traffic can provide small noxa emanation. At some distance (3 km) is a farm of dairy cows, grazing area is border with metallurgic factory. Because of this proximity we can suspicion some nociv influention of heavy metals (Pb, Ar, Hg, Cd), investigation searching to may in evidence theirs presence in blood, milk, muscles or organs (liver, kidney).Heavy metals actions about haemoglobin, building inactiv form methaemoglobin laed, combine with sulphur hydric groups (Cd, As, Hg) wich obstruct activitis of some enzimes, substitute enzimatics fodder calcium (Cd), inhib oxidativ phosphorilation, and decrease ADN sintese.*

1. Introduction

In about three kilometers there is a breeding milk cows farm, which can influence the accumulation in these animal products (milk, meat) of the elements like Pb, Cd, , Co, Cu, Hg – that are polluting in this way even the man is contaminated taking in consideration that the pondery of these animal products in man′s diet.

An additional source of residues in meat is environmental pollution with toxic materials either from natural sources or from industrial pollution of the environment. The seriousness of the problems and consequences of instigating control on these residues have not been fully evaluated.

The animals contamination it could be done in many ways: through the comsuption of the cropped plants from the fields with a higher containing of heavy metals or through the in halting of some powders with the mentioned containing or through the water containing heavy metals.

From many times the chemical manifestations are uninteresting in time, these elements accumulation in the animals organism can produce the transformation of these animals in polluted recesses for man.

2. Experimental

The samples concerning dairy cattles territory coterminous industrial extent. The samples aim at blood, milk, organs prelevation (liver, kidney) and muscles (psoas, gluteus) from cattles wich was slaughter.

These has extravasate from the animals in different ages and varied physiologic states (lactation, gestation).

The blood samples has drawing in the test tube, with steril needles at reduce calibre from jugular vein, after wards these was take at room temperature (25-27°C), `in the timps at 24-36 hours for to praise the serum. For the serum separation at coagulated plasma used one Pasteur dropper, adherent coagulum is detach with these of walls tube test. These operation must making with special atention for avoid haemolysis at someone of coagulum section.After separation the serum was processing imediatly or in maximum 24 hours with aim to stoped some biochemical alterations of serum, in case wich was prolonged examination moment. In this research we took *beef samples* after 1 hour the slaughtering.

Also, we took *milk sample* of dairy farm.

The atomic absorbtion spectrometry was used for determination of heavy metales. The atomic absorbtion spectrometry uses absorbtion of light of intrinsic wavelengths by atoms.

All atoms are classified into those having low energies and those having high energies. The state having low energies is called the ground state and state having high energies is called the excited state.

The atom in the ground state absorbs external energies and is put in the excited state.

The difference between energies in the ground state, and in the excited state is fixed by element and wavelenght of light to be absorbed. The atomic absorbtion spectrometry uses the hollow cathode lamp (HCL).

The HCL gives off light characteristic to the elemental wavelenght being measured. Thus, the light absorbed measures the atomic density. When light of a certain intensity is given to many atoms in the ground state, part of light is absorbed by atoms.

When light of a certain intensity is given to many atoms in the ground state, part of this light is absorbed by atoms. The absorption rate is determined by the atomic density.

The principle mentioned above can be applied to light absorbtion of " Free atoms". A " Free atoms" means an atom not combined with other atoms. However, elements in the sample to be analyzed are not in the free state, and are combined with other elements invariably to make a so-called molecule. Absorbtion cannot be done on samples in the molecule state, because molecules do not absorb light.

The combination must be cut off by some means to free the atoms. This called atomiyation. The most popular method of atomiyation is dissociation by heat –sample are heated to a high temperature so that molecules are converted into free atoms. The flame is produced by a burner for atomization and this is the most popular method.

A typical diagram of the burner is shown in figure 1.
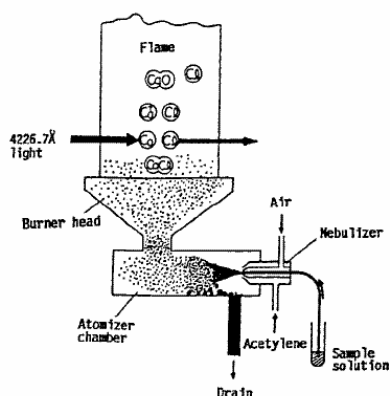
Figure 1. The diagram of the burner

This figure explains measurement of calcium contained in the sample liquid as calcium chloride. The sample is atomized by a nebulizer at first. Then, big water drops are discharged to the drain, and only a fine mist is mixed with fuel, and oxidant in the atomizer chamber and sent to the flame.

When they get in the flame, the mist evaporates instantaneously and fine particles of calcium chloride molecules are produced. When these particles further advance in the flame, calcium chloride is dissolved by heat and free calcium atoms and chloride atoms are produced.

If a beam of light at wavelength 422.7nm(Ca) is introduced through this part of the flame, atomic absorption can be measured. In the upper part of the flame, some of calcium atoms are combined with oxygen to become calcium oxide and some are further ionized. Therefore, atomic absorption does not show sufficient sensitivity even if light is given to such a position.

Many combinations of various gases have been tested as the flame for atomization.

In consideration of analysis sensitivity, safety, easy use, cost and other points; there are four standard flames used: air-acetylene, nitrous oxide-acetylene, air-hydrogen and argon-hydrogen. These flames are used for each element depending on the temperature and gas characteristics.

The equipment must be set at the optimum analysis conditions to obtain the best measurement results.

Optimum conditions generally vary with the element and with the composition of the sample, even if the same elements are contained. Therefore, it is necessary to fully study the measuring conditions in actual analysis.

We have measured the content in Cd, Co, Hg and Pb in accordance with the following preparation methods:

▪ Cd (Cadmium) 1.0mg Cd/m*l* Standard material : Metal cadmium 99.9% up Preparation method of solution : 1,000g of metal cadmium is heated and dissolved with nitric acid (1+1) 30 m*l* and is diluted with water to 1000m*l* accurately after it has cooled.

▪ Co (Cobalt) 1.0mg Co/m*l* Standard material : Metal cobalt 99.9% up Preparation

method of solution : 1.000g of metal cobalt is heated and dissolved with nitric acid (1+1) 30 m and is diluted with water to 1000m*l* accurately after it has cooled.

▪ Pb (Lead) 1.0mg Pb/m*l* Standard material : Metal lead 99.9% up Preparation method of solution : 1.000g of metal lead is heated and dissolved with nitric acid (1+1) 30m*l* and is diluted with water to 1000m*l* accurately.

▪ Hg (Mercury) 1.0mg Hg/m*l* Standard material : Mercury chloride (HgCl2) Preparation method of solution: 1.354g of mercury chloride is dissolved in water and is diluted to 1000m*l* accurately with water.

In the case of milk samples it is necessary to perform a sample pretreatment. This include a nitric acid or perchloric acid decomposition followed by ashing by drying. We have place 5~10 g of sample in a quartz beaker, add 1~3 ml of sulfuric acid, and gently heat on a hot plate at 120°C.

After the components, which are volitilized at low temperatures are driven off, we have continue to heat the sample until carbonization occurs. (At this time, if intense bubbling in the sample occurs, add 0.5 ml of nitric acid.) We place this in an electric furnace, increase heat at a rate of 100°C per hour, and at about 500°C perform ashing over a period of several hours. If ashing is incomplete, we wet with 2~5 ml of 50% magnesium nitrate solution or nitric acid (1+1).

After drying, we have continuing the ashing process. After that, we add 2~4 ml of water to the ash, and after drying, 5 ml of hydrochloric acid to dissolve the salts. We use water to prepare fixed volumes of the measurement solution.

3. Results and discussions

After the affectuation of these determinations it was found that lead has a sensible increasing during the processing stages.

Table 1. Normal content of heavy metales in variable samples, mg/kg

Samples	Pb	Cd	Cu	Hg
Muscles	0,2	0,02	O,1	-
Serum	0,05	0,01	0,05	-
Milk	0,02	0,01	0,02	-

Mercury was absent in all the samples. Cadmium remaind constantly. Cu registered a more important increasing at semiproducts and finished products.

In table no.2, we can observe evolution of these elements in milk and during the processing and the obtaining of finished products.

Increase of heavy metals (lead, cadmium, mercury) in the various tissue can be determinate toxic haemolytic anemy, because the methaemoglobin is oxidabil form hemoglobin, enable to connect reversible the oxygen.

Table 2. Content of heavy metales in samples, mg/kg

Samples	Pb	Cd	Cu	Hg
Muscles	0,05	0,02	1,56	-
Serum	0,07	0,02	2,04	-
Milk	0,05	0,02	2,46	-

The lead amount decrease the hem biosynthesis and erythropoietin , hypochromian anemia show longevity shorter of red sell this process can be injurious of human health if the animals produces will been consummated. The lead contamination is most frequent to young cattle because these present three sensitive factors:

▪ Behavior, calves and young cattle lick one each other;

▪ Physiological, digestive activities is biggest at young cattle;

▪ Metabolism, lead fixation in young tissue is biggest, and born reshuffle mobilize lead.

The handful cadmium action is possible to achieve through inhibition at enzymes with the tiol groups, substitute enzymatic- zinc and can to destroy the testicular tissue structure, and exercise negative influence for the reproductive function, also inhibit oxydative phosphates to mitochondrial level and decrease AND – synthesis.

More over inhibit pancreatic insulin and diminish calcium absorption from fodder.

4. Conclusions

The results was confirmed increase of few heavy metals in fact more alarming but taking in consideration your reminisce and

cumulative affect in animal organism we can opined that increase after normal level may involved about human food.

Cadmium is one of the most toxic heavy metals this influence can be exacerbate of poor fodders in the calcium. Between causes of cadmium contamination can be involved fertilization pasture with mud proceed from combing out station, oils for motors overflow and foods decreases in Ca, Zn, Fe, proteins and vitamin D.

Mercury is present in cinnabar rocks in mixable quantities; in addition, it is a minor component in all the earths surface. It is used in industry to produce chlorine and in agriculture as a fungicide, among many other uses which assure its spread throughout the environment.

Lead have not yet reached the status of major toxicity problems, except that lead poisoning is considered a present and increasing problem in children raised in cities.

Acute toxicity is very low, but all are cumulative poisons with definite threshold-effect level. Thus whys the clinical signs appear, the reversal of symptoms is difficult because of long-term tissue damage and the reservoir of toxic material already in the animal organism.

Is important to be continued this investigations about in special of cattle.

5.References

1. Stănescu, V., 1998, *Igiena şi controlul alimentelor*, Editura Fundaţiei "România de mâine", Bucureşti.
2. Enache, T., and other, 1997, *Medicina legală veterinară, Ediţia a 2-a*, Editura ALL, Bucureşti.
3. Kanehara Publishing Co., *Health Testing Methods Commentary*, Japan Pharmaceutical Publication.
4. Korin C., *Foodstuffs Analysis Methods*, Japan Foodstuffs Manufacturing Society, Foodstuffs Analysis Methods Editorial Commission Publication.
5. Şuţeanu E., Danielescu N., Popescu O., Trif A., *Toxicologie şi toxicoze*, Editura Didactică şi Pedagogică, Bucureşti, 1995, 121-12

METAL SURFACE TREATMENT WITH LASER RADIATION

CĂLIN OROS, SERGIU DINU, GABRIEL DIMA, MARINELA VOICU

Physics Department, "Valahia" University of Targoviste, Romania
oros@valahia.ro

Abstract: The experimental dependence of surface hardness on Nd:YAG laser parameters (laser intensity, laser pulse duration, number of laser shots and laser spot diameter) for aluminum, titanium, nickel, cooper and two kind of steel (21CrMoV57 and 40C130) targets is given. It is show that the target surface hardness increases with laser intensity, with number of laser shots and laser pulse duration. Also, the target surface hardness decreases when the laser spot diameter increases. From these experiments result that the laser hardness is rather a function on laser surface energy density than laser energy.
Subject terms: surface hardness, laser surface energy density

1. Introduction

For many applications it is necessary to generate wear resistant, hard surface layers.

In thermal processing with laser radiation energy deposition and heating in a material are a consequence of the balance between the deposited energy, governed by optical materials proprieties and characteristics of the laser radiation, and the heat diffusion, determined by termophysical materials proprieties and the interaction time. For temperatures below melting temperature the light-induced changes of proprieties occur within the solidus-range. In surface treatment with a laser, the metallic surface is heated locally extremely rapidly and after the laser is switch off it is cools very rapidly. The temperature rises very rapidly to almost melting temperature. Only a thin layer is heated, the other parts of the target remain cold. Due to the high temperature gradients, thermal conduction to the bulk material will cause sufficiently rapid cooling of the heated parts and the resultant structures are often metastable structures with particular proprieties. Heating and cooling rates are of the same order ~10^6 K/s. The advantages and disadvantages of surface treatment with laser beams are thus apparent: precise local treatment, non-equilibrium structures with specific proprieties, difficult procedure for covering large areas with each track influencing the structure of the previous one if the laser beam is moving on the target surface [1]. The laser is not a universal tool and should not be considered simply as a possible substitute for existing methods. It is very effective for treatment of thin surface layers. If thick layers are to be treated then other heat sources are more appropriate. Laser transformation hardening offers decided advantages in local or partial hardening of components or treatments of components which are too large for treatment other by flame hardening.

The hardness of the material is strongly related to its binding behaviour [2]. The metallic binding gives not the highest hardness values but allows a certain amount of plastic deformation. The highest hardness values are obtained for covalent bindings, like diamond. Heteropolar bindings are found for a number of ceramic materials which apart from their hardness show a good oxidation resistance. In reality, the binding behaviour is more complicated and mixed types of binding are possible.

The equation governing absorption of laser energy on the metallic target is given by:

$$I = (1-R)e^{-z\sum_i \alpha_i} \qquad (1)$$

where I is the laser intensity of the absorbed laser beam and I_0 is the intensity of the incident laser beam. The fraction of the incident light intensity reflected by the target is given by R. The factor α_i represents the coefficient for the light absorption by the ith process which summed over the different

absorption processes occurring at the irradiated surface, and z is the penetration depth of the radiation in the material. In the case of laser hardfacing the laser intensity must be below the critical value for melting of material. For same lower laser intensity we account a single term in equation (1) which represent the classical absorption of the electromagnetic radiation by a metallic material.

The critical laser intensity required for melting the surface of the target can be theoretically estimate by the following relationship:

$$I_m = \frac{k_T T_m}{2(1-R)\sqrt{\chi_T \tau_p}} \qquad (2)$$

where T_m and k_T are the melting temperature and the thermal conductivity of the material, respectively.

It is know that in the case of laser interaction with the metallic targets the depth of the damage or the interaction corresponds closely to the depth of thermal penetration l_{th} given by the following relationship:

$$l_{th} = \frac{1}{2}\sqrt{\pi \chi_T \tau_p} \qquad (3)$$

where χ_T is the thermal diffusivity of the metal and τ_p is the laser pulse duration.

2. Laser and targets
Laser

Experiments have been performed with the neodymium-YAG laser of our laboratory operating at 1.064-μm wavelength. The laser delivers Gaussian pulses of 2 ms, 2.5 ms and 3 ms full width at half-maximum (FWHM) with a repetition rate till 20 Hz. The laser output energy can be ranging between 0 and 15 J. The laser spot diameter can also be modify from 0.3 mm to 8 mm. In instance the maxim laser intensity is about 1.06×10^7 W/cm^2. For the hardness experiments we have used lower laser intensities. All experiments were performed in air at normal conditions.

Targets

For experiments we have used metallic targets of aluminum, titanium, nickel, cooper and two kind of steel: 21CrMoV57 and 40C130, with 1.5-mm thick and 10-mm diameter. Their surfaces were polished using a P 1000 grade polishing paper. In order to improve the laser absorption the surface of the targets was painted with a very thin black paint. The measurements of the target surface hardness were performed with a microhardness device.

3. Experimental results

First we have calculated the critical laser intensity for melting the target surface using equation 2. The results for our target materials are given in table 1. Then we have measured the experimental values for critical laser intensity obtained when we use our laser. In order to compare these values the results are given in same table.

Table 1. *Calculated and measured values of critical laser intensity.*

Targets	Al	21CrMoV57	40C130	Ti	Cu	Ni
$I_{cr} \times 10^{-3}$	4.2	17	15	9.5	11	6.5
(W/cm^2)	7.6	6.9	6.5	7.5	7.9	7.5

The calculated depth of thermal penetration, equation 3, is given in table 2 for three values of laser pulse duration.

Table 2. *Calculated values of thermal penetration depth for three laser pulse durations*

	Targets	Al	21CrMoV57	40C130	Ti	Cu	Ni
l_{th}	τ_p=1 ms	261.6	97.1	104.8	68.6	296.5	118.9
	τ_p=2 ms	369.9	137.3	148.2	97.0	380.4	168.2
(μm)	τ_p=3 ms	453.1	168.2	181.5	118.8	513.5	205.9

Figure 1. *Surface target hardness vs. laser intensity*
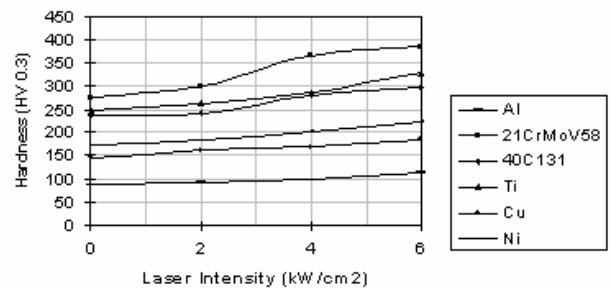
We have performed a first experiment in order to obtain the dependence of surface target material hardness on laser intensity. The results are given in figure 1. The laser irradiation parameters were: pulse duration 2.5 ms, the laser spot diameter 5 mm, and the number of laser shots 600.

In other experiment we have analyzed the dependence of surface target material

hardness on laser pulse duration. The results are given in figure 2. The laser energy for each target material was close below the critical value for melting given by table 1. The laser spot diameter was 5 mm and the number of laser shots was 600 as in previous experiment.
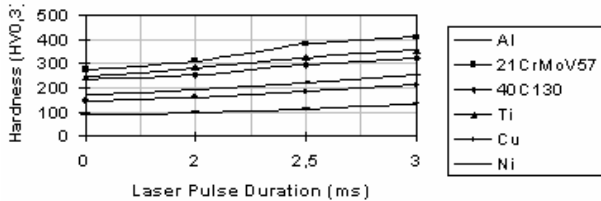

Figure 2. Surface target hardness vs. laser pulse duration
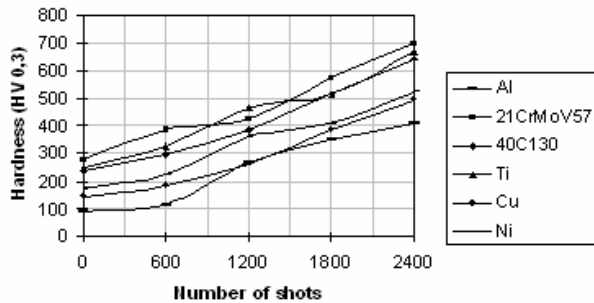
Figure. 3. Surface target hardness vs. number of laser shots

The dependence of surface target material hardness vs. number of laser shots is given in figure 3. The laser energy for each target material and the laser spot diameter were same as in previous experiment.
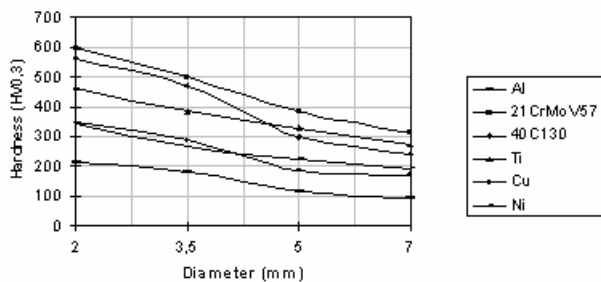
Figure 4. Surface target hardness vs. laser spot diameter

In our last experiment we have analyzed the dependence of surface target material hardness vs. laser spot diameter. The laser pulse duration was 2.5 ms, the laser energy for each target material was same as in previous experiment and the number of laser shots was 600. The results are given in figure 4.

4. Conclusions

We have measured the metallic target surface hardness before and after laser irradiation below melting temperature in order to study the hardness dependence on Nd:YAG laser parameters: laser intensity, laser pulse duration, number of laser shots and laser spot diameter. From our experiments result that the laser surface hardness increases with laser intensity, laser pulse duration, number of laser shots and decreases when laser spot diameter increases.

References
1. A. Gasser, E. W. Kreutz, K. Wissenbach, *"Physical Aspects of Surface Processing with Laser Radiation"*, SPIE, 1020, 70-83 (1989)
2. H.W. Bergmann, R. Kupfer, D. Muller, *"Laser hardfacing"*, SPIE, 1276, 375-390 (1990)

PIXE AND ICP ANALYSIS OF TREES LEAVES

CLAUDIA STIHI[1], GABRIELA BUSUIOC[2], ION V. POPESCU[1]

[1]Valahia University of Targoviste, Faculty of Sciences, Physics Dept., 2 Carol I street, 0200 Targoviste, Romania, e-mail:stihi@valahia.ro

[2] Valahia University of Targoviste, Faculty of Environmental Engineering and Biotechnologies, Carol I street, 0200 Targoviste, Romania

Abstract: *In this paper we present the applications of elemental analysis methods: Particle Induced X-ray Emission (PIXE) and Induced Coupled Plasma (ICP) in biological domain.. These research activities were performed in the frame of collaborations between Valahia University of Targoviste, Institute for Nuclear Physics and Engineering "Horia Hulubei" Bucharest and Special Steel Trust from Targoviste.*

1.Introduction

The microelemental analysis method Particle Induced X-ray Emission (PIXE) [1,4] is based on the fact that the bombardment of the sample with a charged particle beam causes the ionisation of the atomic inner shells followed by a subsequent of the characteristic X-rays. When the X-rays spectrum is detected by high-resolution detector, the well-known Z-dependence of the X-rays energies, as well as the intensities of the individual X-rays line, allow a straightforward determination of the target element.

For PIXE measurements the sample preparation technique does not require a special chemical preparation, which may cause some losses in concentration or some contamination. A quantitative determination of element content in a sample by PIXE method can be done with a great sensibility by relative measurements. The detection limit is 1 ppm.

The Inductively Coupled Plasma (ICP) [2] method is based on the fact that the atoms and ions produced in the plasma are excited and emit light. The intensity of light emitted at wavelengths characteristic of the particular elements of interest is measured and related to the concentration of each element from samples.

These two methods PIXE and has been applied to a wide range of sample types: metals and wide variety of industrial materials, environmental samples (water streams, airborne particles and coal fly ash), and biological and medical samples.

2.Material and method

PIXE measurements of target elements were made using a 3 MeV proton beam extracted from the TANDEM accelerator from IFIN-HH Magurele, Bucharest, and passes through a collimator (3×4 mm) before reaching the target. X-ray spectra were measured with a spectrometric chain having a CANBERRA Ge hyperpure detector (100 mm^2×7mm) with a 160 eV resolution at 6.4 KeV of K_a line of iron. The X-ray spectrum analysis can be made off-line using ORIGIN or LEONE fitting programs. A schematic diagram of PIXE experimental arrangement it is show in figure 1.

At the same time for trace element determinations, we use the **ICP** method. The reason for that choice is the impossibility of measuring the content of Mg with **PIXE** because of the absorption of the X-rays in the windows of the chamber and the detector.

On the other hand, we cannot use only the **ICP** because for that type of measurements the quantity of biological sample needed is proportional to the number of the analyzing elements.

At the same time for trace element determinations, we use the **ICP** method. The reason for that choice is the impossibility of measuring the content of Mg with **PIXE** because of the absorption of the X-rays in the windows of the chamber and the detector. On

the other hand, we cannot use only the **ICP** because for that type of measurements the quantity of biological sample needed is proportional to the number of the analyzing elements. We prefer to use both methods because **PIXE** requires only a "drop" of sample in order to determine all trace elements with atomic number between 13 and 80. We used ICP method to determine the concentration of Mg – element who can not be determined using PIXE method and concentration of Fe to compared experimental results obtained using the both methods [3].
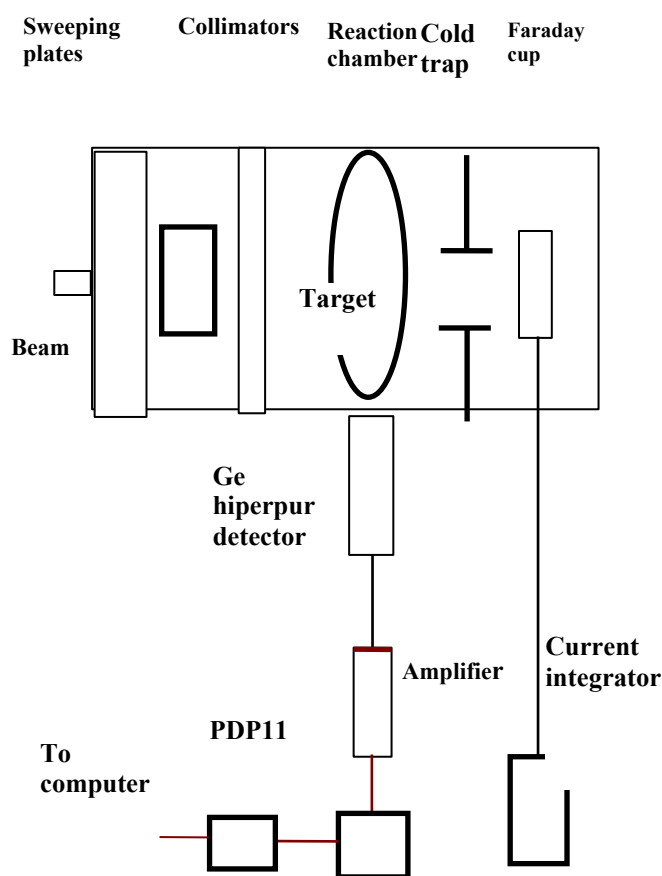
Figure 1: A schematic diagram of PIXE experimental arrangement

The ICP-OES (Inductively Coupled Plasma-Optical Emission Spectroscopy) spectrometer used by us are a Baird ICP2070 - Sequential Plasma Spectrometer (figure 2) which consists of a sample introduction system, a plasma torch, a plasma power supply and an optical measurement system .

The sample must be introduced into plasma in a form that can be effectively vaporized and atomized (small droplets of

solution, small particles of vapor). The plasma torch confines the plasma to a diameter of about 18 mm. Atoms and ions produced in the plasma are excited and emit light. The intensity of light emitted at wavelengths characteristic of the particular elements of interest is measured and related to the concentration of each element from samples. Baird ICP2070 - Sequential Plasma Spectrometer use as a plasma gas Argon and the plasma is sustained in a quartz torch and the plasma is generated using a radio frequency generator at 40.68 MHz. Temperatures of 5000-9000K have been measured in the plasma. The detection systems used are a sequential monochromator with a wavelength range (160-800) nm. The optical emission spectra are made using a personal computer.

Figure2: A schematic diagram of ICP spectrometer

3. Experimental results and discussions

Samples in the PIXE and ICP experiments was:

> ➢ leaves of different trees from different distances of pollution source - Special Steel Trust, Targoviste (table 1)

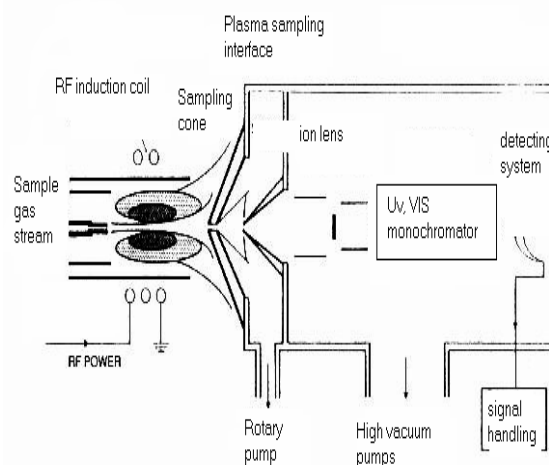**Table 1. PIXE and ICP samples**

Sample	Type of sample
P1	Leave of walnut –2 Km distance from pollution source
P2	Leave of walnut –5 Km distance from pollution source
P3	Leave of apple tree - 2 Km distance from pollution source
P4	Leave of apple tree - 5 Km distance from pollution source
P5	Leave of plum tree - 2 Km distance from pollution source
P6	Leave of plum tree - 5 Km distance from pollution source
P7	Leave of peach tree - 2 Km distance from pollution source
P8	Leave of peach tree - 2 Km distance from pollution source

Sample for ICP experiments was prepared in the following manner: leaves of trees, collected of approximately in some position, have been washed and simply air-dried at a temperature of 105^0 C in a clean box preventing further contamination. The dried leaves have been grained and after powdering, 0.25-g powder leaves have been digested in 5-ml acid nitric. After a set aside in fume cupboard overnight the obtained liquid was gently boiled (without major loss of volume). For a good digestion 10-ml acid perchloric have been added and 1 ml HCl. The cooled solution was diluted with water at 100-ml solution and nebulized into plasma.

Sample for PIXE experiments was prepared in the following manner: the washed leaves were simply air-dried at a temperature of 50^0 in a clean box preventing further contamination. The dried leaves were grained and after powdering a layer of the samples material were deposited on hostaphan foils.

Using the ICP method, we identified and determined in analyzed samples the concentration of Mg, Ca, and Sr with a precision less than 6%.

Using PIXE method we identified and determined analyzed samples the concentration of: Cd, Co, Cu, Zn, Mn, Cr, Fe,

Se, Pb with an instrumental error less than 1% for most of the elements analyzed.

Experimental results obtained by ICP and PIXE methods are presented in tables 2 and 3. The most significant change can be observed at Mg, Ca, Se, Zn, and Fe and Sr concentrations. For leaf trees from a grater distance to pollution source the Sr concentration decreased and the Mg, Ca, se, Zn and Fe concentrations increased. So, we can say that the increase of element mention above can be done by the decrease of Sr in plants.

4. Conclusions

The uses of PIXE and ICP techniques give the possibility to determine the elemental composition of plants with a great sensibility. We identified and determined the concentration of Mg, Ca, Cd, Co, Cu, Cr, Fe, Mn, Se, Zn, and toxic elements Sr, Pb that can put in evidence the presence of these elements in environmental medium. This study demonstrates the potential of PIXE and ICP methods in environmental biomonitoring, and also we can say that the leaves of trees can be used as an indicator for air pollution –the subject of our future works.

5. References

1. Johansson, S.A.E., Campbell, J.l., PIXE: *A Novel Technique for Elemental Analysis*, Campbell's First Book on PIXE, John Wiley&Sons, Inc. 1998,
2. Boumans, R.W.J.M., Inductively Coupled Plasma Emission Spectroscopy, John Wiley and Sons, New York, 1987
3. Stihi, Claudia; Popescu, I.V.; Busuioc, Gabriela; Badica, T.; Olariu, A.; Dima, G.,Particle Induced X-Ray Emission (PIXE) analysis of *Basella Alba L* leaves, Journal of Radioanalytical and Nuclear Chemistry, Vol 246, No 2(2000), p. 445-447.
4. Aspaizu, J; Policroniades, R; Vivero, R; Jimenez, M, Nuclear Instruments and Methods in Physics Research 1995, B 101, p.453-458

Table 2. The concentration (ppm) of elements in samples obtained using ICP method

SAMPLE	MG	CA	SR
P1	7.89	47	0,18
P2	11.6	72.7	NOT DETECTED
P3	8.04	NOT DETECTED	43.1
P4	8.9	NOT DETECTED	NOT DETECTED
P5	11.2	NOT DETECTED	41.1
P6	13.8	42.1	NOT DETECTED
P7	7.01	40.4	0.16
P8	5.72	47	0.2

Table 3: The concentration (ppm) of elements in samples obtained using PIXE method

SAMPLE	CD	CO	CU	CR	FE	MN	PB	SE	ZN
P1	NOT DETECTED	NOT DETECTED	0.29	0.10	8.11	NOT DETECTED	6.14	27.01	1.30
P2	0.7	5.61	3.96	13.22	41.90	12.45	NOT DETECTED	336.85	13.10
P3	NOT DETECTED	NOT DETECTED	NOT DETECTED	0.43	5.87	2.79	0.18	7.65	0.82
P4	NOT DETECTED	NOT DETECTED	1.92	2.68	48.89	12.09	NOT DETECTED	144.52	3.96
P5	NOT DETECTED	NOT DETECTED	NOT DETECTED	5.34	2.45	NOT DETECTED	NOT DETECTED	21.48	0.87
P6	0.07	NOT DETECTED	NOT DETECTED	3.06	3.06	0.69	NOT DETECTED	26.13	0.13
P7	0.06	3.19	1.03	5.77	52.28	15.82	NOT DETECTED	48.24	2.55
P8	0.25	NOT DETECTED	0.63	3.83	31.59	6.75	NOT DETECTED	84.55	3.36

B. CHEMISTRY SECTION

INVESTIGATION OF ROSEMARY EXTRACTS FOR THE PROTECTION OF POLYETHYLENE AGAINST THERMAL OXIDATION

MARIUS BUMBAC[1], LAURA MONICA GORGHIU[1], CRINELA DUMITRESCU[1], SILVIU JIPA[1], RADU SETNESCU[1], TRAIAN ZAHARESCU[2], ION MIHALCEA[3]

[1]Universitatea "VALAHIA" Târgoviste
[2]ICPE C.A. Bucuresti
[3]Universitatea Bucuresti

Abstract : This paper presents the effect of some rosemary extracts on the thermal stabilization of low density polyethylene (LDPE). IR and UV spectra's of these extracts indicates that the major substances are carnosic acid, carnosol and epirosmanol. Chemiluminescence (CL) resulting from the exothermic termination reaction of peroxi radicals was used for the characterization of effectiveness of these extracts for protection of LDPE.

1.Introduction

Rosemary (*Rosmarinus officinalis*) is of a great applicative interest because it exhibits considerable antioxidant properties in comparison to other plants. The main compounds that are responsible for the antioxidant activity of rosemary belong to the phenolic diterpenes [1-3]. Carnosic acid, carnosol, rosmanol and epirosmanol (fig.1) were shown to be the major substances which have been found in leaves of rosemary [4,5].
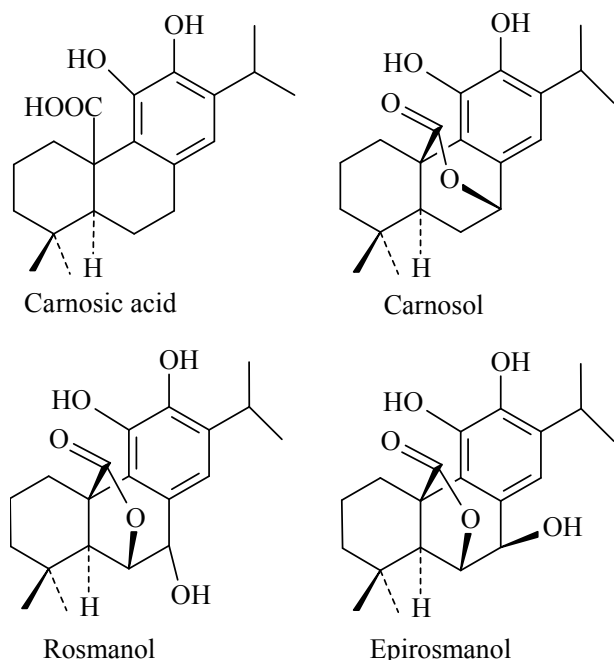

Fig.1 – Antioxidative compounds in rosemary leaves

Wenkert et al [4] reported a concentration of 0,35% carnosic acid in dried leaves. Richheimer et al [6] found a markedly higher concentration of carnosic acid ranging from 1,7% to 3,9%, and the carnosol content amounted to 0,2-0,4% in dried rosemary leaves.

In the presence of oxygen, carnosic acid is converted to carnosol and rosmanol [7].

The problem of stabilizing polyethylene against thermal-oxidative ageing is still of topical interest. Despite the abundance of new stabilizers in the patent literature, further investigation of natural antioxidant compounds have received increasing interest for their use instead of synthetic ones. Interest in employing antioxidants obtained from natural sources is due to the toxic effects of synthetic antioxidants and is connected with the plastic packing for the food industry.

Chemiluminescence (CL) resulting from the exothermic termination reaction of peroxi radicals has proved to be a sensitive technique for antioxidant ranking.

In the present study we have applied the chemiluminescence method for the characterization of the effectiveness of some rosemary extracts for the protection of low density polyethylene (LDPE) against thermal-oxidation.

2.Experimental

Plant material (seeds) was extracted with methanol, chloroform, acetone and diethyl ether, separately. All the solvents were of analytical grad purity. The extraction precipitates were separated from liquid phase by filtration.

The infra-red absorption spectra of rosemary extraction precipitates were recorded

over the range 400 to 4000 cm^{-1} on IR-75 Carl Zeiss Jena spectrophotometer.

Ultra-violet absorption measurements (200 to 300 nm) were made upon a Secomam S-750 spectrophotometer. In these measurements rosemary liquid extracts were examined.

Low density polyethylene (LDPE) provided by the Brazi Chemical Company as K322$^{®}$ type was used as polymeric support. LDPE was purified by precipitation with methanol from hot o-xylene solution. After the removal of remaining solvent, LDPE mass was dried at room temperature.

The rosemary extracts were added to LDPE by intimate grinding of polymer wet (CHCl$_3$) powder. The compounded (0,25 % w/w) samples were dried in a dessiccator at room temperature for 24 h.

Isothermal chemiluminescence measurements were performed in an Oxyluminograph OL-94, which has been previously described [8].

3.Results and discussion

Figure 2 shows a typical infra-red absorption curves obtained for the rosemary extraction precipitates. The absorption bands occurring in the region 1100-1190 cm^{-1} can be ascribed to etheric and carboxylic groups. The 3300-3600 cm^{-1} region show the content of bonded hydroxyl groups. Absorption at 1715 cm^{-1} characterizes the content of C=O groups and absorption at 1650 cm^{-1} belong to monomeric OH groups. The 2000-2300 cm^{-1} region can be attributed to diazo groups or nitrile group [9].

Figure 3 shows a typical ultra-violet absorption curves obtained for the rosemary liquid extracts. These show a maximum in the region 220-230 nm and a shoulder at 260-270 nm. The latter region must be due to the ketonic carbonyl (see [10]) also shown in the infra-red region. According to Bosch et al [11], the UV spectra (230 nm) of all phenolic diterpenes are similar to carnosic acid.

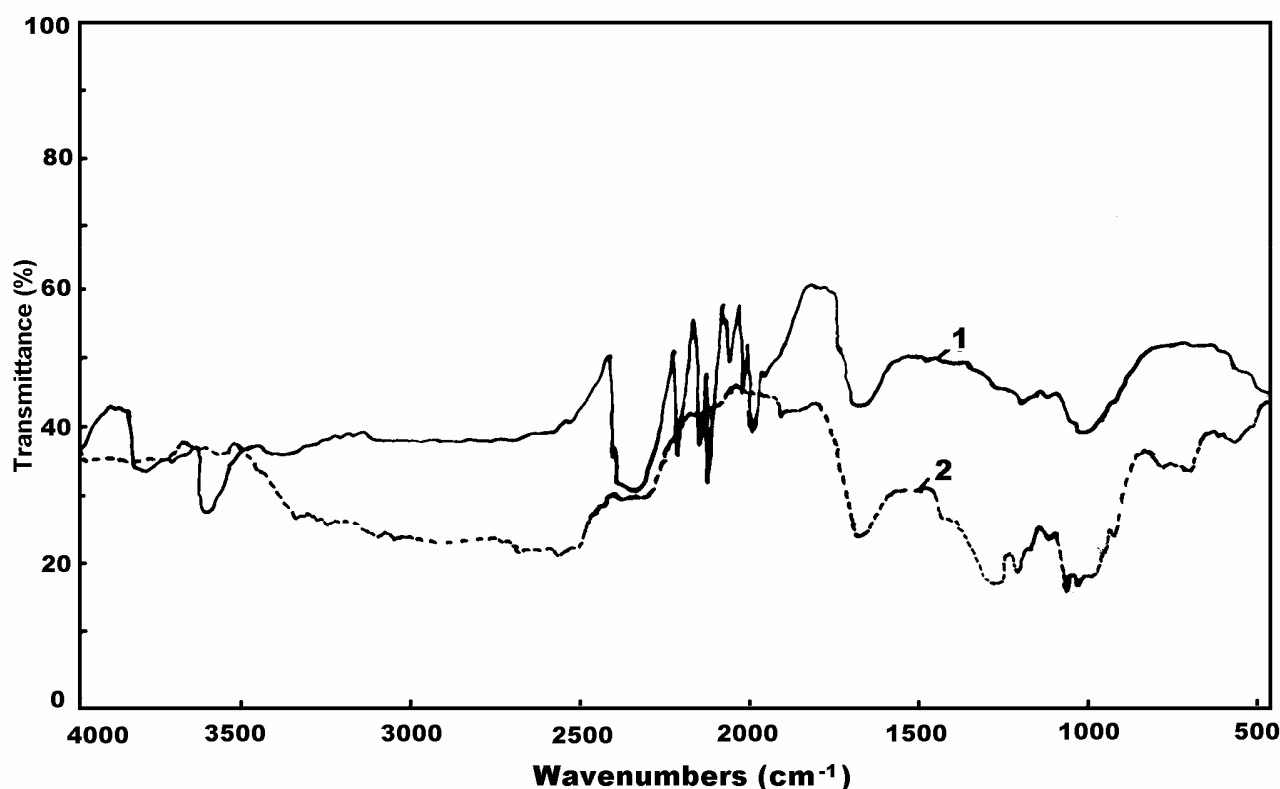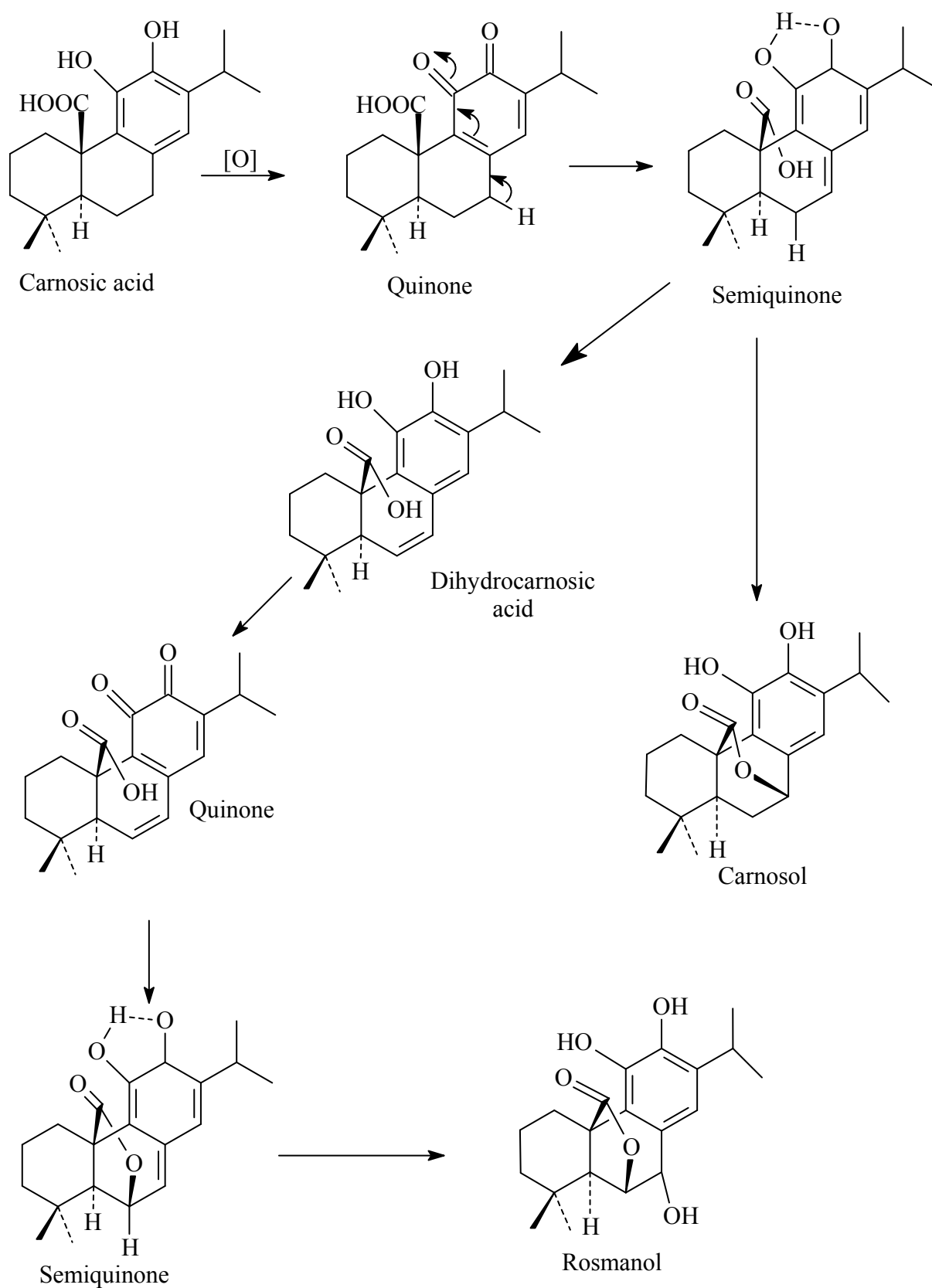Fig.2 – IR – spectra of rosemary extraction precipitate obtained in methanol (1) and acetone (2)

Figure 4 shows the chemiluminescence (200°C, air) of LDPE unstabilized with rosemary extracts. The kinetic parameters of CL data are given in table 1.

Carnosic acid

Quinone

Semiquinone

Dihydrocarnosic acid

Quinone

Carnosol

Semiquinone

Rosmanol

Scheme 1 – Oxidation cascade reactions of carnosic acid

As can be seen all rosemary extracts inhibited LDPE degradation in air at 200°C by trapping the radicals formed in the polymer matrix. It is proved by the increased values of the induction periods (t_i) by comparison with the blank sample. However, the results obtained with extracts from rosemary seeds demonstrate that the type of extraction solvent strongly influences the composition of the extracts and consequently their antioxidation activity.
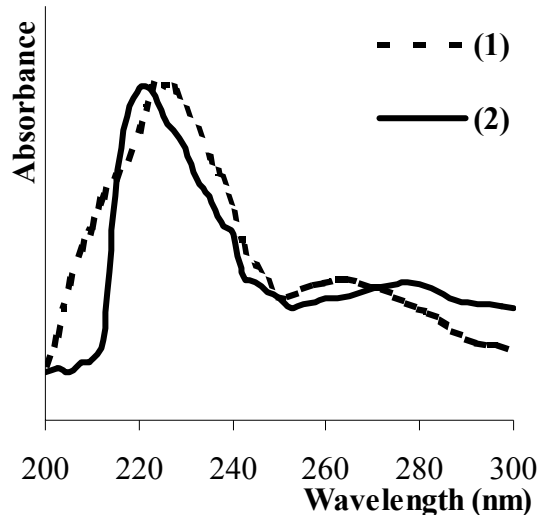

Fig.3 – UV-spectra of rosemary extraction liquids: (1) diethyl ether; (2) methanol
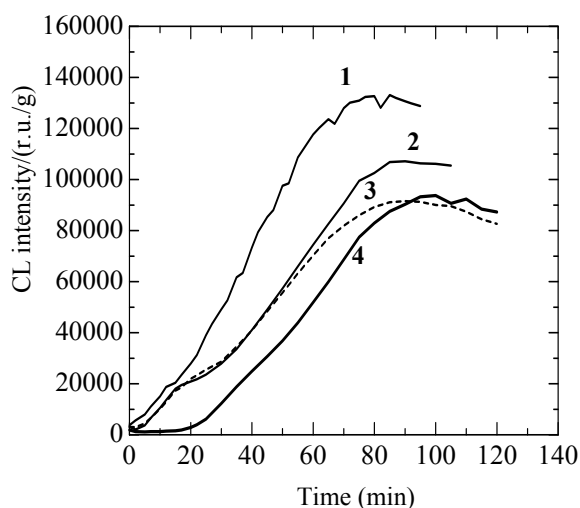

Fig.4 – Isothermal CL curves (200OC, air) for LDPE unstabilized (1) and stabilized (0,25% w/w) with rosemary extraction precipitates resulted from solutions in diethyl ether (2), acetone(3) and methanol (4)

Methanol seems to be the most efficient solvent for the antioxidant extraction. This is proved by the lowest I_O and $\sum\limits_{0}^{20} I_{CL}$ values.

The concentration of carnosic acid in the methanolic extract would be probably situated at the highest level. The scheme 1 shown above illustrates the mechanism through which carnosic acid acts as an efficient antioxidant [12].

When carnosic acid donates a hydrogen to quench a free radical, it forms carnosol, which is also an antioxidant, which in turns forms rosmanol, another antioxidant compound. Therefore, these compounds are oxidized to other compounds that can be rearranged to produce in addition more antioxidants, capable to scavenging more free radicals.

Table 1- Kinetic parameters for thermal oxidation of LDPE in air at 200OC in the presence of studied extracts

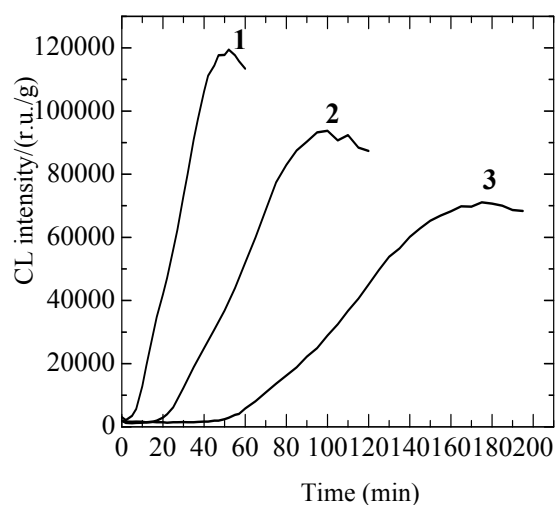| Solvent	Induction period t_i(min)	Initial CL intensity I_O (r.u./g)	Integrated CL signal $\sum\limits_{0}^{20} I_{CL}$ (r.u./g)
—	8.8	3800	134300
Acetone	12	3067	98133
Diethyl ether	14.9	3133	98301
Methanol	24	1900	14767

Fig.5 – CL curves for LDPE stabilized with rosemary extraction precipitate in methanol (1) 210°C; (2) 200°C; (3) 190°C

Figure 5 shows the effect of temperature on the chemiluminiscence of LDPE stabilized (0.25% w/w) with the rosemary extraction precipitate resulted from the methanol solution. The curves from figure 5 were used to calculate the main kinetic features as listed in table 2.Table 2 also includes the kinetic features for the unstabilized LDPE samples.

From t_i and t_{max}, E_i and E_{max} activation energies were calculated respectively. As can be seen in table 2, $E_i>E_{max}$. This difference could be due to the existence of different processes: E_i corresponds for induction period, while E_{max} corresponds to overall process (induction and acceleration of oxidation).

Table 2- The CL kinetic parameters of the LDPE unstabilized and stabilized with rosemary extraction precipitate in methanol

Temp. (^{O}C)	Unstabilized LDPE		Stabilized LDPE	
	Induction time t_i (min)	Maximum oxidation time t_{max} (min)	Induction time t_i (min)	Maximum oxidation time t_{max} (min)
180	36	187	—	—
190	20	92	65	175
200	8.8	84	24	100
210	—	—	10	52
E(Kj/mol)	113.8	71.5	165.8	107.6
lnA	-26.6	-13.9	-38.9	-22.8
Corr. coef.	0.998	0.918	0.999	0.999

The stabilized LDPE presents higher values for the activation energies in comparison with the unstabilized ones.

4.Conclusions
- Rosemary extracts containing carnosic acid or other phenolic compound which derives from carnosic acid, can be used as low temperature antioxidant for LDPE;
- The compounds responsible for the antioxidant activity come from a cascade of oxidation reactions starting with carnosic acid;
- Scavenging of radicals is a suitable method for inhibition of primary oxidation product formation by natural extracts in the plastic packing;
- Chemiluminiscence provides a means for quickly determining the stability of various materials in the presence of different antioxidants. The length of the induction period is a measure of stabilizer efficiency and the initial CL intensity is dependent upon the degree of oxidation.

5.References
[1] Brieskorn,C.H., Domling,J.H., *Z.Lebensm Unters Forsch.*, 141, p.10,1969;
[2] Brieskorn,C.H., Domling,J.H., *Arch. Pharm.*, 302, p.641, 1969;
[3] Scwarz,K., Ternes, W., *Z.Lebensm Unters Forsch.*,195, p.99, 1992;
[4] Wenkert, E., Fuchs,A., McChesney,J.D., *J.Org.Chem.*, 30, p.2931, 1965;
[5] Gonzales,A., Andres,L., Aguiar,Z., Luis,J., *Phytochemistry*, 31, p.1297, 1992 ;
[6] Richheimer,S.L., Bernart, M.W., King,G.A., Kent,M.C., Bailey,D.T., *J.Am.Oil Chem.Soc.*, 73, p.507, 1994 ;
[7] Cuvelier,E., Richard,H., Berset, C., *J.Am.Oil Chem.Soc.*, 73, p.645, 1996;
[8] Jipa,S., Zaharescu,T., Setnescu,R., Setnescu,T., Brites,M.J.S., Silva,A.M.G., Marcelo − Curto,M.J., Gigante,B., *Polym.Int.*, 48, p.414, 1999;
[9] Avram,M., Mateescu,Gh.D., *Spectroscopia in Infrarosu. Aplicatii in Chimia Organica*, Ed. Tehnica, Bucuresti, 1966;
[10] Black,R.M., Charlesby,A., *Int. J .Appl. Rad. Isot.*, 7, p.134, 1959;
[11] Bosch,S.M., Alegre, L., Schwarz,K., *Eur. Foods Technol.*, 210, p.263, 2000;
[12] Wekert,E., Fuchs,A., McChesney,J.D., *J.Org.Chem.*, 30, p.2931, 1965;

AZOIC DYESTUFFS, SYNTHESIS AND CHARACTERIZED

Crinela DUMITRESCU, Laura Monica GORGHIU, Radu Lucian OLTEANU, Silviu JIPA
[1]"Valahia" University of Targoviste, Faculty of Science, Unirii Avenue, 18-20, Targoviste, ROMANIA

Abstract: *The paper presents a class of monoazodyes, derivatives of 6-amino-4-hydroxy-2-naphtalenesulfonic acid („γ acid"). These dyes were obtained by the azo coupling reaction of „ γ acid" with the diazonium salt of primary aromatic amines, in alkali media. IR, UV-VIS, ^{1}H-NMR spectroscopy and elemental analysis characterized the structure of synthesized compounds.*

Introduction

The azo dyes are compounds with azo groups (- N = N -) bounded by hybridised sp^2carbon atoms. By the number of azo groups, the dyes ca be: mono-, dis-, tris-, tetrakis- azo dyes. An intermediate compound very used in synthesis of commercial azo dyes is 6-amino-4-hydroxy-2-naphtalenesulphonic acid ("γ acid").

The coupling reaction of diazonium salt for molecules with hydroxy and amino groups (like as "γ acid") is influenced by pH of reaction medium. Therefore, in acid medium (pH = 4-5) the coupling is oriented by amino groups (is been obtained in large ratio the aminoazoderivatived) and in alkali medium (pH = 8-9) by the hydroxy group (resulting in large ratio the hydroxyazoderivated) [1,2].

Experimental

The 6-amino-4-hydroxy-2-naphtalene sulphonic acid ("acid γ", 7-amino-1-naphtol-3-sulphonic acid, Fluka) technique, 90% purity, was used. The aniline was purified by low-pressure distillation to 99%, m.p. = -6 – (-5) [0] C, b. p. (10 torr) = 70 – 71[0] C, d_4^{20}=1,022 g/ml, n_D^{20}=1,586. Were also used: 4-chloroaniline (1-amino-4-chlorobenzene, Fluka), 99% purity, m.p. = 70-72[0]C, b. p. (10 torr) = 113-114[0]C; 4-nitroaniline (1-amino-4-nitrobenzene, Fluka), 99% purity, m.p. = 146-149[0] C; 3-nitroaniline (1-amino-3-nitrobenzene, Fluka), 98% purity, m.p. = 112-113[0] C; 2-chloro-4-nitroaniline (1-amino-2-chloro-4-nitrobenzene, Fluka), 98% purity, m.p. = 105-108[0]C; 2,4-dinitroaniline (1-amino-2,4-dinitrobenzene, Fluka), 99% purity, m.p. = 176-180[0]C.

It is to mention that the impurities are inorganic soluble salts, which can be removed finally in the filtrate, therefore there will be not involved in reactions. The inorganic reagents and solvents used were of analytical grade purity.

The diazotising of primary aromatic amines was made by usual methods [3].

Synthesis of 6-amino- (2',4'-dinitrophenylazo)-4-hydroxy-2-naphtalenesulphonic acid 6

The „ γ acid" in wet-pulp form (23.8 g, 0,1 mole) is dissolved at 30[0] C in water (190 ml) adding Na_2CO_3 to result a neutral solution; water and ice was added for cooling at 5[0] C and to increase the reaction volume at 460 ml. After that the cooled suspension of 2,4-dinitroaniline diazoderivated was poured under stirring (initially water was added 1:10 for acidity reduction) and Na_2CO_3 was added to obtain an alkali reaction medium (the pH was permanent controlled). The coupling take place rapid but for finishing the reaction the stirring was maintained 3-4 hours. Finally the reaction mass was salted with NaCl (5% in volume) and stirred another 6 hours. After the filter the pressed precipitate was dried at 90 – 100[0] C to obtain 41.9 g product **6** (yield = 92.3%).

Similarly were obtained the monoazo colours **2 –5,7**.

The ^{1}H-NMR spectra were recorded on a VARIAN GEMINI 2000 (300 MHz) spectrometer. The records were performed at ambient temperature, the chemical shifts are given in ppm relative to TMS, and DMSO-d_6 was used as solvent. The chemical shifts were obtained by COSY ([1]H-^{1}H), APT and HETCOR techniques.

The IR spectra were recorded on a BRUKER spectrometer in KBr pellet a 400-4000 cm^{-1}. For calibration of the frequencies (cm^{-1}) was used polystyrene as standard.

The UV-VIS spectra were performed with SECOMAM S 750 apparatus in quartz cells (l = 1 cm) for aqueous solution (thermal controller at 20-25[0]C) of c = 10^{-4}-10^{-5}M of synthesized compounds.

CARLO-ERBA M1106 apparatus performed the analysis calculated for C, H and N.

The thin layer chromatography was made by one-dimensional ascending technique using silica gel as stationary phase (MERCK DC Plastiffolien Kieselgel 60 F 254 plates) with 0.2 mm thickness of absorbent layer and for elution the solvents mixtures 1-buthanol:ethanol:water = 2:1:1 (v:v:v) and 1-buthanol:1-propanol:ethyl-acetate:water = 2:4:1:3 (v:v:v:v).

Results and discussions

Were obtained monoazo colours by the coupling reaction between 6-amino-4-hydroxy-2-naphtalenesulphonic acid and the diazonium salts of some primary aromatic amines, in alkali medium (reaction 1) [3]:
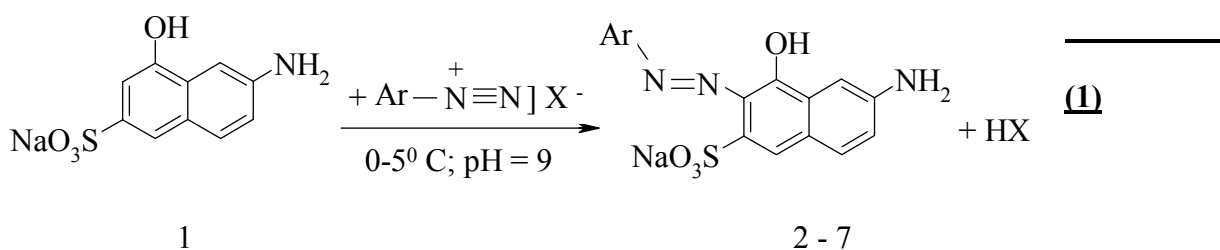
The removal of inorganic salts was made by the acidification of aqueous sodium salt solutions of azoic dyes to precipitate such as free acids. The obtained precipitate was washed with HCl 2% solution (to pass the salts in filter liquor). The salts tracks were filtered again. To obtain the sodium salt of the colour, NaOH was added. After concentration from mass reaction precipitate the sodium salt dyes [4].

The synthesis of **2-7** compounds was performed at 92.3-98.7% yields (table 1).

Table 1. Azoic compounds, derivatives of 6-amino-4-hydroxy-2-naphtalenesulphonic acid

Compound	Yield, (%)	Ar
2	98.7	C_6H_5
3	94.5	$4-O_2N- C_6H_4$
4	94.9	$3-O_2N- C_6H_4$
5	98.2	$4-Cl- C_6H_4$
6	92.3	$2,4-O_2N- C_6H_3$
7	95.0	$2-Cl-4-O_2N- C_6H_3$

Also was obtaining in small quantities the **8-13** isomers as secondary products [5, 6]. The presence of these compounds in the reaction mixture was observed by the apparition of two spots in thin layer chromatograms (table 2).

8-13 (secondary products)
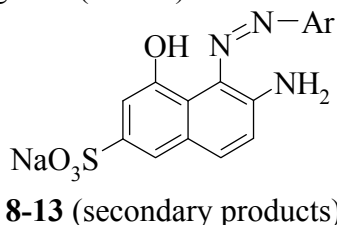
The columns chromatography was used for separation of hydroxyazo from aminoazoderivative isomers. The used stationary phase was silicagel and for the elution the solvent system C_4H_9OH : C_2H_5OH : NH_3 : pyridine (4 : 1 : 3 : 2, v : v : v : v) [5].

The azo dyes and also the secondary reaction products were characterized by the absorption peeks in visible spectra (table 3, 4). Also, in the UV – molecular spectra of studied compounds the vibrations due to naphthalene ring (220 – 290 nm).

In the IR spectra (made in KBr) were present absorption bands of OH (3430 – 3455 cm^{-1}), NH$_2$ (3250 – 3350 cm^{-1}) groups, the nitro groups vibrations (asymmetrical 1433 – 1588 cm^{-1} and symmetrical 1360 – 1390 cm^{-1}, in 3, 4, 6, 7 compound) and SO$_3^-$ Na$^+$ groups (1041 – 1098 and 1156 – 1190 cm^{-1}). Can be mentioned also the vibration deforming bands of naphtalenic ring (661 – 953 cm^{-1}) and there armonics (≈1614 cm^{-1}) [7].

In the ^{1}H-NMR spectra (DMSO – d$_6$,

300 MHz) were identified the signals: 6.85 – 8.78 ppm (m, Ar$\underline{H}$), 2.8 – 3.9 ppm (2H, s, N$\underline{H}_2$) and water signal, both overlap, 10 – 12 ppm (1H, s, O$\underline{H}$) – coalescent signal [8].

The results of elemental analysis (table 5) show a good correlation between experimental and calculated data.

Table 2. R_f values in thin layer chromatograms

Compound[1]	R_f	Mobile phase
2, **8**	0.51 ; 0.65	1-buthanol : ethanol : water
	0.59 ; 0.71	1-buthanol : 1-propanol : ethyl acetate : water
3, **9**	0.56 ; 0.68	1-buthanol : ethanol : water
	0.63 ; 0.75	1-buthanol : 1-propanol : ethyl acetate : water
4, **10**	0.57 ; 0.69	1-buthanol : ethanol : water
	0.63 ; 0.76	1-buthanol : 1-propanol : ethyl acetate : water
5, **11**	0.55 ; 0.67	1-buthanol : ethanol : water
	0.62 ; 0.74	1-buthanol : 1-propanol : ethyl acetate : water
6, **12**	0.53 ; 0.66	1-buthanol : ethanol : water
	0.60 ; 0.73	1-buthanol : 1-propanol : ethyl acetate : water
7, **13**	0.58 ; 0.70	1-buthanol : ethanol : water
	0.65 ; 0.77	1-buthanol : 1-propanol : ethyl acetate : water

Table 3. Characteristics of UV-VIS spectra of 2-7 compounds

Compound	λ_{max} nm, (A)	
	UV (10^{-5} M)	*VIS (10^{-4} M)*
2	237.5 (0.485); 347.3 (0.137)	497.7 (0.107)
3	*237.3 (0.768); 292.0 (0.419)*	*503.0 (0.361)*
4	*235.9 (0.718);*	*477.4 (0.243)*
5	*237.4 (0.719); 289.4 (0.448)*	*477.2 (0.264)*
6	*237.1 (0.729); 295.6 (0.478)*	*512.8 (0.498)*
7	*238.5 (0.729); 291.8 (0.643)*	*485.0 (0.351)*

Table 4. Characteristics of VIS spectra of 8-13 compounds

Compound	8	9	10	11	12	13
λ_{max}, nm, (A)	485.2 (0.235)	492.7 (0.348)	465.8 (0.273)	466.0 (0.280)	498.5 (0.483)	471.9 (0.325)

Table 5. Elemental analysis of 2-7 azoic dyestuffs

Compound	Formula	Elemental analysis, (%)					
		C		H		N	
		calcd	found	calcd	found	calcd	found
2	$C_{16}H_{12}N_3O_4SNa$	52.60	52.65	3.28	3.21	11.50	11.59
3	$C_{16}H_{11}N_4O_6SNa$	46.83	46.89	2.68	2.60	13.65	13.70
4	$C_{16}H_{11}N_4O_6SNa$	46.83	46.81	2.68	2.66	13.65	13.62
5	$C_{16}H_{11}ClN_3O_4SNa$	48.06	48.01	2.75	2.73	10.51	10.47
6	$C_{16}H_{10}N_5O_8SNa$	42.19	42.15	2.19	2.17	15.38	15.36
7	$C_{16}H_{10}ClN_4O_6SNa$	43.19	43.17	2.24	2.21	12.59	12.60

---

[1] Isomers in the mixture

The **2–7** monoazo derivatives structure was confirmed by correlation between elemental and spectral analysis data.

Conclusions

- Were obtained by coupling in alkali media with different aromatic diazoderivatives, six monoazo dyes derivated from 6-amino-4-hydroxi-2-naphtalenesulfonic acid.
- The secondary reaction products presents in small ratio – aminoazo- and hydroxiazoderivatives – (in function of pH – media), appear because that the coupling reaction doesn't have a high selectivity. The column chromatography was used to isolate these compounds in pure form; their properties are relatively the same, the differences can be observed only in VIS absorption pecks.
- The synthesis colours were characterized by elemental analysis, UV-VIS, IR, ^{1}H-NMR spectroscopy. The obtained data confirm the proposed structures.

References

1. Floru L., Urseanu F., Tărăbăşanu-Mihăilă C., Palea R., Chimia şi tehnologia intermediarilor aromatici şi a coloranţilor organici, Editura Didactică şi Pedagogică, Bucureşti, 1980.
2. Dumitrescu C., Gorgiu L. G., Olteanu R. L., *Revista de Chimie*, 54(11), 2003, p. 890-894.
3. Sanielevici H., Urseanu F., Sinteze de coloranţi azoici, 1, 2, Editura Tehnică, Bucureşti, 1987.
4. Sanielevici H., Urseanu F., Analize de intermediari aromatici şi de coloranţi organici, Editura Tehnică, Bucureşti, 1985.
5. Lycka A., Jirman J., *Dyes and Pigments*, **8**, 1987, p. 315-325.
6. Skrabal P., Zollinger H., *Dyes and Pigments*, **9**, 1988, p. 201-207.
7. Avram M., Mateescu G. D., Spectroscopia în infraroşu. Aplicaţii în chimia organică, Editura Tehnică, Bucureşti, 1966.
8. Balaban A. T., Banciu M., Pogany I., Aplicaţii ale metodelor fizice în chimia organică, Editura Ştiinţifică şi Enciclopedică, Bucureşti, 1983.

CHEMILUMINESCENCE STUDY OF IR-LASER IRRADIATION OF LOW DENSITY POLYETHYLENE

LAURA MONICA GORGHIU, SILVIU JIPA, CĂLIN OROS,
CRINELA DUMITRESCU, RADU LUCIAN OLTEANU
Valahia University of Targoviste, 18-22 Unirii Boulevard, Targoviste

Abstract: There is a considerable interest in thermal stabilization of commercial polyolefins because their service life depends on a large extent by the stabilization efficiency of additives.
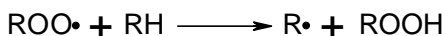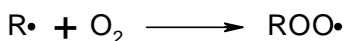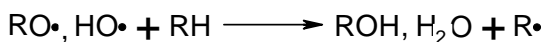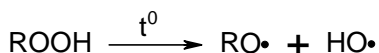
One of the most sensitive procedures used for the determination of antioxidative ability is chemiluminescence.

The triazines compounds are an important class of antioxidants that has a continuous developing. In the case of these compounds an important decrease of the oxidation effect in comparison with the same effect of the simple phenolic or aminic antioxidants is observed.

In this paper the influence of IR – laser over some stabilized LDPE samples with new triazinic antioxidants is studied. The stabilization efficiency of these additives is also studied. Heating the IR – laser irradiated samples above $200^{0}C$ rapidly decomposes all peroxidic groups and gives a CL emission that is proportional to peroxide content.
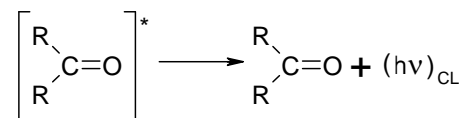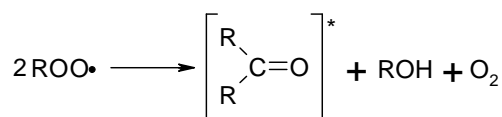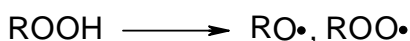
The oxidation of polyolefins is an important cause of the premature failure of articles made from these polymers. The oxidation processes may be heat, light, mechanical action or high energy radiation.

Hydroperoxide groups are widely recognized as key intermediates in the oxidative degradation of many polymers [1-3]. They are present in polymers as impurities generated by oxidation during storage, processing or use. Hydroperoxides in polyolefins are thermally labile. Free radicals generated by this hydroperoxide decomposition reaction begin new oxidative chain reactions by attack on the polymer matrix (RH) [4]:

$$ROOH \xrightarrow{t^0} RO\bullet + HO\bullet$$

$$RO\bullet, HO\bullet + RH \longrightarrow ROH, H_2O + R\bullet$$

$$R\bullet + O_2 \longrightarrow ROO\bullet$$

$$ROO\bullet + RH \longrightarrow R\bullet + ROOH$$

The chemiluminescence (CL) method has been recognized as a useful tool for the study of the oxidative degradation of polymers and also for the assessment of stabilizers [5-8].

The predominating chemiluminescence mechanism is assumed to be the Russel mechanism described as follows [9]:

$$ROOH \longrightarrow RO\bullet, ROO\bullet$$

$$2\,ROO\bullet \longrightarrow \left[\begin{matrix} R \\ R \end{matrix} C=O \right]^{*} + ROH + O_2$$

$$\left[\begin{matrix} R \\ R \end{matrix} C=O \right]^{*} \longrightarrow \begin{matrix} R \\ R \end{matrix} C=O + (h\nu)_{CL}$$

The main luminescence species present in polyolefins are the excited carbonyl groups [10].
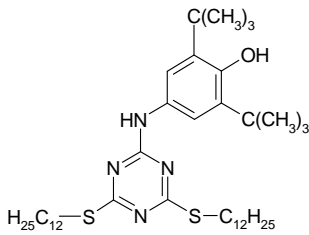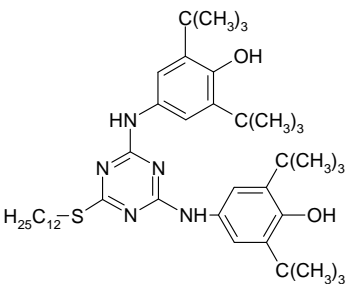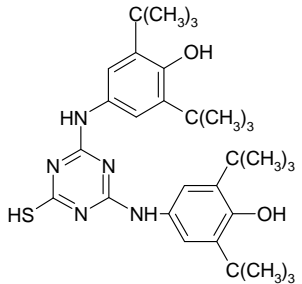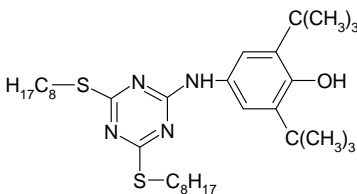
In this paper the chemiluminescence method was applied to evaluate the thermal oxidative degradation of polyolethylene, induced by laser irradiation and the effect of various antioxidants on the chemiluminescence behaviours.

Experimental
Low density polyethylene (LDPE) provided by the Brazi Chemical Company (Romania) as K322® type was used. Some polymer characteristics are density 0.920 g/cm³, crystalinity 45,5%, number of –CH₃ per 100 carbon atoms 3. LDPE was dissolved in hot o-xylene and its precipitation was achieved by pouring methanol into the solution. The precipitate was filtered, washed with acetone and dried at room temperature.

Table 1 presents the molecular structure of the mercapto - triazines used as stabilizers in this paper. Details on their synthesis are presented elsewhere [11].

Tabel 1 – Molecular structure and chemical name of studied additives

Code	Structure and denomination
T_5	2,6-thio-bis-(lauryl)-4-(4-hydroxy-3,5-di-tert-butyl-aniline)-1,3,5-triazine
T_6	2,4-bis (4-hydroxy-3,5-di-tert-butyl-aniline)-6-thio-(lauryl)-1,3,5-triazine
T_7	2,4-bis-(4-hydroxy-3,5-di-tert-butyl-aniline)-6-mercapto-1,3,5-triazine
Irganox-565	2,4-bis (n-octyl-thio)-6-(4-hydroxy-3,5-di-tert-butyl-aniline)-1,3,5-triazine

The addition of a stabilizer (0.25%w/w) was carried out by a wet route. Polymer was brought in a slurry state with chloroform and the appropriate amounts of each additive solution in $CHCl_3$ were separately poured during gentle homogenization. The compounded polyethylene samples were dried in a desiccator at room temperature for 24 h.

Then thin films were pressed at 140^0C for 2 min to a thickness of about 120 ± 20 μm.
Irradiation was carried out by means of a IR-laser NdYAG type, Spic3 ($\lambda = 1.06$ μm, mean energy/pulse = 5 – 7 J, laser pulse duration τ_p = 3 ms). The IR-radiation produced by the NdYAG laser was directed toward polymer film. The irradiation temperature was below the melting point of the polymer.
Isothermal chemiluminescence measurements were performed in air at 210^0C in an Oxyluminograph OL-94 which has been previously presented [12]. The weights of the laser – oxidized samples varied between 0.05 and 0.07g.

Results and discussion
The chemiluminescent behavior of a typical low density polyethylene stabilized with 0.25% w/w of different triazines is shown in figure 1. The chemiluminescence intensity rose to a maximum, then dropped off. The rate of rise (i.e maximum oxidation rate, v_{ox}^{max}) appeared to vary as a function of the stabilizer structure.

Fig.1 – Isothermal CL curves from unirradiated LDPE (210^0C, air) samples containing 0.25%w/w of different triazines:
(1) free of additive; (2) T_7; (3) Irganox-565; (4) T6 (I×0.7); (5) T_5

The stabilization efficiency order in LDPE of the studied antioxidants can be expressed by the following sequence, irrespective of the level of laser – irradiation (fig. 2):

T_5 > T_6 > Irganox-565 ≥ T_7

This order is clearly detailed by the values of kinetic parameters (table 2). Because oxidation induction time OIT) characterizes the modifications occurring during the early stage of thermal degradation in air, it could be considered an appropriate parameter for the assessment of stabilization efficiency.

The chemiluminescence intensity (I) may be directly associated with the accumulation of hydroperoxide and carbonyl groups in the polymer during its thermooxidation while the initial CL intensity (I_0) seem to be associated with the degradation of polymer caused by laser irradiation.

On the other hand, OIT show the effect of the laser – irradiation as can be observed in figures 3 and 4. OIT decreases with the intensity of the laser treatment. This means that the antioxidant is consumed during the laser irradiation of the polymer. A simple and adjusted scheme (see [13]) of laser induced oxidation process for polyethylene sample is shown in figure 5.
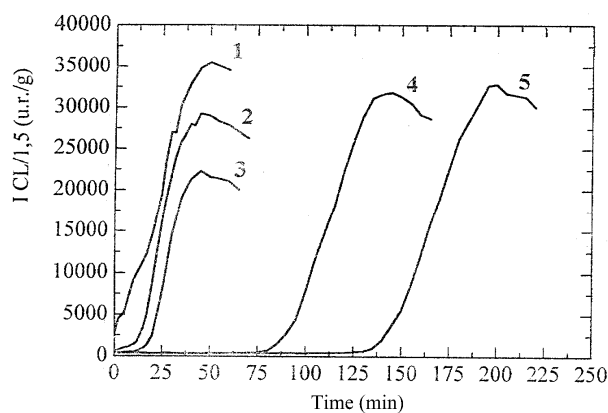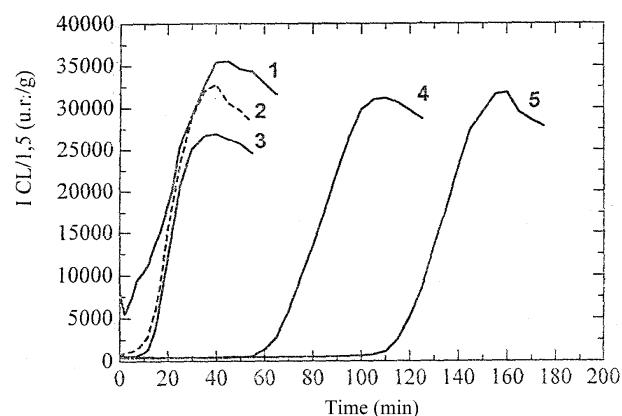

Fig. 2 - Isothermal CL curves from laser - irradiated LDPE (210^0C, air) samples containing 0.25% w/w of different triazines:
(1) free of additive; (2) T_7; (3) Irganox-565; (4) T6 (I×0.7); (5) T_5 (Irradiation condition: 2 min 6J; 3ms; 30Hz + 1min 7.5J ; 3ms ; 30Hz)

Table 2 – Kinetic parameters for thermal oxidation (2100C, air) of the IR laser irradiated LDPE in the presence of studied mercapto – triazines

Antioxidant	t_i (min)	$t_{1/2}$ (min)	t_{max} (min)	I_0 (r.u./g)	I_{max} (r.u./g)	v_{ov}^{max} (r.u./g·min)
Unirradiated sample						
None	9	23	50	2747	35463	1286
T_5	142	166	200	496	32851	705
T_6	90	111	145	664	45529	1026
T_7	13	23	45	591	29249	1398
Irganox-565	19	27	45	451	22283	1372
Irradiated (30 s; 4.5 J; 3 ms; 15 Hz) sample						
None	7	23	55	3186	31853	985
T_5	125	154	200	832	31005	534
T_6	71	90	120	933	46242	1171
T_7	11	21	50	579	27178	1330
Irganox-565	21	29	50	707	24266	1386
Irradiated (2 min; 6 J; 3 ms; 30 Hz + 1 min; 7.5 J; 3 ms; 30 Hz) sample						
None	3	19	45	8127	35541	1281
T_5	116	133	160	565	31856	854
T_6	62	82	110	688	44565	1186
T_7	10	21	40	629	32835	1352
Irganox-565	13	21	40	618	26893	1672

Fig. 3 – Decrease of OIT for LDPE (210^0C, air) stabilized (0.25% w/w) with T_5 triazine by laser irradiation
(1) Unirradiated sample; (2) Irradiated sample (30s; 4.5J; 3ms; 15Hz); (Irradiated sample (2 min; 6J; 3ms; 30Hz + 1min; 7.5J; 3ms; 30Hz)
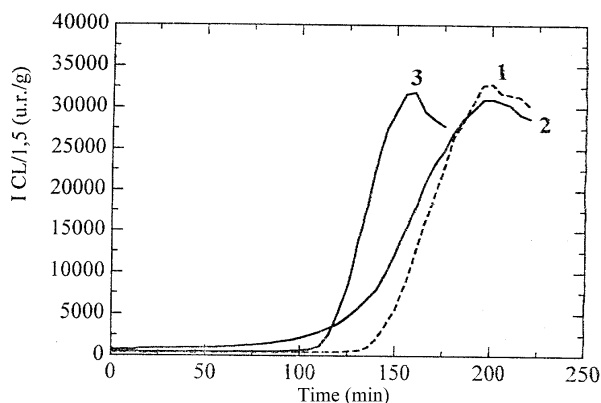

Fig. 4 – Decrease of OIT for LDPE (210^0C, air) stabilized (0.25% w/w) with T_6 triazine by laser irradiation
(1) Unirradiated sample; (2) Irradiated sample (30s; 4.5J; 3ms; 15Hz); (Irradiated sample (2 min; 6J; 3ms; 30Hz + 1min; 7.5J; 3ms; 30Hz)
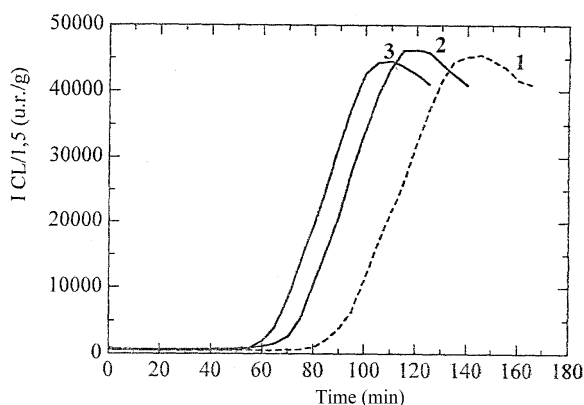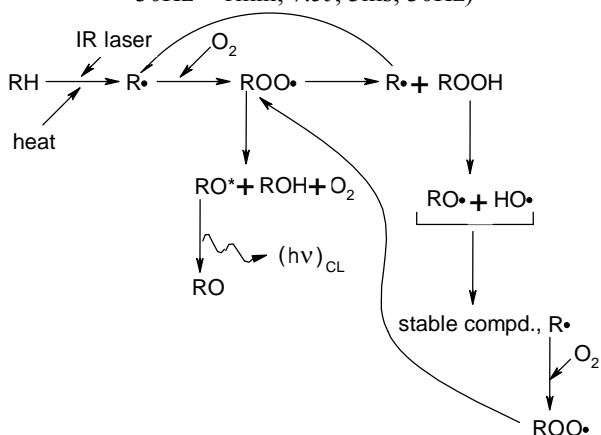

Fig. 5 – Simple scheme of laser – induced oxidation and CL process for polyethylene

Radical species (R•) produced by main chain scission which is caused by the action of IR-laser light and heat, react with O_2 and form peroxy radical (ROO•). The bimolecular reaction of ROO• is known to be able to excite a product ketone up to its first triplet state (RO*). Visible chemiluminescence is emitted as it returns to its ground state. The CL intensity is proportional to the rate of the bimolecular colligation of ROO•.

The radicals stabilization can be explained by the following reactions [14]:

$$ROO\bullet + AH \longrightarrow A\bullet + ROOH$$

$$A\bullet + ROO\bullet \longrightarrow ROOA$$
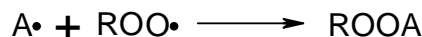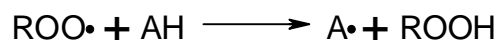
The peroxy radicals are intercepted by the added antioxidant (AH). The complete consumption of an inhibitor by the above reactions at elevated temperatures is marked by a suddent increase in the chemiluminescence emission due to the peroxy – peroxy reactions.

Conclusions

- Heating the IR – laser irradiated samples above 200^0C rapidly decomposes all peroxidic groups and gives a CL emission that is proportional to peroxide content;
- The addition of triazine antioxidants to polyethylene increases their thermooxidative stability as indicated by a delay of degradation;
- The chemiluminescence method provide a sensitive technique in polymers thermal oxidative stability evaluation. Chemiluminescence gives quantitative information such as: induction time, oxidation rate, extent of oxidation, etc.

References
1. Carlsson, D. J., Wiles, D. M., *J. Macromol Sci. Rev. Macromol. Chem.*, **C14**, 1976, p.67
2. Petruj, J., Marchal, J., *J. Radiat. Phys. Chem.*, **16**, 1980, p.27
3. Gardette, J. L, Lemaire, J., *J. Polymer Photochem.*, **7**, 1986, p.409
4. Carlsson, D. J., Lacoste, J., *Polym. Degrad. Stab.*, **32**, 1991, p.377
5. Jipa, S., Setnescu, T., Setnescu, R., Cazac, C., Mihalcea, I., *Rev. Chim. (Bucuresti)*, **44**, 1993, p.65
6. Jipa, S., Zaharescu, T., Setnescu, R. Setnescu, T., Giurginca, M., Wurm, D., *Materiale Plastice*, **37**, 2000, p.63

7. Jipa, S., Setnescu, R. Setnescu, T., Zaharescu, T., *Polym. Degrad. Stab.*, **68**, 2000, p.159

8. Jipa, S., Zaharescu, T., Setnescu, R. Setnescu, T., Herdan, J., Gorghiu, L. M., *Polym. Testing*, **21**, 2002, p. 353

9. Russel, G. A., *J. Am. Chem. Soc.*, **79**, 1957, p. 3871

10. Zlatkevich, L., (Ed.) *Luminescence Techniques in Solid – State Polymer Research*, Marcel Dekker, New York, 1989, Chap. 3

11. Giurginca, M., Herdan, J. M., Cira, L., Văleanu, G. Ivan, G., *Polym. Degrad. Stab.*, **36**, 1992, p. 53

12. Jipa, S., Zaharescu, T., Setnescu, R. Setnescu, T., Brites, M. J. S., Silva, A. M. G., Marcelo-Curto, M. J., Gigante, B., *Polym. Int.*, **48**, 1999, p. 414

13. Kihara, H., Hosoda, S., *Polym. J.*, **22**, 1990, p. 763

14. Mendenhall, G. D., *Angew. Chem. Int. Ed. Engl.*, **29**, 1990, p. 362

STABILITY ANALYSIS OF VITAMIN A IN PHARMACEUTICAL PRODUCTS

ANA - MARIA HOSSU, CRISTIANA RĂDULESCU, IONICA IONIȚĂ[1], VASILE MAGEARU[2]

[1] University « Valahia » Targoviste, Department of Chemistry, Blvd. Unirii No. 18-20, Targoviste, Romania
[2] University of Bucharest, Faculty of Chemistry, Department of Analytical Chemistry, Sos. Panduri, No. 90, 76229, Sector 5, Bucharest, Romania

Abstract: *In this paper there are presented the research results regarding the establishing of the optimal conditions for the stability of fat-soluble vitamin A in multivitamin pharmaceutical products. Vitamins are generally sensitive to light, high temperatures and moisture. They should be kept in properly closed containers, protected from humidity and light at temperature of maximum 21^0C. The analyzed technique used was the HPLC method for analytical characterization of this.*

1. Introduction

Most of the fat-soluble vitamins present in pharmaceutical preparations or in natural products are accompanied by a number of closely related compounds. This explains why chromatographic methods are so frequently used in analysis of these compounds. HPLC is almost ideally suited for these compounds because of its simplicity, speed, selectivity and sensitivity.[1-6]

Vitamin A (formula 1) was chromatographed in the form of the alcohol, the acid or the respective ester in the presence of its isomers or other vitamins, especially D_2, D_3 and tocopherol [7-10]. Reverse-phase chromatography with a mobile phase of methanol and water (96:4 or 95:5) was used for the quantitative determination of vitamins A [11-14]. The retinol was determined in serum with high sensitivity over a wide linear range using UV detection at 340 or 280 nm and using retinyl acetate as the internal standard.
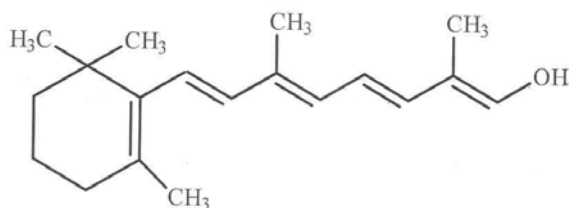
Formula 1

A number of HPLC modifications for the simultaneous analysis of vitamin A in pharmaceutical preparations and biological material have been worked out. These methods usually used UV, fluorimetric or electro-chemical detection [15,16]. This vitamin was determined using elution with aqueous methanol and detection at 325 nm. [17]

In this paper the influence of temperature on the stability of this vitamin fat-soluble is analyzed using the HPLC method, during 30 months. The stability of this is influenced in principal by temperature, light and moisture and also by the preservation conditions.

2. Experimental part

Investigations were carried out with a Spectra-Physics Analytical Model P 4000 liquid chromatograph with a Model 2000 UV detector (Spectra-Physics Analytical). This system was connected to a computer Pentium III 800MHz.

The pump P 4000 is conceived to reach the performances and the maximal capacities. It presents features of vanguard: four solvents, eleven files users of the names of files and solvents, and a waiting line for the link of the files.

The UV 2000 is a detecting UV/vis doubles length of wave, programmable, entirely equipped. It functions as well in simple fashion that length of wave doubles in fashion, in the UV ranges and visible. The UV 2000 also offers the spectral sweep, a file develop (for the development of the methods), the storage of several files, a waiting line (for the link of the files), and more. We place the

detector to a length of wave $\lambda = 326$ nm for vitamin A.

A mobile phase composed of methanol and water (98/2) allowed a very good separation of vitamins A on LC 18 column.

The vials of oral solution Biosol (Biokim Istanbul Turkey) were stored in special climate shelves. The vials were kept at temperatures of $+5^0$C, $+15^0$C, $+21^0$C and $+37^0$C.

The following tests have been executed:
- optical appearance of the product;
- qualitative and quantitative analysis of the active ingredient (vitamins A).

3. Results and discussion

For vitamin A, the European Pharmacopoeia gives the following storage instructions: "store in a well-closed, well-filled container, protected from light, between 8^0C and 15^0C. When the container has been opened, its contents should be used as soon as possible; any part of the contents not used at once should be protected by an atmosphere of inert gas (e.g. nitrogen)".

The limits for the contain in vitamin A for each vial are 45000-55000 U.I./mL.

The results of the determinations for each temperature, test period 30 months, are presented below in tables.

Assay	Vitamin A (U.I./mL)
Nominal value	50000
Date of manufacture	55000
6 months	54000
12 months	54000
18 months	53000
24 months	51000
30 months	50000

Table 1. The results obtain at temperature $+5^0$C (refrigerator)

Assay	Vitamin A (U.I./mL)
Nominal value	50000
Date of manufacture	55000
6 months	54000
12 months	53000
18 months	51000
24 months	50000
30 months	49000

Table 2. The results obtain at temperature $+15^0$C (cool cabinet)

Assay	Vitamin A (U.I./mL)
Nominal value	50000
Date of manufacture	55000
6 months	54000
12 months	52800
18 months	51000
24 months	49500
30 months	48000

Table 3. The results obtain at temperature $+21^0$C (room temperature)

Assay	Vitamin A (U.I./mL)
Nominal value	50000
Date of manufacture	55000
6 months	52000
12 months	49000
18 months	47000
24 months	41000
30 months	37000

Table 4. The results obtain at temperature $+37^0$C (climate cabinet)

Figure 1. Variation of contain in Vitamin A with time test at different temperatures

[12] Nierenberg, D. W., Lester, D. C., *J. Chromatogr.*, 345, 1985, 275.
[13] Russel, M. J. et al., *J. High Resolut. Chromatogr.,* 9, 1986, 281.
[14] Sanz, D. C., Santa-Cruz, M. C., *J. Chromatogr.*, 380, 1986, 140.
[15] Mulholland, M., et al., *J. Chromatogr.*, 350, 1985, 285.
[16] Huang, M. L., et al., *J. Chromatogr.*, 380, 1986, 331.
[17] ****Farmacopeea Romana*, ed X, Editura Medicala, Bucuresti, 1993.
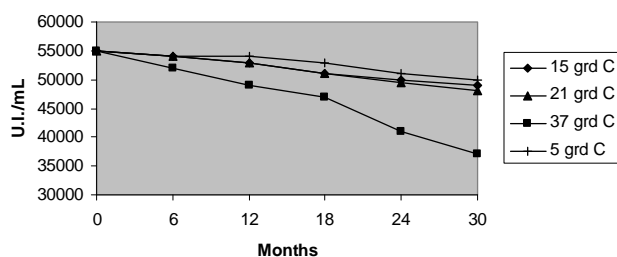
The oral solution of Biosol in the original vial is stable and retains its activity when stored at room temperature (18-21^{0}C). Under high temperatures (37^{0}C climate cabinet), the solution is showing an intensifying colouring after longer storage and looses activity, which are even below the tolerances of the declared value.

4. **Conclusions**

The stability tests show that during a storage period of 2 years an adequate stability is provided, when the product is stored at room temperature (< 21^{0}C) and protected from light. The choice of the storage temperature plays an important roll for the stability of the pharmaceutical products of vitamins.

REFERENCES

[1] Pellerin, F., Dumitrescu, D., *Talanta*, 27, 1980, 243.
[2] Thompson, J. N., *Trace Anal.*, 2, 1982, 1.
[3] Wachob, G. O., *Liq. Chromatogr. HPLC Mag.*, 1, 1983, 110.
[4] Zonta, F., Stancher, B., *Riv. Ital. Sostanze Grasse*, 60, 1983, 65.
[5] Roeck-Holtzhauer, Y., Montel, E., *Ann. Falsif. Expert. Chem. Toxicol.,* 76, 1983, 331.
[6] Cannelle, T., Bichi, G., *Boll.Chim. Farm.,* 122, 1983, 205.
[7] B. Stancher, B., Zonta, F., *J. Chromatogr.*, 238, 1982, 217.
[8] Zonta, F., Stancher, B., *J. Chromatogr.*, 287, 1984, 353.
[9] Chaudhary, L. R., Nelson, E. C., *J. Chromatogr.*, 294, 1984, 466.
[10] Zonta, F., Stancher, B., *J. Chromatogr.*, 301, 1984, 65.
[11] Driskell, W. J. et al., *Clin. Chem.*, 27, 1981, 1031.

AZOIC DYES DERIVATIVES
OF PHENYLAMINOMETHYLENSULPHONIC ACID

Ionica IONIȚĂ, Cristiana RĂDULESCU, Ana-Maria HOSSU

University ''Valahia'' Târgoviște, Faculty de Science, Department of Chemistry, 18-22 Unirii Bdvl.

Abstract: The paper presents the synthesis and characteristics of a two dyes, derivatives of phenylaminomethylensulfonic acid. In future the synthetized structures will be included on macromolecular catena to obtain some stable photochromic materials with special applications.

Synthesis contained following stage: diazotizing even *p*-anilines[1] and the coupling salt of diazonium with the phenylaminomethylensulfonic acid [2].

The way of thing for diazotizing even established anilines on base variation of the next parameters of reaction: order of reactant load, the molar ratio, the influence of the addition time of sodium nitrite and the reaction time.

Synthesis of phenylaminomethylensulphonic acid – A mixture of NaHSO$_3$ solution and formaldehyde solution is heated at 70^{0}C, where it is maintained for 0,5h.

The resulted solution is cooled at 25^{0}C, then the aniline is added and the mixture is heated for 3h at 25-30^{0}C and then 1h at 35^{0}C. The mixture was diluted with water, cooled to 20^{0}C and the precipitated product.
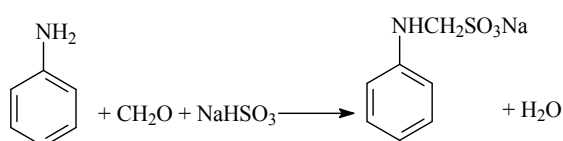
The ^{1}H-NMR spectra for phenylaminomethylensulphonic acid:
- H^4 triplet δ_H: 6.48 ppm, with the coupling constants orto J(4,3) = 7.68 Hz
- (H^2) H^6 split doublet δ_H: 6.69 ppm, with the coupling constants orto J(2,3) = 8.16 Hz
- (H^5) H^3 triplet δ_H: 6.69 ppm, with coupling constants orto J(3,4) = 7.29 Hz
- NH – triplet at 5.96 ppm, constants J = 6.61 Hz
- the signals of 3.88 ppm has been attributed the presence of group –CH$_2$, constants J = 6.61 Hz

The ^{13}C-NMR spectra present signals for carbon atoms: C^3, C^5 δ: 128.694 ppm, C^2, C^6 δ: 112.677 ppm, C^4 δ: 115.864 ppm, and carbon atom from CH$_2$- group present δ: 60.613 ppm.

The results at the elementary analysis proved the presence of synthetized compound.

Synthesis at diazoniu salts and preparation of the dyes:
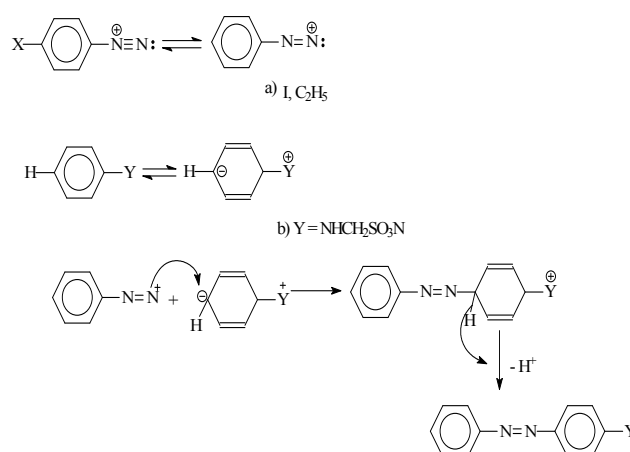
a) Electrofil active forms of diazoniu derivatives
b) Active form of coupling component

Purification methods for the azo dyes which were obtained. The purification of the azo dyes was achieved through recrystallization from solvents (ethanol and CCl$_4$).

The purity was checked by chromatography[3] on thin layer.

The obtained spots were distinguishing units with R$_f$ values 0.83 and 0.86.

Physic-chemical[4] characterization of the synthesised compounds was done by UV, IR and NMR spectroscopy.

The spectra UV were recorded on a SECOMAM S750 spectrophotometer, utilizing the vat from quartz, for solution of concentration 2.10^{-5} mol/l in DMF.

Table 1.*Results of UV-VIS analysis of azo dyes*

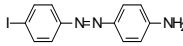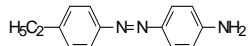| Dye / Value	$I-\bigodot-N=N-\bigodot-NH_2$ (1)	$H_5C_2-\bigodot-N=N-\bigodot-NH_2$ (2)
λ_1 (nm)	294	263
λ_2 (nm)	405	405

The synthetized compounds were characterized by NMR spectroscopy [4] using an Varian Gemini 300BB apparatus, the frequency of registration be in the case ^{13}C-NMR of 75 MHz, and in the case ^{1}H-NMR of 300 MHz, using deuterated dimethyl-sulfoxide as a solvent.

The ^{1}H-NMR values of dyes are presented in table 2.

Table 2.*The ^{1}H-NMR values of compounds*

Code	δ(ppm) (1)	δ(ppm) (2)
$H^2(H^6)$	7.87^d $J^o_{2,3}$=8.00Hz	7.33^d $J^o_{2,3}$=8.07Hz $J^m_{2,6}$=1.55Hz
$H^3(H^5)$	7.68^d $J^o_{3,2}$=8.7Hz	7.67^d $J^o_{3,2}$=8.14Hz $J^m_{3,5}$=1.55 Hz
$H^8(H^{12})$	7.70^d $J^o_{8,9}$=8.64Hz	7.63^d $J^o_{8,9}$=8.85Hz $J^m_{8,12}$=1.6Hz
$H^9(H^{11})$	6.72^d $J^o_{9,8}$=8.64Hz	-
NH_2	-	3.97^s
CH_3	-	112^t J=7.2Hz
CH_2	-	2.66^c J=7.2Hz
R	I	C_2H_5

s = singlet; o = orto; m = meta; d = doublet; t = triplet; c = cvartet

The ^{13}C-NMR values of dyes are presented in table 3.

Table 3.*The ^{13}C-NMR values of compounds*

Code	δ(ppm) (1)	δ(ppm) (2)
C^1	59.700	59.853
$C^2(C^6)$	137.819	122.724
$C^3(C^5)$	122.934	121.996
C^4	119.909	124.665
C^7	115.427	112.580
$C^8(C^{12})$	130.15	129.162
$C^9(C^{11})$	139.81	128.726
CH_3	-	15.458
CH_2	-	27.641
R	I	C_2H_5
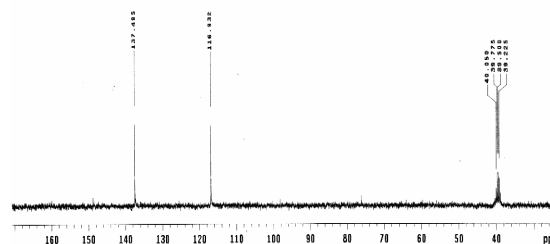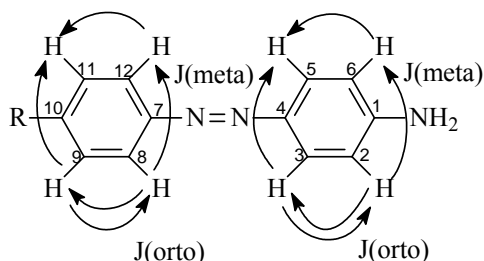
Figure 1.*The ^{13}C-NMR spectra of compound (1)*
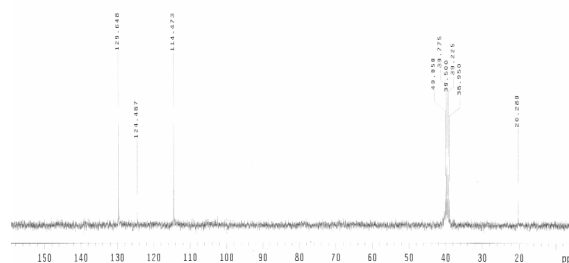
Figure 2. *The ^{13}C-NMR spectra of compound (2)*

References:

* E-mail address: ioana67@hotmail.com

[1]. H. Sanielevici, F. Urseanu, *Sinteze de intermediari aromatici*, Vol.II şi II, **145**, Ed. Tehnică, Bucureşti, 1983

[2]. L. Floru, H.W. Langfeld, C. Tărăbăşanu-Mihăilă, *Coloranţi azoici*, **296**, Ed. Tehnică, Bucureşti, 1981.

[3]. V. Pelloni-Tamas, F. Iohan, *Cromatografie pe strat subţire*, Ed. Tehnică, Bucureşti, 1971

[4]. A.T. Balaban, M. Banciu, I. Pogany, *Aplicaţii ale metodelor fizice în chimia organică*, Ed. Ştiinţifică şi Enciclopedică, Bucureşti, 1983

SYNTHESIS AND CHARACTERISTICS OF COMPACT CONDENSED SYSTEM 2-AMINOTHIAZOLO[5,4-f]INDAZOLE

CRISTIANA RĂDULESCU, IONICA IONIȚĂ, ANA MARIA HOSSU
"Valahia" University of Târgoviste, Faculty of Science, Department of Chemistry, Unirii Bdvl. 18-20, Târgoviste, Romania, mail: radulescucristiana@yahoo.com.

Abstract: *In this present study an original heterocyclic compact condensed system with thiazolic ring, 2-aminothiazolo[5,4-f] indazole was synthesized. In laboratory was tested an original alternative for the synthesis of this heterocyclic system by obtaining intermediary N-6-thiazolotioureea.*

The liquid chromatography of high performance, HPLC, was applied in this case, leaded at the separation and purification of the heterocyclic compound 2-aminothiazolo[5,4-f]indazole.

IR, UV-VIS, NMR spectroscopy and elemental analysis characterized the structure of heterocyclic system synthesized.

Introduction

The compact condensed heterocyclic systems with thiazolic ring are easy to be synthesized, using a variety of methods: either classic methods of heterocycles starting from compounds in which the thiazolic ring already preexist, or generating the thiazolic ring from the diverse heterocyclic structures of aromatic type. The compact condensed heterocyclic systems are solid products with very high melting points having the tendency to decompose before reaching them.

The thiazolic ring determines a great stability doubled by a remarkable biological activity, this fact leads to their application in many fields of interests.

Experimental part

Heterocyclic system 2-aminothiazolo [5,4-f]indazole was obtained by synthesis, in pharmaceutical scope, using a quotation method in the specific literature[1] for some thiazolo-indazolic compounds – sulphocyanuration of 5-aminoindazole with dirodan, generated "in situ" by bromine action about $Cu(SCN)_2$.

The original synthesis was proposed[2-4] lead at stage presented in figure no.1.

The nitration reaction of *o*-toluidine was realized by analogy with a quoted method in specialty literature[5]; this method was required a nitric mixture formed of 84% sulphuric acid, 7,36% nitric acid and 6,9% water.

The results of my experimental researches is referring at dependence of selectivity nitration reaction by concentration sulphuric acid in nitric mixture, utilizing at the ratio molar *o*-toluidine: $HNO_3=1:1,02$ is presented.

The disadvantage of this method was: the transformation of *o*-toluidine in ammonium salt is not total and from this reason in the nitration reaction resulted 2-aminotoluen in great quantity. The elimination of this disadvantage was tested moreover the original methods of synthesis:

1. The increase of sulphuric acid concentration in the nitric mixture moves the equilibrium of the *o*-toluidine protonation reaction in the right part.
2. The adding Na_2SO_4 in the reaction mass, when the formatting sulphuric acid of *o*-toluidine was favorized by "common ion effect" (because the concentrate sulfuric acid was dissociated much less). The dependence of selectivity nitration reaction of *o*-toluidine in according with concentration sulphuric acid in nitric mixture and with the concentration Na_2SO_4 in reaction mass was presented in figure no. 2.
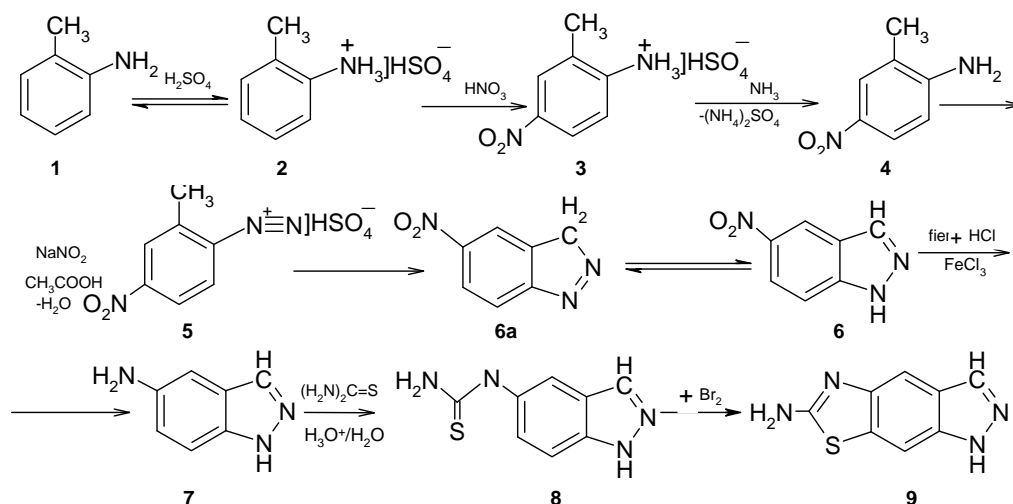
Figure no.1. Synthesis of heterocyclic system 2-aminothiazolo[5,4-f]indazole
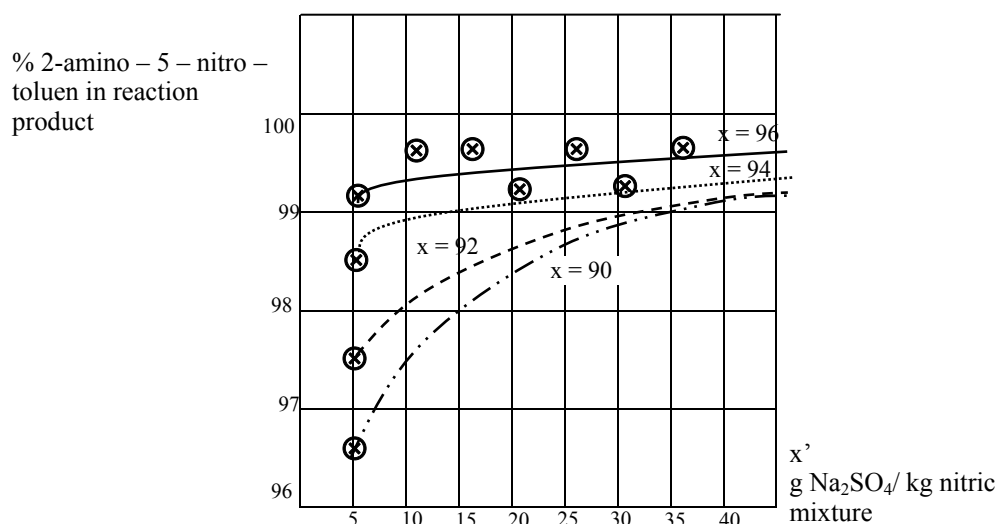
Figure no. 2. The dependence of selectivity nitration reaction in according with the concentration sulphuric acid in nitric mixture and with the concentration Na$_2$SO$_4$

In case of these two methods a significant increase of selectivity nitration reaction was observed, because was added sulphuric acid with concentration situated between 94-96% in the nitration mass. The increase of concentration acid cannot lead at significant increase of selectivity, probably was due at small variation of the dissociation degree of sulphuric acid in same time with the increasing concentration. The conclusions were:

- The results of research presented in figure no.1 were obtained at the concentrations H$_2$SO$_4$, in nitric mixture, situated between 90-96% (90 ≤ x ≥ 96), when the selectivity of process it's already remarkable (figure no.2). The adding Na$_2$SO$_4$, 25 ≤ x' ≥ 30,

leads at the increase, in each case, of total selectivity nitration reaction.

- The increase of the concentration Na$_2$SO$_4$ effect in reaction mass is significant at the x value near as 90. The concentration of sulphuric acid in nitric mixture is greatest and the adding Na$_2$SO$_4$ effect is very small significant under selectivity aspect. This fact is normal, because both factors (the increase of x and x' values) were acted about qualitative system in same way (the increase of anion HSO$_4^-$ concentration) they were compensate with quantitative aspect.

The determination of product reaction composition was realized after purification by

recrystallization and continued of elution column by HPLC chromatography.

For to assure the homogeneity of reaction mass before nitration, *o*-toluidine was dissolved in sulphuric acid 100% (molar ratio H_2SO_4:*o*-toluidine=6,1:1). Also, the increase of selectivity nitration reaction in according with the increase of x can be attributed to diminution of concentration as amine in reaction mass and this thing leaded at the increase homogeneity of system, prevented the precipitation of sulphat acid of *o*-toluidine, difficult soluble in H_2SO_4 concentrated. In this case the reaction rate was small and in this motive was necessary a long time as reaction, over 12 hours. This time, over 12 hours, leads at the total conversion of *o*-toluidine and for that motive the selectivity of process may be assimilate with global yield.

Under thermic aspect, the process most be operated at temperature -12^0C for to decrease the oxidant effect of nitric acid about amino group. When the nitration was finished, the reaction mass was added over water at temperature under 60^0C and then the suphat acid of 2-amino-5-nitrotoluene precipitate was separated as o-toluidine, soluble, then was filtrated. In next stage, the sulphat of 2-amino-5-nitrotoluene was dissolved in water at 50^0C, then was treated with NH_3 25% until pH~7,5 and finally precipitate compound **4**.

5-Nitroindazole was synthesized in accordance with method presented in specialty literature[6].

The reduction of 5-nitroindazole was nest stage and for obtaining of optimal yield was necessary a selection both a reducing agent and a reaction conditions, because can appeared secondary product: aromatics amine by degradation of indazolic ring, azoxiderivatives, azoderivatives, etc.

Consulting the literature[5] was chose the reducing agent: iron in presence of electrolytes solution, in very thin acid medium or neutral medium (reduction Béchamps). The work conditions for this reaction for synthesis of 5-aminoindazole was: the electrolyte $FeCl_2$, was formed in reaction mass by treating the iron with HCl dilutee solution, at the reflux temperature, under stirred, and the optimal molar ratio was 13,88 moles water:0,16 moles HCl 36%:0,80 moles iron; then was added 5-nitroindazole, in small quantity, in one hour, under stirred, the molar ratio chose was 0,80 moles iron:0,1 moles 5-nitroindazole and the pH=5,5-6; in permanence was verified the end of reduction reaction by the analysis of aureole formed as black iron oxides. For an efficient reduction and for obtaining a good yield, the time of reduction reaction was 8 hours. Finally, the reaction mass was alkalinized with NaOH solution until at pH~7,5. For diminution[2] of reaction time, in the beginning in reaction medium was added 1-5% zinc, because in this case was realized an efficient "chemical corrosion" of iron, leading to the increase of chemical rate of reduction process.

In laboratory[2] was tested a *new original method for synthesis of 2-aminothizolo[5,4-f]indazole*, **9**. In this alternative N-(5-indazolile) tioureea was obtained by direct arilation of tioureea with 6-aminoindazole in acid catalyze. The optimal parameters for this synthesis was: molar ratio 6-aminoindazole:tioureea=1:5; reaction medium is HCl solution 5% and reflux temperature was applied in process; time for reaction was 12 hours; the isolation of N-(5-indazolile) tioureea was realized by alkaline treatment with NH_3 solution 25%.

Results and discussion

The purification of the synthesized organic compounds was realized by recrystallization of organic solvent for eliminating the resinous product and by HPLC chromatography. Also, the purity verification was effected by thin layer chromatography and by melting points determination. For to separate the trace of impurities, the final compounds was analyzed, developing was realized with Erlich reactive or by diazotation - cupling reaction with aromatic amine N-substitute or N,N-substitute. The results were centralized in table no.1.

**Table no. 1. The purification methods of organic compounds *4 - 9***

Compound	The purification method	Melting point, ^{0}C	λ_{max}, nm (Extincţia)
5-nitro-*o*-toluidine, **4**	• *Recrystallization* of ethylic alcohol, resulted yellow-orange prisms. • *Thin layer chromatography:* -*Substratum*: silica gel (F_{254}-Merck) on aluminium layer. - *Eluent* : ethylic alcohol: CH_3COOH = 10 : 90 (vol / vol) R_f = 0,82; unitary spot, pure substance • *The high performance liquid chromatography (HPLC)* -*Column* and *flow*: Nucleogen® 4000-7 DEAE, 2 mL/min -*Eluent*: 0,5 M NaCl, 6M urea, 25 mM phosphate of sodium -*Detection*: λ_{max} = 356,1 nm	108 – 109	219,6 (0,791) 244,1 (0,753) *356,1 (0,262)*
5-nitroindazole, **6**	• *Recrystallization* of ethylic alcohol, resulted yellow crystals • *Thin layer chromatography:* - *Substratum*: silica gel (F_{254}-Merck) on aluminium layer. -*Eluent* : ethylic alcohol : acetic acid = 10 : 90 (vol / vol) R_f = 0,75; unitary spot, pure substance • *The high performance liquid chromatography (HPLC)* -*Column* and *flow*: Nucleogen® 4000-7 DEAE, 2 mL/min -*Eluent*: 0,5 M NaCl, 6M urea, 25 mM phosphate of sodium -*Detection*: λ_{max} = 329,5 nm	208 – 209	207,8 (1,711) 243,8 (2,207) 279,3 (1,564) *329,5 (0,602)*
5-aminoindazole **7**	• *Recrystallization* of ethylic alcohol obtained aces white - gray. • *Thin layer chromatography:* - *Substratum*: silica gel (F_{254}-Merck) on aluminium layer. - *Eluent* : ethylic alcohol : acetic acid = 10 : 90 (vol / vol) R_f = 0,64; unitary spot, pure substance • *The high performance liquid chromatography (HPLC)* -*Column* and *flow*: Nucleogen® 4000-7 DEAE, 2 mL/min -*Eluent*: 0,5 M NaCl, 6M urea, 25 mM phosphate of sodium -*Detection*: λ_{max} = 377,5 nm	210 – 211	210,9 (1,363) 288,8 (0,446) *377,5 (0,165)*
2-aminotiazolo [5,4-f] indazole, **9**	• *Recrystallization* of ethylic alcohol, obtained brown powder. • *Thin layer chromatography:* - *Substratum*: silica gel (F_{254}-Merck) on aluminium layer. - *Eluent* : ethylic alcohol : acetic acid = 10 : 90 (vol/vol) R_f = 0,52; unitary spot, pure substance • *The high performance liquid chromatography (HPLC)* -*Column* and *flow*: Nucleogen® 4000-7 DEAE, 2 mL/min -*Eluent*: 0,5 M NaCl, 6M urea, 25 mM phosphate of sodium -*Detection*: λ_{max} = 378,2 nm	218 – 219	210,8 (0,559) 239,9 (1,178) 286,4 (0,326) *378,2 (0,020)*

The high performance liquid chromatography was applied in this case, using apparatus JASCO 800, for leading at the separation and purification of the compounds synthesized. For this case were used the gel-permeable columns, Nucleogen® 4000-7 DEAE, (Table no. 1) considered to be the best and the most appropriate because they allow retention times long enough for an efficient separation and do not present the colmation phenomenon for the heterocyclic system.

The UV-VIS electronic spectra[7] were performed with SECOMAN S 750 apparatus in quartz cells for ethylic alcohol of c ~ $2 \cdot 10^{-5}$ M of the synthesized compounds. The absorption bands characterized by maximum wave length are presented in same table.

The IR spectrum were made including the synthesized compounds in KBr disks, absorption been measured with SPECORD 75 IR apparatus and the results were analyzed by O'Sullivan[8] for a general structure:
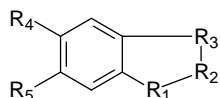
and R_1, R_2, R_3 can be CH_2, NH, O, CO, SO_2, CH, NH and demonstrated R_4 and R_5 groups modified a little the IR spectrum for this general structure (in spectrum will find characteristics of vibration for R_4 and R_5 that can be NO_2, NH_2, COOH, CN). The O'Sullivan theory must emphasized same characteristic vibrations for indazolic and benzothiazolic, heterocyclic systems "fused" in molecule.

The IR spectrum of general heterocyclic system presented bands at the 1600, 1460, 1390, 1310, 1270, 1250, 1200, 1160, 1100, 1060, 1020, 950, 890, 850 and 750 cm^{-1}.

- The IR spectrum of 5-nitroindazole was characteristics band at 1660, 1480, 1325, 1265, 1140, 1110, 1040, 850 and 750 cm^{-1} and these values was presented, also, 5-aminoindazole and 2-aminothiazolo[5,4-f] indazole.

- The indazolic derivatives can exist under more tautomere forms. The behavior of atoms group –N=N-, respectively –C=N- was less differentiates in IR spectrum, stabilized at 1620 cm^{-1} values. We propose as by analysis of IR spectrum, in case of indazolic compounds, establishing of preponderant tautomere forms. In these products the weight of hydrogen bond intermolecular N – H ….N is very important, because the large band attested the implication of NH group in very strong hydrogen bond.

- The values ν_{NO_2} symmetric = 1359 cm^{-1}, respectively ν_{NO_2} asymmetric = 1537 cm^{-1} confirming the fact these groups isn't implicated in hydrogen bond.

- The –NH_2 groups were observed, in IR spectra, about sharps bands of vibrations; the band more high correspond to asymmetrical valence vibration, (3400 cm^{-1} for 5-aminoindazole and 34250 cm^{-1} for 2-aminothiazolo[5,4-f]indazole), and this with the more small correspond of symmetrical valence vibration (3350 cm^{-1} for 5-aminoindazole and 3340 cm^{-1} for 2-aminothiazolo[5,4-f]indazole).

- The bands situated at 655 and 625 cm^{-1} corresponding C – S bond.

- The structures proposed was confirmed in accordance with the values found about the benzothiazolic and thiazolic systems: ν=1620, 1580 respectively, 980, 920 and 850 cm^{-1}.

- The bands of indazolic ring ν_{NH} = 3385 cm^{-1}, ν_{CH} = 3050 cm^{-1} and 2935 cm^{-1} confirming the structure proposed.

The study of IR spectrum[9] attested the structure propose suggesting the next fact: all derivatives studies that included the indazolic structures there is preponderant under azometinic tautomere.

The compounds **4-9** were analyzed by NMR spectroscopy using VARIAN GEMINI 300 BB apparatus, with frequency of registration in case ^{1}H-NMR is 300 MHz and in case ^{13}C-NMR the frequency is 75 Hz. The purified prove was soluble in DMSO and signals was reported at TMS. We select compounds **9** to present in NMR spectra.

^{1}H-NMR spectrum for 2-aminotiazolo [4,5-f]indazole leads at the signals (figure no.3)

- At benzene nucleus the protons was: H^1 – *singlet*, δ_H : 6,72 ppm and H^4 – *singlet*, δ_H : 5,96 ppm (the coupling constants, J, were zero, because in position 2 and 6, respectively 3 and 5, the carbon atoms of benzene ring cannot have protons, in accordance with structures **9** and **9a**). .

- The signals of proton, –CH=, was attributed of δ_H: 8,50 ppm, *split doublet*, with the coupling constant J = 8,60 Hz emphasized tautomere structure **9**).

- The protons of group –CH_2, were attributed of δ_H : 7,25 ppm, *split doublet,* with the coupling constant J = 8,60 Hz.

- The signals of 4,66 ppm, *singlet*, has been attributed the presence of amino group.

- The proton of –NH group present signal at 4,76 ppm, *singlet.*
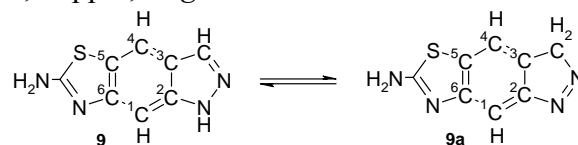
The presence a two tautomere forms for system 2-aminothiazole[4,5-f]indazole was indicated as the same coupling constant, J = 8,60 Hz, for both protons.
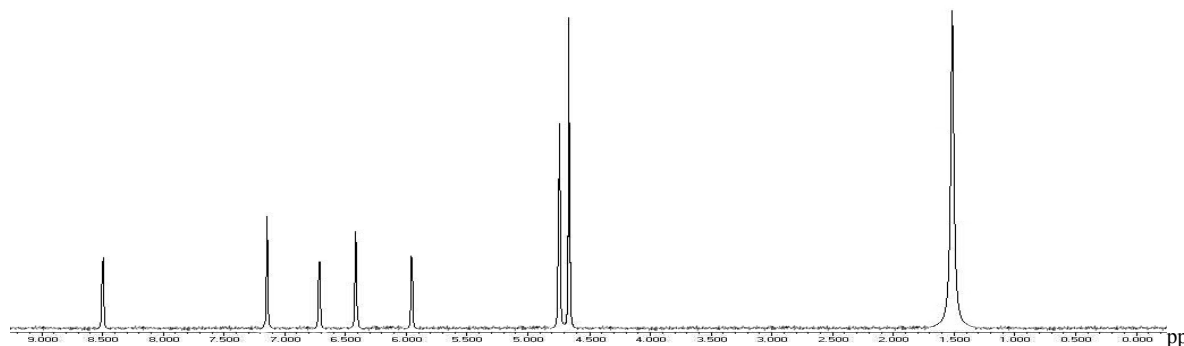
m

Figure no. 3. The ^{1}H-NMR spectra of compound 2-aminothiazolo[5,4-f]indazole

The ^{13}C-NMR spectra (figure no. 4) present next signals for carbon atoms:
- The carbon atoms present signals, for both tautomere forms: 123,7 and 110,9(C^5); 107,0 and 95,6 (C^1); 137,9 and 143,9(C^2); 108,7 and 117,9(C^3); 149,0 (C^6) and 128,9(C^4) ppm.

- The carbon atoms of –CH= and –CH$_2$ groups present the signals δ: 140,0, respectively 59,0 ppm.
- The signal, δ: 130,0 ppm, has been attributed at carbon atom on thiazolic ring.

ppm

Figure no. 4. The ^{13}C-NMR spectra of compound 2-aminothiazolo[5,4-f]indazole

The elementary analysis results were presented in table no. 2.

Table no. 2. Elemental analysis of compounds *4 - 9*

Comp.	C	%	N	%	O	%	S	%
	Calc.	Exp.	Calc.	Exp.	Calc.	Exp.	Calc.	Exp.
4	55,26	55,12	18,42	18,41	21,05	21,03	-	-
6	55,26	55,09	25,76	25,61	19,63	19,59	-	-
7	55,26	55,01	31,57	31,32	-	-	-	-
9	50,52	50,39	29,47	29,13	-	-	16,84	16,76

Conclusions

A new original synthesis methods of 2-aminothiazo[5,4-f]indazole was elaborated by intermediary preparation of derivate N-piridil tioureici, which were oxidized with liquid bromine.

Was obtained a new compact condensed system by an original methods, very profitable both technological and economical.

The synthesized compounds were characterized by *IR, UV-VIS* and *RMN* spectroscopy, thin layer chromatography, HPLC, elementary analysis and decomposition points.

References

[1] Bellavita, C., Maratani, N., Avialdo, *F.A., Ann. Chem*, 1968, **58**, 823.

[2] Radulescu C., *Ph. Dr.*, 2003, Faculty of Industrial Chemistry, Bucharest, Romania

[3] Radulescu C., Tarabasanu Mihaila C., *The Chemistry Review,* 2004, **55(1)**., 25-30, Bucharest, Romania

[4] Radulescu C., Tarabasanu Mihaila C., *The Chemistry Review,* 2004, **55(2)**, p. 94, Bucharest, Romania

[5] Sanielevici, H., Floru, L., *The synthesis of aromatics intermediary and of dyes,* 1971, vol. I and II, E.D.P, Bucharest

[6] Meunier, J., *Bull.Soc.Chem*, France, 1904, 641

[7] Balaban A. T., Banciu M., Pogany I*., The applications of physic methods in organic chemistry*, 1983, Ed. Scientific and Encyclopedic, Bucharest, Romania

[8] O'Sullivan, D.G., *J. Chem. Soc*. 1960, **8**, 3278
    Avram, M., Mateescu, Gh., *"The IR spectroscopy. The application in organic chemistry"*, Ed. Technique, Buchares

CATIONIC DYES DERIVATIVES OF COMPACT CONDENSED SYSTEM 2-AMINOTHIAZOLO[5,4-f]INDAZOLE

CRISTIANA RĂDULESCU[1] ANA MARIA HOSSU[1], IONICA IONIȚĂ[1]

[1]University ''Valahia'' Târgoviste, Science Faculty, Chemistry Department, 18-22 Unirii Bdvl., Târgoviste, Romania, mail: radulescucristiana@yahoo.com

Abstract

The synthesis and characterization of some new cationic dyes derivatives from heterocycle system with thiazolic ring, 2-aminothiazolo[5,4-f]indazole were described. These dyes were elucidated by chemical and spectral analyses, UV-VIS, NMR and infrared analyses, confirming the structures propose. The results obtaining by dyeing polyacrylic fibers (intense and brightness color, fastness to washing, fastness to perspiration, fastness to boiling and to blenching, exposure to sunlight, ability to be absorbed a beginning from retained by the fiber) and the relationship between chemical structure of some cationic dyes and perspiration/light fastness was discussed.
Keywords: *2-aminothiazolo[5,4-f]indazole, dimetilsulphate, cationic dye, polyacrylic fiber*

Introduction

The cationic dyes derivatives from heterocycle system 2-aminothiazolo[5,4-f] indazole were obtained for first time by original synthesis.

In these synthesis the cationic dyes never been quoted in the specific literature and never been purified by classic methods of purification. And this thing was happened because the diazotizing reaction was incomplete and resulted big quantity of phenolic products by decomposition of diazonium salts.

The results of my research were leaded to the diminution of phenolic compounds in reaction mass and the removing these.

In the paper was investigated the synthesis of new cationic dyes (blues); were studied by chemical, UV-VIS, NMR, infrared analyses and the results of dyeing polyacrylic fibers.

Experimental part

The heterocycle system 2-aminothiazolo[5,4-f] indazole was diazotized in phosphoric acid 80% medium with $NaNO_2$ 25% solution, at -12^0C, time 4-5 hours. Diazonium salt obtained was treated with varied coupling compounds (table no.1) in phosphoric acid 80% and acetic acid in excess,

at -10^0C; the time necessary was 2-3 hours. Finally about 8 hours, precipitated the disperse dyes, reds (figure no. 1); these dyes were purified by recrystallization of ethyl alcohol and separated by HPLC.[1-3]

The disperse dyes were methylated with dimethyl sulfate at acetic acid medium, at excess, molar ratio was $(CH_3)_2SO_4$:disperse dye=3:1, at $60-70^0C$, time 12-14 hours, (the cromatograma indicated total conversion), under stirred. The next stage was the condition with NaCl, time 15 minutes, at 70^0C, when resulted blues cationic dyes (figure no. 1 and table no. 1); these were purified by recrystallization in ethyl alcohol and HPLC.[2]

The cationic dyes synthesized were used for dyeing polyacrylic fibers and cotton/PNA texture (mixture). The polyacrylic fiber and the texture had been scoured at 60^0C, at time ½ hour, and dried under vacuum for 48 hours at room temperature prior to dyeing.

The dyebath (200 ml) was prepared at room temperature with cationic dye (2,0% aqueous solution) acetic acid 1% solution and sodium sulphate 10% solution and adjusted to Ph = 1; the fleet rapport was 1:40. The dyebath temperature was raised to 60^0C, 70^oC and 100^0C and held constant during the whole dyeing process. The dyed polyacrylic fiber (similar the texture) was rinsed first in cold water and then boiling water to remove unfixed dye and dried at room temperature.[4]
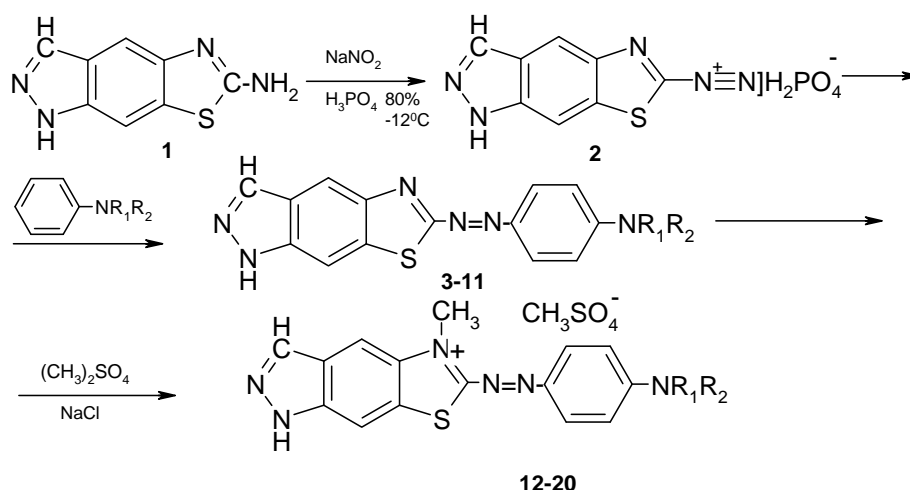
Figure no.1. The stages of synthesis cationic dyes **12-20**

Table no. 1. The cationic dyes obtaining by synthesis

Nr. crt	R_1	R_2	Colour coupler	Cationic dye	Color λ_{max}, nm and ε_{max}
12	H	CH_3			Blue light 590 nm 12300
13	CH_3	CH_3			Blue light 594 nm 12510
14	H	C_2H_5			Blue light 591 nm 12400
15	C_2H_5	C_2H_5			Blue light 595 nm 12850
16	H	C_2H_4OH			Blue 601 nm 12980
17	C_2H_4OH	C_2H_4OH			Blue 605 nm 13100
18	CN	C_2H_5			Blue 608 nm 13400
19	CH_3	C_2H_4OH			Blue 604 nm 13200
20	C_2H_5	C_2H_4OH			Blue 607 nm 13330

Results and discussions

Purification methods (recrystallization of ethyl alcohol and chromatographic methods) the melting points and yields of cationic dyes are presented in table no. 2.

Disperse and cationic dyes were studied employing chemical, UV-VIS, NMR and IR spectroscopy, confirming the structures proposed.

Table no. 2. The purification methods, melting points and the yields of cationic dyes

Cationic dyes	Chromatographic thin layer method	HPLC method	Melting point, ^{0}C	Yield, %
12 - 20	*Substratum*: silica gel F_{254} (Merck) on aluminium layer *Eluent:* dioxane: formic acid : water=1:3:1 *Solvent*: water, sol. 0,01%	*Column*: Nucleosil® 100-5 C_{18}PPN *Eluent A*: Trimethylammonium acetate 0,1M : acetonitrile : water = 90:5 (v/v) *Eluent B*: Trimethylammonium acetate 0,1M : acetonitrile : water = 30:70 (v/v) *Linear gradient* from 15% at 40% B. *Flow*: 1 mL/min. *Detection,* λ_{max}= 590-608 nm	>250	58,1-67,2

In case of cationic dyes **12-20** the problem that appeared was: in where place was fixed the –CH_3 group resulted by the metylation with dimetylsulphate, at nitrogen atom from indazolic ring or at nitrogen atom from thiazolic ring.

The grafting position of –CH_3 group for the thiazolobenzothiazols compounds was established by differential analysis[11] and by ^{1}H-NMR spectroscopy correlated with results obtained by IR analysis.[2]

The UV-VIS electronic spectrum were performed with *SECOMAN S 750* apparatus in quartz cells (L=1cm) for ethyl alcohol of c~2 10^{-5} M of the synthesized compounds. The molar extinction coefficient, ε_{max}, characterized by maximum wave length are presented in table no. 1.[5]

The IR spectrum[5,12] was made including the synthesized compounds in KBr disks, absorption been measured with *SPECORD 75 IR* apparatus and the results were:

• The IR spectra of disperse and cationic dyes confirm the proposed structures in accordance with the values found about the thiazolic ring: ν = 1610, 1055-1100 and 2100-2400 cm^{-1}.

• The bands of indazolic system ν_{NH}=3155 cm^{-1}, ν_{CH}=3060 cm^{-1} and 2930 cm^{-1}, but and specific bands placed between 1380-1071, respectively 850–740 cm^{-1} confirming the structure proposed.

• The –$N(CH_3)_2$ group was identified at all disperse and cationic dye because the absorption band for this group (especially when is bound to aromatic ring) is one single and appear at 2800 cm^{-1}.

• The azo chromophore group, -N=N-, was characterized as faints absorptions, as small intensity, at 1500-1600 cm^{-1} and 1020-1050 cm^{-1}.

• The alkylated nitrogen was identified at cationic dyes at 1260-1290 cm^{-1} frequency, for two bands.

The disperse and cationic dyes were analyzed by NMR spectroscopy[5] using *VARIAN Gemini 300 BB* apparatus, with frequency of registration in case ^{1}H-NMR is 300 MHz and in case ^{13}C-NMR the frequency is 75 Hz. The purified prove was soluble in DMSO-d_6, and the signals was reported at TMS. We select illustrative, cationic dye **13** to present in NMR spectra.

The ^{1}H-NMR spectra for cationic dyes blue**, 13** purified by HPLC, lead to the signals:
H^1 – *singlet*, δ_H: 6,41 ppm.
H^4 – *singlet*, δ_H: 7,02 ppm.
H^8, H^{12}–*split doublet*, δ_H:6,67 ppm, with coupling constants *orto* J(9,8) = 8,00 Hz and *meta* J(8,12) = 1,50 Hz.
H^9, H^{11}–*split doublet*, δ_H:6,10 ppm, with coupling constants *orto* J(9,8) = 8,00 Hz and *meta* J(9,11) = 1,50 Hz.
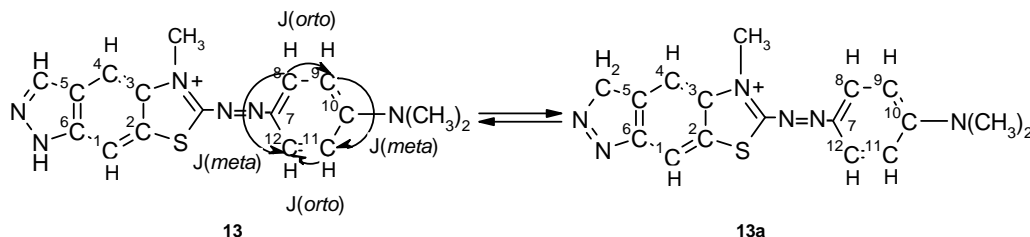
The six protons of –N(CH$_3$)$_2$ group present signal at 2,49 ppm, *singlet* and the protons of –N$^+$-CH$_3$ group present signal of 2,30 ppm, *singlet*.

The proton of –NH group, indazolic ring, was attributed to signal of 4,76 ppm, *singlet*.

The proton from –CH, indazolic ring, was attributed the *triplet* of 7,10 ppm.

The ^{13}C-NMR spectra present next signals for carbon atoms:

The carbon atoms C^1 and C^4 present signals of δ: 110,0 ppm, respectively 127,9 ppm.

The carbon atoms C^2, C^3, C^5, C^6, present signals of δ: 113,7; 137,0; 133,4; 101,0 ppm.

The carbon atoms C^8, C^{12} and C^9, C^{11}, present next signals δ: 122,2 ppm and 112,2 ppm; C^7 and C^{10} δ: 140,6 ppm and 152,1 ppm.

The signal δ: 125,0 ppm has been attributed at carbon atom on thiazolic ring.

The signals 7,70 ppm and 43,6 ppm were attributed to carbon atoms from –N$^+$-CH$_3$ and–N(CH$_3$)$_2$ groups.

13   **13a**

The polyacrylic fiber and cotton/polyacrylic fiber textures were submitted the qualitative tests by estimation fastness shades with grey scale; the results were expressed by note from 1 at 5.[6,13]

Table no. 3. The fastness* test of cationic dyes on polyacrylic fibers

Cationic dye	Cool water fastness	Light fastness	Washing fastness 40^{0}C	Perspiration fastness acid (pH=5,5)	Perspiration fastness alkali (pH=8)	Ironing fastness	Friction fastness
12	4	4	3-4	4	4	3-4	4
13	4	4	3-4	4	4	3-4	4
14	4	4	3-4	4	4	3-4	4
15	4	4	3-4	4	4	3-4	4
16	4	4	4	4	3-4	4	4
17	4	4	4	4	3-4	4	4
18	4	4	4	4	3-4	4	4
19	4	4	4	4	3-4	4	4
20	4	4	4	4	3-4	4	4

These fastness measures were made in accordance with strength standards.

The perspiration/light fastness at cationic dyes increases if used colorant solution 2-3%. This aspect determines the improvement at the dyeing fastness with ½-1 tone.[7-9]

The cationic dyes derivatives from 2-aminothiazolo [5,4-f] indazole dyeing polyacrylic fibers and cotton/polyacrylic fiber texture in bright blue shades, with good perspiration/light fastness, good ironing fastness and friction fastness, but was less good the washing fastness at 40^{0}C (table no. 3 and no. 4).

The relationship between colour and perspiration/light fastness test was influenced by coupler colorant. Also, the number of electrons donating group in cationic dye molecule lead at displace of absorption maximum at greatest wave lengths and implicit at light fastness diminution.[10]

The affinity of synthesized cationic dyes depend on presence of the functional groups in dye molecule, also the dispersion degree at dye and the polyacrylic fiber nature dyeing submitted.

Table no. 4. The fastness[*] test of cationic dyes on cotton/polyacrylic fibers texture

Cationic dye	Cool water fastness	Light fastness	Washing fastness 40^{0}C	Perspiration fastness acid (pH=5,5)	Perspiration fastness alkali (pH=8)	Ironing fastness	Friction fastness
12	4	4	3	4	3-4	4	4
13	4	4	3	4	3-4	4	4
14	4	4	3	4	3-4	4	4
15	4	4	3	4	3-4	4	4
16	4	4	3	4	3-4	4	4
17	4	4	3	4	3-4	4	4
18	4	4	3	4	3-4	4	4
19	4	4	3	4	3-4	4	4
20	4	4	3	4	3-4	4	4

Conclusions

Were obtained new cationic dyes derivatives of 2-aminothiazolo[5,4-f]indazole, by an original method, very profitable both technological and economical. The synthesized cationic dyes were characterized by IR, UV-VIS and NMR spectroscopy, thin layer chromatography, HPLC and decomposition points. These dyes were used with success in dyeing process of polyacrylic fibers and the fastness values tests and this thing is proved.

References

[9] Radulescu C., *The Chemistry Review*, 2003**, 54(12)**, p. 965-968 , Bucharest, Romania

[10] Radulescu C., *Ph. Dr.*, 2003, Faculty of Industrial Chemistry, Bucharest, Romania

[11] Radulescu C., Tarabasanu Mihaila C., *The Chemistry Review,* 2004**, 55(2),** p. 102-105, Bucharest, Romania

[12] H. Sanielevici, L. Floru, *The synthesis of aromatics intermediary and of dyes,* 1971, *vol. I and II*, E.D.P, Bucharest

[13] Balaban A. T., Banciu M., Pogany I.*, The applications of physic methods in organic chemistry*, 1983**,** Ed. Scientific and Encyclopedic, Bucharest, Romania

[14] Radulescu C., Tarabasanu Mihaila C., *The Chemistry Review,* 2004**, 55(1),** p. 25-30, Bucharest, Romania

[15] Ball, P., Nicholls, C. H., *Dyes Pigments*, **3, 5**, 1982

[16] Okada, Y., Kato, T. and Morita, Z., *J. Japan Res. Assoc Textile End Uses*, **32 , 171**, 1991

[17] Okano, S., *J. Japan Assoc Textile*, **32, 194,** 1991

[18] K. Kelemen, *Dyes Pigments,* **3,27**, 1982

[19] Tarabasanu, C.M., Floru, E., Balta, P., *Rev. Roumaine Chimie*, **18, 889**, 1973

[20] Avram, M., Mateescu, Gh., *IR spectroscopy. Applications in organic chemistry*, 1966, Bucharest

[21] Radulescu C., Tarabasanu Mihaila C., Ionita I., Hossu A. M., *The Ist International Conference of Moldavian Chemical Society*, 2003, **189**, Chisinau, Republic of Moldova

OXIDATION OF EDIBLE OILS AS STUDIED BY CHEMILUMINESCENCE (CL) METHOD

Radu SETNESCU[a,b*], Tanţa SETNESCU[a,b], Silviu JIPA[a,b], Nicoleta BĂLAŞA[c], Ion MIHALCEA[c]

[a]Valahia University of Târgovişte, Faculty of Science, Dept. of. Chemistry, Bd. Regele Carol I, nr. 2, Târgovişte, ROMANIA
[b]Research Institute for Electrical Engineering (ICPE-CA), Laboratory for Radiation Processed Materials and Luminescence Techniques, Splaiul Independenţei 313, Sector 3, Bucharest, ROMANIA
[b]University of Bucharest, Faculty of Chemistry, Dept. of Physical Chemistry, Laboratory of Radiation Chemistry, Bd. Regina Elisabeta 4-13, Sector 3, Bucharest, ROMANIA

*Corresponding author; e-mail: rsetnescu@yahoo.com

Abstract:

A possible correlation between chemiluminescence (CL) emission and oxidation of edible oil at elevated temperatures, usual for frying processes, has been studied based on similarity of the chemical structure of the oils and hydrocarbon polymers. CL emission was found to be dependent on temperature, activation energy values calculated from various CL parameters indicating the occurrence of an inhibited oxidation and oxygen diffusion controlled process. Specific CL curves were recorded from various types of oils, suggesting that CL could be used as an analytical technique for identification of nature, grade or origin of edible oils. Previous thermal oxidation at 130° induced a degradation that has been evidenced by changes in both CL parameters and IR spectra. Because CL and IR data are consistent, it was drawn the conclusion that CL could be used as a marker of thermal oxidative degradation. α-tocopherol induced a weak antioxidative effect that seems to increase as decreasing the temperature. In fact, a very slight improvement in stability was observed

1. Introduction

Lipid oxidation is a very important process related to foods preparation and degradation (alteration) and also to ageing processes in living organisms [1-5].

Several oxygen active species were identified as initiators of oxidation, and two main types of oxidation processes, namely thermal- and photo-oxidation are responsible for lipid oxidation [6, 7, 8]. Beside these mechanisms there is also the enzymatic peroxidation [1, 5].

It is well known that oxidation processes occur by mean of hydroperoxides and radicals, as a chain process that could be described by a Bolland Gee scheme [9-11]. In fact, similar scheme is used to explain the oxidation of hydrocarbons and of some polymers (such as natural rubber or polyethylene), that are more simple systems. In these cases, chemiluminescence (CL) emission is well related to oxidation and it becomes a useful method to investigate the oxidation kinetics, mechanism or to evaluate the effectiveness of various stabilizers [12-16].

Lipid systems are considerably more complicated than mineral oils or pure polymers. Therefore, is often difficult to apply traditional methods to study their oxidation, because the results could be contradictory, being influenced being influenced by various compositional factors. CL is very attractive to study lipid oxidation, because luminescence signal could be directly related to the reactions of hydroperoxides and peroxyl radicals, i.e. the

same species involved in oxidation mechanism. Actually, it was shown that there are several differences between lipids systems and hydrocarbons, and extrapolations should be carefully made.

CL was used to characterize the oxidation of some model compounds, such as linoleic acid [17]. In paper [18] a direct correlation of CL and oxidation extent (as it was described by concentration of malonic dialdehyde - a major product of lipid peroxidation) was reported. Similar results were reported also in papers [19, 20].

Recently, it was reported that CL signal increased after hydroperoxide concentration vas level of, that is the decomposition of lipid hidroperoxides lead to peroxyl radicals which react to product excited species responsible for light emission [21]. In other words, under these conditions, oxidation occurs before an increasing in CL signal. It was also tentatively applied to check the oxidation level (to detect the rancidity, or its beginning state) in various foods, such as vegetal edible oils [22, 23], milk powder and instant Chinese noodles [23], breakfast cereals and soda crackers [24] a.s.o. Cash and colab. tentatively estimated the shelf time of some vegetal edible oils, based on CL induction time, i.e. the period before the non-linear increasing of CL. They considered that traditional methods, such as analysis of concentration of secondary oxidation products, sub-evaluate the shelf time at low temperature [22]. However, the smell and coloration of the model system clearly appeared before the end of the induction period. Several standardized procedures were also proposed, but it is clear the field is not enough explored [25].

The aim of this work was to preliminary study the CL emitted from several edible oil samples during isothermal oxidation in order to check if CL could be a valuable test for characterization of oxidation at elevated temperatures (specific to frying processes). On the other hand, we intended to observe if CL curves are specific, to be applied as marker of the oil origin or grade.

2. Experimental

2.1. Materials

Commercial available grade edible oils were used in this study, namely:

- refined sunflower oil, recommended for both salad and frying; two different grades, produced by different enterprises and called "sample A" and "sample B" were analyzed;
- ground sunflower oil, sample C;
- olive oil, sample D.

All samples are viscous, clear liquids and yellow colored liquids, the most intense color (yellow-brown) being exhibited by sample C.

Pure d-α - tocopherol, has been used as an antioxidant. It was included in oil sample (5 cm^3) after accurate weighting and mixed by a glass rod. All samples were kept in refrigerator to avoid the effect of heat and light.

2.2. Methods

CL emission from initial or oxidized oil samples has been recorded by CL-RTL 97/03M apparatus, made by ICPE CA Bucharest (see Fig. 1a, b).
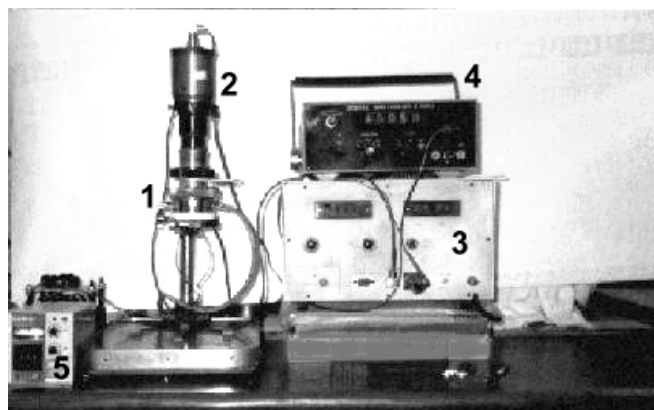

Fig. 1a - General view of the apparatus CL-RTL 97/03M (ICPE-CA): 1- sample unit (furnace and measuring cell); 2-photo-multiplier tube; 3- measuring unit, including high voltage supply; 4- thermometer; 5- temperature controller
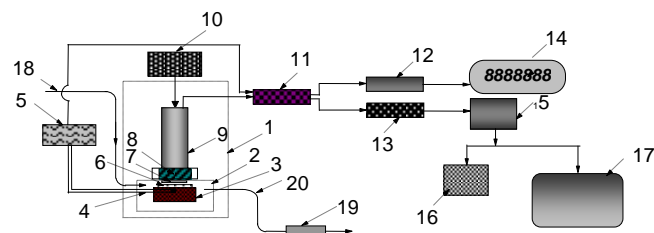

Fig. 1b - Bloc schema of the apparatus CL-RTL 97/03M (ICPE-CA): - light tight box; 2- oven; 3- heater; 4- thermocouple;

5- temperature controller; 6- sample; 7- lens; 8- shutter; 9- PM tube; 10- high voltage supply; 11- amplifier; 12- A/D converter; 13- interface; 14- digital data display; 15- computer; 16- printer; 17- computer display; 18- gas inlet; 19- flowmeter; 20- gas exit

A typical CL curve and parameters describing the oxidation kinetics are presented in Fig. 2 and Table 1 respectively.
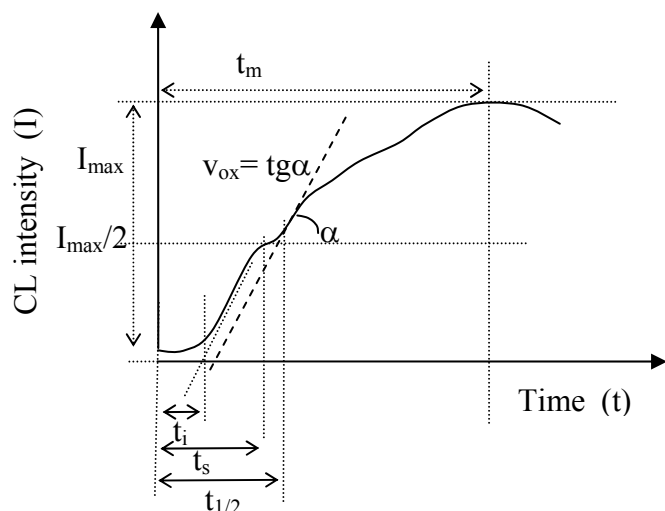

Fig. 2 - Typical CL curve from isothermal oxidation of an organic material

Weight loss of the samples during oxidation has been determined by sample weighting before and after measuring of CL. The calculation has been made using the formula:

$$\Delta_m = \frac{m_f - m_i}{m_i} \cdot 100 \qquad (1)$$

where m_i and m_f are the initial and respectively the final (after CL measurement) weight of the sample.

Table 1 - CL parameters related to oxidation process and their signification

Parameter	Significance
t_i	oxidation induction time
$t_{1/2}$	time requested for reaching half of CL intensity
t_S	time to reaching first CL shoulder
v_{ox}	oxidation rate
t_m	time requested for reaching maximum of CL intensity
I_{max}	maximum of CL intensity

The thermo-oxidative pre-treatment at 130° has been made in aluminum cells (50 mm in diameter and 8 mm in height), that where exposed in an air oven; the thickness of oil layer was 5 mm.

Infrared spectra were recorded in transmission using a Specord 75 IR (Karl Zeiss Jena) on oil films of about 100μ deposed between two PE thin films (20μm) separed by a spacer.

3. Results and discussion

3.1. Effect of the nature of oil on the CL curves

The analyzed oil samples exhibited different CL curves that seem to be dependent on the oil type or grade (see Fig. 3 and Table 2). Thus, we can observe that CL signal start to increase considerable latter with olive oil as compared to sunflower oil samples. This means that olive oil is more stable to thermal oxidation than other analyzed samples. It is well known that oil olive is recommended to be used in cooking and also that several oils, among them being included sunflower oil are sensible to oxidation because of their high content in polyunsaturated fat acids [26, 27]. Our result is in agreement with these observations, proving a higher oxidation susceptibility of olive oil.

On the other hand, we can observe some differences between the CL curves from the sunflower samples (A, B and C). Thus, the ground oil seems to be less emissive as compared to refined samples that emit more CL. This could be caused by some composition effects. We can suppose that there are some components in non-refined oil, which could play an antioxidative role. Another possibility is that one removable component is a quencher or light absorber of CL emission. First hypothesis is supported by the observation that CL increased slower, and I_{max} was reached latter in the case of ground sample as compared to samples A (see t_{max} values in Table 2).
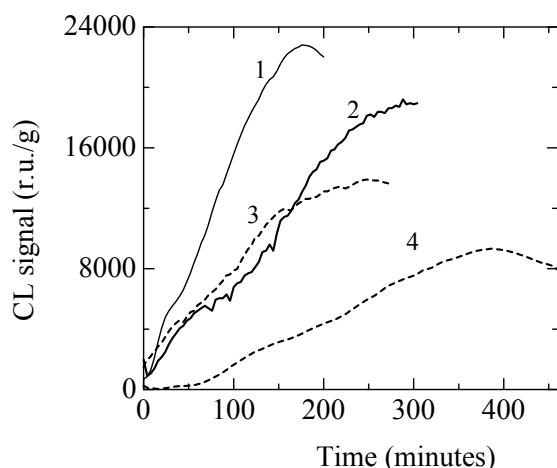
Fig. 3 - CL curves at 150° from some edible oils: 1 - refined sunflower oil (sample A); 2 - refined sunflower oil (sample B); 3- ground (non-refined) sunflower oil (sample C); 4 - refined olive oil (sample D)
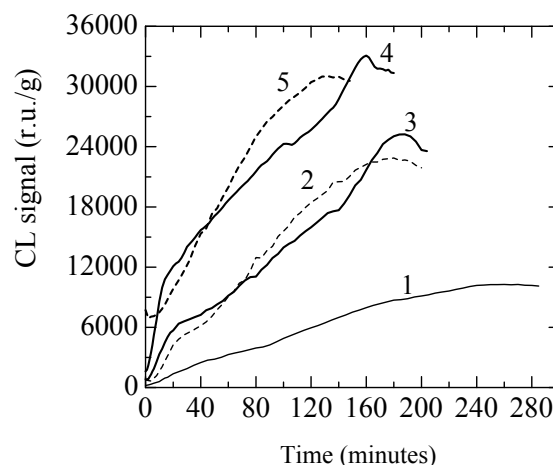
Fig. 4 - CL curves from sample A (refined sunflower oil) at various temperatures:
1- 140°C; 2 - 150°C, 3 - 160°C, 4 - 170°C; 5 - 180°C

Table 2 - CL parameters of oxidation at 150° of various oil samples

Sample	t_i (min.)	$t_{1/2}$ (min.)	t_m (min.)	v_{ox}[a]	I_{max} (u.r./g)	t_s (min.)
A	5	75	180	190	22800	23
B	8	140	299	33	19200	64
C	4	84	245	44	13400	40
M	64	208	384	30	9400	128

[a]measured in r.u/g.min.

On the other hand, there are some differences in oxidation kinetics in the case of samples A and B. This would be assigned to different stabilization effectiveness in these two samples.

A rancidity smell has been detected in the region of the first CL shoulder (see t_s values in Table 4). This suggests that t_i and/or t_s values could be related to the loss of comestible quality of the oil during oxidation. In this case, t_m and $t_{1/2}$ parameters, which are often used to characterize the polymer oxidation, could lose their importance.

3.2. Effect of temperature

It is well known that increasing of temperature leads to an increasing in oxidation rate, and as a result, CL intensity tends usually to increase. Similar tendency we can observe in the case of sunflower oil sample A when the CL intensity has been lower at lower temperatures (see Fig. 4).

We can observe sigmoid-shape curves, similar to those recorded from polymers but, in this case, especially at low temperatures, the oxidation rate seems to change for several times during oxidation, resulting several shoulders that could be assigned to oxidation of various oil components. In fact, CL curves from vegetable oils seem to be a composition of jointed sigmoids which would result either as successively oxidation of several components, or as successive oxidation of various oil layers. It was observed that, during oxidation, solid oxidized layers were successively separated toward the border of the cell.

CL parameters describing the oxidation kinetics are presented in Table 3.

Table 3 - CL parameters from oxidation of sunflower oil (sample A) at various temperatures

T (°C)	t_i (min.)	$t_{1/2}$ (min.)	t_m (min.)	v_{ox}[a]	I_{max} (u.r./g)	t_s (min.)	Δm ((%)
140	7,5	105	258	52	10 200	45	-13,88
150	6	62	188	111	21 240	30	-15,61
160	2	70	187	121	25 340	24	-20,57
170	0	45	162	139	33 425	13	-24,23

[a] in r.u./g.min.

It should be noticed also that at the end of the measurement (at t_{max}) all samples were solid films, exhibiting a rubber-like

consistency and yellow colored, the color being more intense as increasing the temperature.

We can also observe in Table 3 an increasing in weight loss of the samples during oxidation, as increasing the oxidation temperature. The observed weight changes are the result of several process which are competing during the oxidation: one is the oxygen uptake and crosslinking and it should result in an increasing in sample weight; another process is the loss of volatile products - low molecular weight components initially existing in the oil, or appeared from scission-oxidation processes.

When CL parameters in Table 3 are plotted in Arrhenius coordinates, straight lines were obtained as it is shown in Fig. 5. Activation energy values, corresponding to various stages of oxidation were derived from these curves (Table 4).

The value of E_a calculated from t_s (61.6 kJ/mol, i.e. 14.74 kcal/mol) suggest a contribution of both oxygen diffusion and antioxidative effects. On the other hand, this value is typical for decomposition of hydroperoxides in organic compounds [28]. Similar values of E_a were obtained from v_{ox} and I_{max}, while with Δ_m, (30.7 kJ/mol) considerably lower value has been provided. This last value of E_a is similar to those derived from $t_{1/2}$ and t_{max} and suggests that weight loss and intense oxidation (described by t_m and $t_{1/2}$) are strongly related.
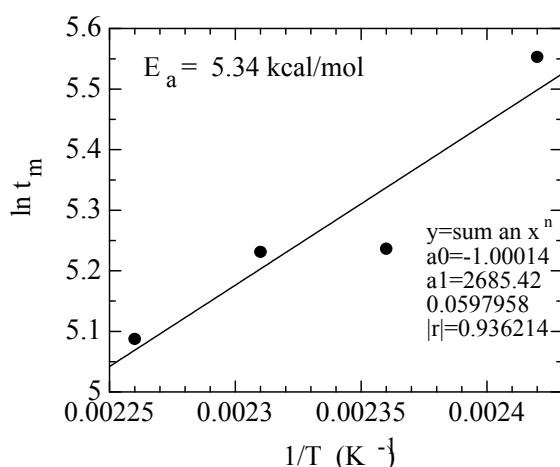
Table 4 - Activation energy and other parameters of Arrhenius plots for oxidation of sunflower oil (sample A) at various temperatures

	CL parameter used for E_a calculation					
	t_i	$t_{1/2}$	t_s	t_m	I_{max}	v_{ox}
E_a (kJ/mol)	97.5	38.4	61.6	22.3	59.2	48.6
ln A	26.25	6.61	14.11	1.00	26.61	18.28
Correlation	0.914	0.905	0.980	0.936	0.962	0.909

3.3. Thermooxidative pre-treatment at 130°C

Thermal oxidation at 130°C at various exposure times resulted in an expected decreasing in stability of the samples. This decreasing is proportional to the duration of the exposure (see CL parameters of pre-oxidized samples in Table 5). Pre-oxidized samples did not exhibit any induction period (t_i). The values of t_s decreased also quickly as a function of pre-oxidation time, as it is shown in Fig. 6.

Table 5 - CL parameters (at 150°C) and weight loss of pre-oxidized samples (exposed at 130°C for various times)

hours	t_i (min.)	$t_{1/2}$ (min.)	t_m (min.)	v_{ox}[a]	I_{max} (u.r./g)	t_{s1} (min.)	Δm ((%)
0	6	62	188	111	21 240	30	-15,61
2	-	86	196	105	19580	12	-14,36
4	-	45	141	148	31360	6	-6,43
8	-	50	185	133	24640	-	-5,6
12	-	36	165	87	26600	-	-5,26

[a]in r.u./g.min

Fig. 5 - Arrhenius plot of t_m as a function of temperature for oxidation of sunflower oil (sample A) at various temperatures
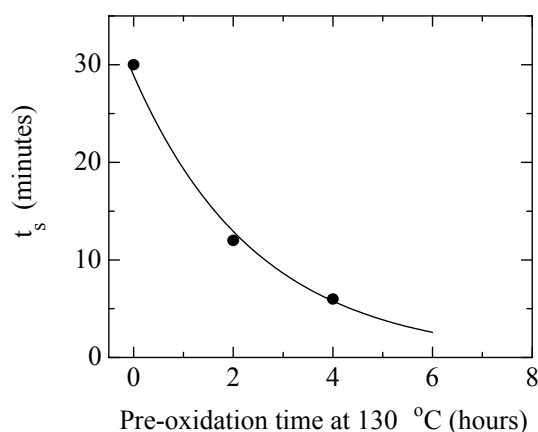

Fig. 6 - Decreasing in t_s values (at 150°C) of sunflower oil (sample A) pre-oxidized at 130°C for various periods

The shapes of CL curves from exposed samples seem to become more simple by disappearance of several shoulders that would be assigned to oxidation of several components.

The CL intensity from exposed samples is higher than in the case of unexposed ones; therefore CL (by means of t_s or I_{max} values) could be a marker of thermal oxidation exposure of oils.

Infrared spectra were also sensitive to oxidative changes, especially in the region of 3480 cm^{-1} (hydroperoxides, see Fig. 7) and 1720cm^{-1} (ketone carbonyl groups). However, this latter band is overlapped by the more intense absorption at 1760 cm^{-1}, due to carbonyl ester groups.

The hydroperoxide content increased after 4 hours exposure. This moment is corresponding to the disappearance of the first shoulder (t_s became 0) in CL curve, being an evidence to support the above hypothesis that related t_s oil and comestibility.
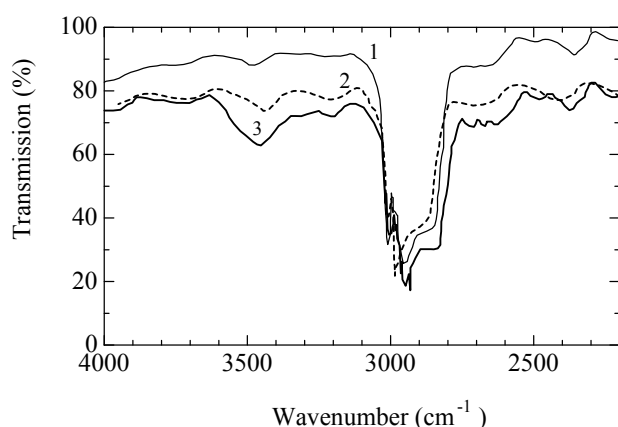

Fig. 7 - IR spectra in region of 4000 - 2200 cm^{-1} from some sunflower oil samples (A) previously submitted to thermal oxidation at 130°C: 1 - initial; 2 - 4 hours; 3 - 12.5 hours.

3.4. Effect of tocopherol

Tocopherol is well known as a fat soluble antioxidant [2, 3], being involved in various processes of lipid oxidation. The inhibition mechanism consists in radical trapping. Our experiments, carried out at elevated temperature, revealed a low antioxidative activity of α-tocopherol, as suggest a comparison of data presented in Table 6 and 3. We can clearly observe that the stability is basically the same, excepting a slight increasing in t_i and t_s values in the case of tocopherol containing samples.

Table 6 - CL parameters for oxidation at various temperatures of tocopherol containing sunflower oil (sample A)

T (°C)	t_i (min.)	$t_{1/2}$ (min.)	t_m (min.)	v_{ox} u.r./g.min.)	I_{max} (u.r./g)	t_s (min.)
140	18.5	86.5	233	86	14720	49
150	5	59	135	200	25760	20
160	4	60	141	314	47500	14,5
170	-	52	99	468	51600	6

This increasing in stability seems to be more significant at lower temperatures than at higher ones, and could be related to the known decreasing in activity of tocopherol at elevated temperatures [29]. A higher effectiveness is therefore expected at lower temperatures, which are not used in frying processes.

On the other hand, it is known that the antioxidative effectiveness of tocopherols decreases as increasing vitamin E [29], thus α-tocopherol should exhibit the weakest effect as antioxidant among the tocopherols. Similar results concerning a weak antioxidative effect of α-tocopherol in stabilization of several polyolefins were recently reported [30]. Moreover, antagonistic effects of tocopherol and some stabilizers added or contained in the oil could be supposed, because similar behavior has been observed in the case of oxidation of oil samples containing phenols, in spite that they exhibited very high activity in polyolefins. These results will be reported elsewhere.

The values of the activation energy calculated from various CL parameters concerning the oxidation of tocopherol containing oil, could be gathered in three main categories, namely:

- low values, in the cases of t_m and $t_{1/2}$ indicating a low influence of the temperature and a significant oxygen diffusion control on oxidation process;

- intermediate values, as in the case of I_{max} parameter;

- high values, for E_a calculated from t_i, t_s and v_{ox}, suggesting the occurrence of some inhibition effects.

A comparison of E_a values for oxidation of sample A (in initial, blank state and in

presence of tocopherol) is presented in Fig. 8. We can observe that E_a values seem to be slightly higher in presence of tocopherol.

Conclusions

A possible correlation between CL and edible oil oxidation at elevated temperatures has been studied based on the similarity of the chemical structure of oils and hydrocarbon polymers. Similar (sigmoid) CL curves are observed in both cases.
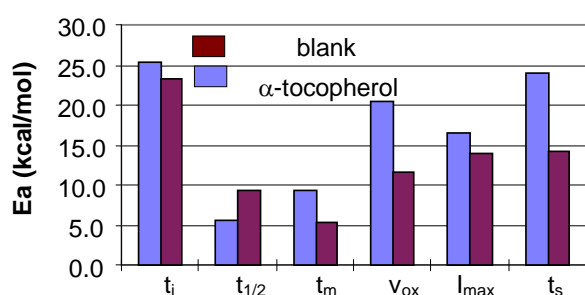

Fig. 8 - Comparation of E_a values calculated from various CL parameters for oxidation of sunflower oil, sample A, blank and α - tocopherol containing.

Different CL curves were provided under the same conditions by olive oil and sunflower oil, thus CL would be applied as an analytical test to discriminate between different kinds of edible oils. CL curves from different grades of sunflower oils are also different, suggesting that CL could be also applied to discriminate between oils of different origin or grade.

Activation energy values corresponding to various oxidation steps can be derived from CL measurements, and the results suggest the occurrence of a diffusion controlled process and an influence of inhibitors at the beginning of oxidation.

Previous thermal oxidation at 130°C induced an oxidative degradation that has been evidenced by changes in CL parameters. Thus, CL could be a marker of oxidative stress. IR data are in good agreement with those of CL.

α-tocopherol induced a weak antioxidative effect that seems to increase as

decreasing the temperature. In fact, a very slight improvement in stability was observed.

References

[1] Allen J.C., Hamilton R.J. (Eds.), "*Rancidity in food*", Appl. Sci. Publ., London, 1983

[2] Byung P.L., „*Mitocondrial Aging and Lipoperoxidative Products*", Ann. Acad. Sci. New York, vol. 786, p. 44-56 (1996)

[3] Leonte M., Florea T., *Chimia alimentelor*, p. 251 - 344, Ed. Pax Aura Mundi, Galaţi 1998

[4] Farmer E.H., *Trans Faraday Soc.* **38**, 340 (1942)

[5] Olinescu R., *"Peroxidarea în Cimie, Biologie şi Medicină"*, Ed. Ştiinţifică şi Enciclopedică, Bucureşti 1982

[6] Bruna E., *Lipids,* **24**, 970 (1990)

[7] Porter N.A., *J. Am. Chem. Soc.* **103**, 6447 (1981)

[8] Porter 1995 - Porter N.A., *Lipids* **30**, 277 (1995)

[9] Bolland, J.L., Gee, G., *Trans Farad. Soc.*, **42**, 236 (1946)

[10] Bolland, J.L., *Quart. Rev. Chem. Soc.,* **3**, 1 (1949)

[11] Bolland J., in: *"Review in Autooxidation and Antioxidants"* Lundberg WO Ed., Wiley, NY 1961

[12] Rychla-Matisova L., Rychly J., "*Inherent Relations of Chemiluminescence and Thermooxidation of Polymers*", in "*Polymer Durability*", Am. Chem. Society , 175 (1996)

[13] Audouin-Jirackova, L., Verdu, J., *J. Polym. Sci. A : Polym Chem.,* **25,** 1205 (1987)

14. Billingham 1990 - Billingham, N.C., George, G. A., *J. Polym. Sci. Polym. Phys.*, **28** (1990) 257

[15] Celina, M., George, G. A., Billingham, *N. C., Polym. Degrad. Stab*., **42**, 335 (1993)

[16] R. Setnescu, S.Jipa, Z. Osawa, *Polym. Degrad. Stab.* **60**, 377 (1988)

[17] Olinescu R., Greabu M., „*Chemilumines-cenţa şi bioluminescenţa*", Ed. Tehnică Bucureşti 1987

[18] Wright J.R., Rumbaugh H.D., Colby H.D., Miles P.R., *Arch. Biochem. Biophys.*, **192,** 344 (1979)

[19] Puntatrulo, S., Cederbaum Al., *Arch. Biochem. Biophys.*, **264**, 482 (1988)

[20] Noll T., De Groot H., Sies H., *Arch. Biochem. Biophys*., **252**, 284 (1987)

[21] Tilbury L.N., Miller H., *Chemilumines-cence from the Oxidation of Model Lipid Systems* - Scool of Chemical and Physical Sciences, Victoria University of Wellington 2003

[22] Cash G.A., George G.A., Bartly J.P., *J. Sci. Food. Agric.*, **43**, 277 (1988)

[23] Usuki R., Kaneda T., Yamagishi A., Takyu C., Inaba H., *J. Food. Sci.*, **44** (1979) 1573

[24] Mendenhall, G. D., *Angew. Chem. Ed.,* **16**, 225 (1977)

[25] Laeliger J., Sancy F., *J. Luminol.*, **31**, 908 (1984)

[26] Laubli 1986 - Laubli M.W., Bruttel P.A., *J. Am. Oil Chem. Soc.*, **63**, 792 (1986)

[27] Neumann M.M., Fusero S.N. Garcia N.A., *J. Am. Chem. Soc.,* **68**, 662 (1991)

[28] Fisher, W. K., *J. Indust. Irrad. Technol.,* **3,** 167 (1985)

[29] Packer L., Ong A.S.H., "*Biological Oxidants and Antioxidants: Molecular Mechansims and Health Effects*", 1999 AOCS Press, Champaign IL

[30] Zaharescu 2000 - Zaharescu T., Jipa S., Surmeian M., *Rev. Roum. Cheim.* **45**, 863 (2000)

C. MATHEMATICS SECTION

MATHEMATICAL CLASSIFICATION WITH FUZZY PARTITIONS. DEFUZZIFICATION OF OPTIMAL PARTITIONS

ALINA CONSTANTINESCU
Valahia University Târgoviste - 0200 Targoviste, Romania
e-mail: alina@valahia.ro Tel.: +40 45 611079; +40 92 342736

Abstract: *The propose of this paper is to present the defuzzyfication of the optimal partition obtained from "n-medium Fuzzy" (Fuzzy – Isodata) algorithm classification .*

1.Introduction.

The optimal partition is denoted:
P = {A$_1$, A$_2$, . . ., A$_n$} and it is a fuzzy partition. There interpretation is given by a classical partition:

$$\overline{P} = \left\{ \overline{A}_1, \overline{A}_2, \ldots, \overline{A}_n \right\}$$

which is defined such as:

$$x \in \overline{A}_i \Leftrightarrow A_i(x) = \underset{j=1\ldots n}{\text{maximum}} A_j(x)$$

We provide that the rule of choosing a classical partition $\overline{P}$ is not equivalent to minimizing the distance between P and $\overline{P}$. According to my calculation I considered the definition of the distance from Fuzzy-Isodata algorithm.

2.Defuzzification of optimal partitions

If X = {x^1, x^2, . . ., x^P}, x^i ∈ R^d a data set,
P = {A$_1$, . . ., A$_n$} a fuzzy partition,

A$_i$: X→[0, 1], obvious $\sum_{i=1}^{n} A_i(x^j) = 1$ for any
x^j ∈ X.
Each fuzzy set A$_i$ describes a class (cluster) of elements.
We represent fuzzy partition with a matrix A with n lines and p columns.
$A = \left(A_{ij} \right)_{\substack{i=1\ldots n \\ j=1\ldots p}}$, A$_{ij}$ = A$_i$ (x^j) ∈ [0, 1] with

$$\sum_{i=1}^{n} A_{ij} = 1 \text{ for any } j = 1 \ldots p$$

If matrix norm A: $\|A\| = \max_{i,j} |A_{ij}|$ and

distance d(P, P') = ‖P – P'‖ for any P, P' fuzzy partitions of X.

3.Theorem:

If $\overline{P} = \left\{ \overline{A}_1, \ldots, \overline{A}_n \right\}$ with x^j ∈ $\overline{A}_i$ if and only if :

$$A_i(x^j) = \max_k A_k(x^j).$$

Then $d(P, \overline{P}) > d(P, P')$, for some P' different fuzzy partition. In other words, $\overline{P}$ cannot minimize the chosen distance between P and $\overline{P}$.

Proof: $d(P, \overline{P}) \le d(P, P')$ for any P' if and only if
$\|P - \overline{P}\| \le \|P - P'\|$ for any P' if and only if

$$\max_{i,j} |A_i(x^j) - \overline{A}_i(x^j)| \le \max_{i,j} |A_i(x^j) - A'_i(x^j)|$$

If A and $\overline{A}$ is associated matrix to P respectively $\overline{P}$.

$$\overline{A} = \left(\overline{A}_{ij} \right)_{\substack{i=1\ldots n \\ j=1\ldots n}} ;$$

$$\overline{A}_{ij} = \begin{cases} 1 \text{ if } A_i(x^j) = \max_k A_k(x^j) \text{ with } j = 1 \ldots p \\ 0, \text{ as for the rest} \end{cases}$$

$$\left| A_{ij} - \overline{A}_{ij} \right| = \begin{cases} \left| 1 - A_i\left(x^j\right) \right| = \sum\limits_{\substack{k=1 \\ k \neq i}}^{n} A_{kj}, \\ \\ , \text{ if } A_i\left(x^j\right) = \max\limits_k A_k\left(x^j\right) \\ \\ \left| A_{ij} \right| = A_{ij}, \text{ as for rest} \end{cases}$$

Let P with $A_{ij} - A_{rj} = \varepsilon$ extremely small and with:

$$A_{ij} = \max_k A_k\left(x^j\right)$$
$$A_{rj} = \max_{k \neq i} A_k\left(x^j\right)$$

If we consider P' different partition, namely

$A'_{ij} = A_{ij} - \varepsilon$ and
$A'_{rj} = A_{rj} + \varepsilon$,
where $\varepsilon = \left| A_{ij} - A_{rj} \right|$
and $A'_{kl} = A_{kl}$ as for the rest.

Then:
$$d(P,P') = \max_{i,j} \left| A_i\left(x^j\right) - A'_i\left(x^j\right) \right| =$$
$$= \max\{\varepsilon, 0\} = \varepsilon$$

But $d(P, \overline{P}) = \max_{i,j} \left| A_i\left(x^j\right) - \overline{A}_i\left(x^j\right) \right| =$

$$= \max_j \sum_{\substack{k=1 \\ k \neq i}}^{n} A_{kj}$$

Because:

$$\max_j \sum_{\substack{k=1 \\ k \neq i}}^{n} A_{kj} > \varepsilon$$

Then $d\left(P,\overline{P}\right) > d\left(P,P'\right)$.

4.Conclusion: Empirical rule of choosing a classical partition $\overline{P}$ is not equivalent to minimizing the distance between P and $\overline{P}$ if the distance is defined like in Fuzzy- Isodata algorithm.

References:
[1.] Dumitrescu D.: Mathematical Principles of Classification Theory - Academic Press, Romania, 1999.
[2.] Dumitrescu D.: Fuzzy Hierarhical Classification Methods in Analytical Chemistry - D.H. Rouvray (editor), Fuzzy logic in Chemistry, Academic Press, New York, 1997
[3.] Ichihashi H.: A Neuronal Interior Point Algorithm for Solving Hard and Fuzzy Clustering Problems - EDAN'97 Barcelona 1997.

CANTOR-BERNSTEIN THEOREM AND APPLICATIONS

CRISTINEL MORTICI

Valahia University of Targoviste Dept. of Mathematics
Bd. Unirii 18, Targoviste, ROMANIA
Email: cmortici@valahia.ro

Abstract. *We give in this note an interesting proof for Cantor-Bernstein theorem. Then we show how this theorem permits us to develop an ordering relation on the set of cardinals and finally some applications are given.*

Let U be a system of sets also called univers. We say that two sets $A, B \in U$ are equipotent if there exists a bijection $f : A \to B$. We denote:

$$A \sim B \Leftrightarrow \exists f : A \to B \text{ bijection}$$

or simply $A \overset{f}{\sim} B$. Easy, "$\sim$"is an equivalence relation, as we can see from the following scheme:

$$\begin{cases} (\textit{reflexivity}) & A \overset{1_A}{\sim} A \\ (\textit{symmetry}) & A \overset{f}{\sim} B \Rightarrow B \overset{f^{-1}}{\sim} A \\ (\textit{transitivity}) & A \overset{f}{\sim} B, B \overset{g}{\sim} C \Rightarrow A \overset{g \circ f}{\sim} C \end{cases}.$$

Now by cardinal of the set A, denoted $card A$ we mean the equvalence class of A,

$$card A = \{ B \mid B \in U, B \sim A \}$$

In consequence, we have

$$card A = card B \Leftrightarrow \exists f : A \to B \text{ bijection}.$$

On the other side, we can define an ordering relation on the sets of cardinals. Indeed, we will say that
$$card A \le card B \Leftrightarrow \exists f : A \to B \text{ injection}.$$
It is not hard to prove that the following equivalent definition holds true:
$$card A \le card B \Leftrightarrow \exists g : B \to A \text{ surjection}.$$
For any set $A \in U$ we have $card A \le card A$ because the identity function $1_A : A \to A$ is injective.
If $A, B, C \in U$ satisfy:

$$card A \le card B, card B \le card C,$$

then there exist injections $f : A \to B$ and $g : B \to C$.

Their product $g \circ f : A \to C$ remains injective, so $card A \le card C$.

In this way, we established the reflexivity and transitivity of the relation $"\le"$. The antisymmetry property is not obvious. There are a lot of proofs for that. It also follows from the next basic theorem:

Theorem (Cantor-Bernstein). *Assume that for two given sets A and B there exist injections $f : A \to B$ and $g : B \to A$. Then there exists a bijection $h : A \to B$.*

Solution. We will say that $b \in B$ is ancestor of an element $a \in A$ if
$$\underbrace{(g \circ f \circ g \circ ... \circ f \circ g)}_{2k+1 \, times}(b) = a \quad, \quad \text{for some}$$
integer $k \ge 0$. Similarly, we will say that $a \in A$ is ancestor of an element $b \in B$ if
$$\underbrace{(f \circ g \circ f \circ ... \circ g \circ f)}_{2k+1 \, times}(a) = b,$$
for some integer $k \ge 0$. Finally, $a' \in A$ is ancestor of $a \in A$ if $f(a') \in B$ is ancestor of a and $b' \in B$ is ancestor of $b \in B$ if $g(b') \in A$ is ancestor of b, in the sense of the previous definitions.
Let us denote by M_1, M_2, M_∞ the set of all elements of A which have an odd, even, respective an infinite number of ancestors. Analogue, let N_1, N_2, N_∞ the set of all elements of B which have an odd, even, respective an infinite number of ancestors.
We will prove that the function $\varphi : A \to B$ given by
$$\varphi(x) = \begin{cases} g^{-1}(x) &, & x \in M_1 \cup M_\infty \\ f(x) &, & x \in M_2 \end{cases}$$

is bijective.

Indeed, its inverse is $\psi : B \to A$ given by

$$\psi(y) = \begin{cases} f^{-1}(y) & , \quad y \in N_1 \\ g(y) & , \quad y \in N_2 \cup N_\infty \end{cases}.$$

If $x \in M_1 \cup M_\infty$, then $\varphi(x) = g^{-1}(x) \in N_2 \cup N_\infty$, so

$$\psi(\varphi(x)) = g(\varphi(x)) = g(g^{-1}(x)) = x.$$

If $x \in M_2$, then $\varphi(x) = f(x) \in N_1$, so $\psi(\varphi(x)) = f^{-1}(\varphi(x)) = f^{-1}(f(x)) = x$.

In consequence, $\psi \circ \varphi = 1_B$ and analogue, $\varphi \circ \psi = 1_A$.

A direct application of Cantor-Bernstein theorem is the following

Proposition. $card\mathbf{N}^* = card(\mathbf{N}^* \times \mathbf{N}^*)$.

Solution. The idea is to use the function $f : \mathbf{N}^* \to \mathbf{N}^* \times \mathbf{N}^*$,

$$f(n) = (n,1)$$

and the function $g : \mathbf{N}^* \times \mathbf{N}^* \to \mathbf{N}^*$ given by

$$g(m,n) = 2^{m-1} \cdot 3^{n-1}.$$

It is easy to see that *f* and *g* are injections and according to the Cantor-Bernstein theorem, there exists a bijection $h : \mathbf{N}^* \to \mathbf{N}^* \times \mathbf{N}^*$. That is $card\mathbf{N}^* = card(\mathbf{N}^* \times \mathbf{N}^*)$.

References

[1] – C. Mortici, *Lectii de Analiza Matematica,* Editura Ex Ponto, Constanta, 2000.
[2] – C.P. Niculescu, *Analiza Matematica,* Editura Academiei Romane, Bucuresti, 2001.
[3] – G.E. Silov, *Analiza Matematica,* Editura Stiintifica si Enciclopedica, Bucuresti, 1989

SOME REMARKS ON THE STUDY OF THE NONLINEAR DIFFUSION EQUATIONS

DINU TEODORESCU

Department of mathematics, Valahia University of Targoviste

Abstract: *In this paper we consider two models of nonlinear diffusion for which we show that is possible a reduction to a more convenient form.*

Let D be an open and bounded subset of R^n.

For T>0, let $D_T = \{(t,x)/\, 0 < t < T; x \in D\}$.

We consider the problem of finding a function $u = u(t,x)$ satisfying

(1.1) $\dfrac{\partial u}{\partial t} = div(a(u)gradu)$ in D_T,

(1.2) u(0,x)=0, $x \in D$,

(1.3) u(t,x)=0, $x \in \partial D, 0 < t < T$.

The problem (1.1),(1.2), (1.3) is known as the homogeneous initial-boundary value problem for the nonlinear diffusion-convection equation.

We suppose that the coefficient $a : R_+ \to R$, $a = a(s)$ is given and satisfies:

$c \le a(s) \forall s \ge 0 (c > 0)$, $a \in C^1([0,\infty))$.

The right term of (1.1) can be written as:

$$\sum_{i=1}^{n} \frac{\partial}{\partial x_i}\left(a(u)\frac{\partial u}{\partial x_i} \right) =$$

$$\sum_{i=1}^{n}\left(a'(u)\left(\frac{\partial u}{\partial x_i}\right)^2 + a(u)\frac{\partial^2 u}{\partial x_i^2} \right)$$

$$= a(u)\Delta u + a'(u)\sum_{i=1}^{n}\left(\frac{\partial u}{\partial x_i}\right)^2,$$

where $\Delta u = \sum_{i=1}^{n}\dfrac{\partial^2 u}{\partial x_i^2}$.

So, the equation (1.1) becomes:

$$\frac{\partial u}{\partial t} = a(u)\Delta u + a'(u)\sum_{i=1}^{n}\left(\frac{\partial u}{\partial x_i}\right)^2.$$

Let us consider now the function:

$$F_a : R_+ \to R, \; F_a(y) = \int_0^y a(s)ds.$$

We have $F_a'(y) = a(y) > 0$ and then F_a is invertible.

For $u(t,x)$ a solution of (1.1), (1.2), (1.3) define:

(2) $v(t,x) = F_a\big(u(t,x)\big)$.

We obtain:

$$\frac{\partial v}{\partial t} = F_a'(u)\frac{\partial u}{\partial t} = a(u)\frac{\partial u}{\partial t} = a\big(F_a^{-1}(v)\big)\frac{\partial u}{\partial t} \text{ and}$$

$$\Delta v = \sum_{i=1}^{n}\frac{\partial^2 v}{\partial x_i^2} = \sum_{i=1}^{n}\frac{\partial}{\partial x_i}\left(F_a'(u)\frac{\partial u}{\partial x_i} \right) =$$

$$= \sum_{i=1}^{n}\frac{\partial}{\partial x_i}\left(a(u)\frac{\partial u}{\partial x_i} \right).$$

Also, we have:

$v(0,x) = F_a\big(u(0,x)\big) = F_a(0) = 0$ for $x \in D$

and

$v(t,x) = F_a\big(u(t,x)\big) = F_a(0) = 0$,for

$x \in \partial D, 0 < t < T$.

It results, using the transformation (2), that the problem (1.1), (1.2), (1.3) becomes:

(2.1) $\dfrac{\partial v}{\partial t} = b(v)\Delta v$ in D_T ,

(2.2) v(0,x)=0, $x \in D$,

(2.3) v(t,x)=0, $x \in \partial D, 0 < t < T$,

where $b(v) = a\big(F_a^{-1}(v)\big)$.

The advantage of the equivalent problem (2.1), (2.2), (2.3) is that the nonlinear term containing $\sum \left(\dfrac{\partial}{\partial x_i}\right)^2$ does not appear any more.

Consider now the nonlinear equation (3)

$|u|^\alpha \dfrac{\partial u}{\partial t} = \Delta u \ (\alpha > 0) \text{ in } [0,\infty) \times R^n$.

From the viewpoint of physics (3) is known as a model of the fast diffusion. Let $w = w(x)$ be a solution of the nonlinear equation $\Delta w = |w|^\alpha w$ in R^n. We define:

(4) $u(t,x) = (\alpha t + \beta)^{\frac{1}{\alpha}} w(x)$ $(\beta > 0)$ for

$x \in R^n$, $t \in [-\dfrac{\beta}{\alpha}, \infty)$.

We have :

$\Delta u = (\alpha t + \beta)^{\frac{1}{\alpha}} \Delta w = (\alpha t + \beta)^{\frac{1}{\alpha}} |w|^\alpha w$ and

$|u|^\alpha \dfrac{\partial u}{\partial t} = (\alpha t + \beta)|w|^\alpha w \cdot \dfrac{1}{\alpha}(\alpha t + \beta)^{\frac{1}{\alpha}-1} \cdot \alpha =$

$= (\alpha t + \beta)^{\frac{1}{\alpha}} |w|^\alpha w$.

It results that $u = u(t,x)$ given by (4) is a solution for the equation (3).

So the evolution equation (3) is reduced to the stationary equation

(5) $\Delta w = |w|^\alpha w$.

References

[1]   P. DuChateau, Monotonocity and Uniqueness Results in Identifying an Unknown Coefficient in a Nonlinear Diffusion Equation, SIAM Journal on Applied Mathematics, vol. 41, nr. 2(1981), pp. 310-323

[2] K. Hayasida, Unique continuation for fast diffusion , Tsukuba Journal of Mathematics, vol. 27, nr. 1(2003), pp. 175-187

ON THE ASYMPTOTIC REPRESENTATIONS OF THE REGULAR LACUNARY FINITE SUMS ASSOCIATED TO A GIVEN SERIES

ANDREI VERNESCU

"Valahia" University,Dept.of Mathematics, 18 , Unirii Blvd., Targoviste
e-mail: avernescu@pcnet.ro

Abstract: *We present here (as a generalization of our previous works [1] and [2]) a general method for obtaining in certain natural conditions of the asymptotic expressions for a finite sum with the indices in an arithmetical progression (a so-called regular lacunary sum)starting from a given series.*

1. In the previous Conference (Iassy, 1999) we have given an asymptotic representation for the regular lacunary sums (i.e. having the indices in an arithmetical progresion) of the harmonic sum $H_{n,\alpha}^{(r)} = 1 + \frac{1}{2} + \frac{1}{3} + \ldots + \frac{1}{n}$. Let $r > 1$ be a natural, fixed number $\alpha = \{1,2,3,\ldots,r\}$. These sums are

(1.1)

$$H_{n,\alpha}^{(r)} = \frac{1}{\alpha} + \frac{1}{\alpha+r} + \frac{1}{\alpha+2r} + \ldots + \frac{1}{\alpha+(n-1)r}$$

To answer this purpose, we have used the asymptotic expression (of first order) of H_n, namely $H_n + \ln n = \gamma + \varepsilon_n$[2], where $\gamma = \lim_{n\to\infty}(H_n - \ln n) = 0,577\ldots$ is the famous Euler's constant, and $(\varepsilon_n)_n$ is a sequence which converges to 0 for $n \to \infty$. Also, we have used the generating function $G_n^{[r]} : \mathbb{C} \to \mathbb{C}$ of the finite sequence $\left\{1, \frac{1}{2}, \frac{1}{3}, \ldots, \frac{1}{rn}\right\}$, defined by the equality

(1.2) $G_n^{[r]}(u) = \frac{u}{1} + \frac{u^2}{2} + \frac{u^3}{3} + \ldots + \frac{u^{rn}}{rn}$.

We have expressed the sums $H_{n,\alpha}^{(r)}$ as linear combinations of the values of the generating function in the points ω_l ($l = 0,1,2,\ldots,r-1$),

where $\omega_0, \omega_1, \ldots, \omega_{r-1}$ are the roots of order r of the unity i.e. the roots of the equation $z^r = 1$.

So, we have obtained the formula:

(1.3) $H_{n,\alpha}^{(r)} = \frac{1}{r}\left(H_{rn} + \sum_{i=1}^{r-1}(\omega_l^\alpha)^{-1} G_n^{[r]}(\omega_l)\right)$

We have established the following asymptotic representation for the $G_n^{[r]}$:

(1.4) $G_n^{[r]}(u) = -\log(1-u) - I_n^{[r]}(u)$,

where for the complex logarithm we have considered an unspecified but fixed branch and where we have $I_n^{(r)}(u) = \int_0^u \frac{z^{rn}}{1-z}dz$ ($u \in \mathbb{C}\setminus[1,\infty)$) and, for any $u \in \mathbb{C}\setminus\{1\}$, with $|u| = 1$, we have $\lim_{n\to\infty} I_n^{(r)}(u) = 0$.

So, we have obtained the following asymptotic representation

(1.5)

$$H_{n,\alpha}^{(r)} = \frac{1}{r}\left(H_{rn} - \sum_{i=1}^{r-1}(\omega_l^\alpha)^{-1}\log(1-\omega_l)\right) + o(1)$$

where $o(1)$ denotes, as usual, a function of natural variable n which converges to 0, when $n \to \infty$.

Replacing in (1.5) H_{rn} by its asymptotic expression and also ω_l^α and $\log(1-\omega_l)$ by their expressions, we have obtained:

---

[2] We denote by ln the natural (neperian) logarithm of a strictly positive real number and by log the complex logarithm.

$$H_{n,\alpha}^{(r)} = \frac{1}{r}\left[\ln n + \ln r + \gamma - \sum_{l=1}^{r-1}\left(\cos\frac{2\alpha l\pi}{r}\ln\left(2\sin\frac{l\pi}{r}\right) + \frac{(2l-r)\pi}{2}\sin\frac{2l\pi}{r}\right)\right] + o(1).$$

We give, as particular examples, obtained in [2], the formulas for $r = 3$ and $r = 4$; the apparition of a term in π is due to the complex logarithm.

a) The case $r = 3$

$$H_{n,1}^{(3)} = 1 + \frac{1}{4} + \frac{1}{7} + \ldots + \frac{1}{3n-2} =$$

$$= \frac{1}{3}\ln n + \frac{1}{3}\left(\gamma + \frac{3}{2}\ln 3 + \frac{\pi\sqrt{3}}{6}\right) + o(1)$$

$$H_{n,2}^{(3)} = \frac{1}{2} + \frac{1}{5} + \frac{1}{8} + \ldots + \frac{1}{3n-1} =$$

$$= \frac{1}{3}\ln n + \frac{1}{3}\left(\gamma + \frac{3}{2}\ln 3 - \frac{\pi\sqrt{3}}{6}\right) + o(1)$$

$$H_{n,3}^{(r)} = \frac{1}{3} + \frac{1}{6} + \frac{1}{9} + \ldots + \frac{1}{3n} =$$

$$= \frac{1}{3}\ln n + \frac{1}{3}\gamma + o(1)$$

b) The case $r = 4$

$$H_{n,1}^{(4)} = 1 + \frac{1}{5} + \frac{1}{9} + \ldots + \frac{1}{4n-3} =$$

$$= \frac{1}{4}\ln n + \frac{1}{4}\left(\gamma + 3\ln 2 + \frac{\pi}{2}\right) + o(1)$$

$$H_{n,2}^{(4)} = \frac{1}{2} + \frac{1}{6} + \frac{1}{10} + \ldots + \frac{1}{4n-2} =$$

$$= \frac{1}{4}\ln n + \frac{1}{4}(\gamma + 2\ln 2) + o(1)$$

$$H_{n,3}^{(4)} = \frac{1}{3} + \frac{1}{7} + \frac{1}{11} + \ldots + \frac{1}{4n-1} =$$

$$= \frac{1}{4}\ln n + \frac{1}{4}\left(\gamma + 3\ln 2 - \frac{\pi}{2}\right) + o(1)$$

$$H_{n,4}^{(4)} = \frac{1}{4} + \frac{1}{8} + \frac{1}{12} + \ldots + \frac{1}{4n} =$$

$$= \frac{1}{4}\ln n + \frac{1}{4}\gamma + o(1)$$

All these questions were published *in extenso* in [2]. These suggest the generalization which follows.

2. Now we consider a series of real or complex numbers, $S = \sum_{n=1}^{\infty} a_n$, with $a_n \underset{(n\to\infty)}{\to} 0$ and let $r, \alpha \in \mathsf{N}$ be $r > 1$, $\alpha \in \{1, 2, 3, \ldots r\}$. We note:

(2.1) $S_{n,\alpha}^{(r)} = a_\alpha + a_{\alpha+r} + a_{\alpha+2r} + \ldots + a_{\alpha+(n-1)r}$

These are the sums mentioned in the title (associated to the series S); these are subsums of the rn-th partial sums of S $\left(S_{rn} = \sum_{k=1}^{rn} a_k\right)$.

Our purpose is to obtain in certain conditions some asymptotic representations for the sums (2.1).

We consider the generating function of the finite sequence $\{a_1, a_2, a_3, \ldots, a_{rn}\}$,

$G_n^{[r]} : \mathsf{C} \to \mathsf{C}$, defined in a natural way by the equality

(2.1) $G_n^{[r]}(u) = a_1 u + a_2 u^2 + \ldots + a_{rn} u^{rn}$

The conditions which we consider are the following:

(i) For the partial sum S_n of S we have an asymptotic representation

(2.3) $S_n = \varphi(n) + \lambda + o(1)$

where φ is a function of the natural variable n, λ is a constant and $o(1)$ is as usual; the expression $\varphi(n)$ is the so-called principal part of S_n.

(ii) The generating function $G_n^{[r]}$ has an asymptotic representation of the form

(2.4) $G_n^{[r]}(u) = F(u) + \varepsilon_n^{[r]}(u)$,

where, for all $u \in C$ with $|u| = 1$, we have

$\lim_{n\to\infty} \varepsilon_n^{[r]}(u) = 0$

Using the methods of our also mentioned paper [2], we obtain first (without the hypothesis (i) and (ii)), the following

THEOREM 1. For any $r \in N$, $r > 1$ and $\alpha \in (1, 2, 3, \ldots r)$, fixed, we have

$(2.5)\ S_{n,\alpha}^{(r)} = \frac{1}{r}\sum_{l=0}^{r-1}(\omega_l^{\alpha})^{-1}G_n^{[r]}(\omega_l)$,

or equivalent

$(2.6)\ S_{n,\alpha}^{(r)} = \frac{1}{r}\left(S_{rn} + \sum_{l=0}^{r-1}(\omega_l^{\alpha})^{-1}G_n^{[r]}(\omega_l)\right)$

Now, in the hypothesis (i) and (ii), we obtain the asymptotic formula given by the following

THEOREM 2. If (i) and (ii) are satisfyied, we have
(2.7)

$S_{n,\alpha}^{(r)} = \frac{1}{r}\left(\varphi(rn) + \lambda + \sum_{l=1}^{r-1}(\omega_l^{\alpha})^{-1}F(\omega_l)\right) + o(1)$

3. This method is general and the application depends only on the conditions (i) and (ii); in the previous case, of the sums of harmonic nature, fortunately the conditions were satisfied.

Another example can be produced now.

Taking into account that the sum $E_n = \sum_{k=0}^{n}1/k!$

"begins" from the term coresponding to $k=0$, we must made some little, not essential, modifications concerning the indices. It consists in the obtaining of the asymptotic expressions of the regular lacunary sums defined starting from the sum of exponential type

$E_n = 1 + \frac{1}{1!} + \frac{1}{2!} + \ldots + \frac{1}{n!}$,

i.e. $E_{n,\alpha}^{(r)} = 1 + \frac{1}{\alpha!} + \frac{1}{(\alpha+r)!} + \ldots + \frac{1}{(\alpha+n)!}$

where r are as previous, but $\alpha \in \{1,2,3,\ldots r-1\}$.

We have the asymptotic expression $E_n = e - \frac{\theta}{n!}$, with $\theta \in (0,1)$ and the generating function is $G_n^{[r]}: \mathbb{C} \to \mathbb{C}$,

$G_n^{[r]}(u) = 1 + \frac{u}{1!} + \frac{u^2}{2!} + \ldots + \frac{u^{rn}}{(rn)!}$.

Let $I_n^{(r)}(u) = \int_0^u e^{-z}z^{rn}dz$, $z \in C$ be. So, as in the real domain, we have the well-known

formula, obtained by an integration by parts and an iteration, which, with our notations is:

$(3.1)\ \frac{e^u}{(nr)!}I_n^{(r)}(u) = e^u - G_n^{[r]}(u)$

and therefore

$(3.2)\ G_n^{[r]}(u) = e^u - \frac{e^u}{(nr)!}I_n^{(r)}(u)$

where, if $|u| = 1$, we have $\lim_{n\to\infty}I_n^{(r)}(u) = 0$. So, we have $G_n^{[r]}(u) = e + o(1)$.

And so, we have satisfied the two conditions (i) and (ii). We obtain succesively

$E_{n,\alpha}^{(r)} = \frac{1}{r}\sum_{l=0}^{r-1}(\omega_l^{\alpha})^{-1}G_n^{[r]}(\omega_l) =$

$= \frac{1}{r}\sum_{l=0}^{r-1}(\omega_l^{\alpha})^{-1}\left(e^{\omega_l} - \frac{e^{\omega_l}}{n!}I_n^{(r)}(\omega_l)\right) =$

$= \frac{1}{r}\left(E_{rn} + \sum_{i=1}^{r}(\omega_l^{\alpha})^{-1}e^{\omega_l}\right) + o(1)$

($\alpha = 0,1,2,\ldots,r$) or finally:

$(3.4)\ E_{n,\alpha}^{(r)} = \frac{1}{r}\left(e + \sum_{l=1}^{r}(\omega_l^{\alpha})^{-1}e^{\omega_l}\right) + o(1)$

4. Particular cases

a) *The case $r = 2$*
(Therefore $\alpha = 0$ or $\alpha = 1$)

$E_{n,0}^{(2)} = 1 + \frac{1}{2!} + \frac{1}{4!} + \ldots + \frac{1}{(2n)!} =$

$= \frac{1}{2}\left(e + \frac{1}{e}\right) + o(1) = \text{ch}\,1 + o(1)$

$E_{n,1}^{(2)} = \frac{1}{1!} + \frac{1}{3!} + \frac{1}{5!} + \ldots + \frac{1}{(2n+1)!} =$

$= \frac{1}{2}\left(e - \frac{1}{e}\right) + o(1) = \text{sh}\,1 + o(1)$

b) *The case $r = 3$*
(Therefore $\alpha = 0$ or $\alpha = 1$ or $\alpha = 2$)

$E_{n,0}^{(3)} = 1 + \frac{1}{3!} + \frac{1}{6!} + \ldots + \frac{1}{(3n)!} =$

$= \frac{1}{2}\left(e + \frac{2}{\sqrt{e}}\cos\frac{\sqrt{3}}{2}\right) + o(1)$

$$E_{n,1}^{(3)} = \frac{1}{1!} + \frac{1}{4!} + \frac{1}{7!} + \ldots + \frac{1}{(3n+1)!} =$$

$$= \frac{1}{3}\left(e + \frac{2}{\sqrt{e}}\cos\left(\frac{2\pi}{3} - \frac{\sqrt{3}}{2}\right)\right) + o(1)$$

$$E_{n,2}^{(3)} = \frac{1}{2!} + \frac{1}{5!} + \frac{1}{8!} + \ldots + \frac{1}{(3n+2)!} =$$

$$= \frac{1}{3}\left(e + \frac{2}{\sqrt{e}}\cos\left(\frac{2\pi}{3} + \frac{\sqrt{3}}{2}\right)\right) + o(1)$$

c) *The case r = 4*
(Therefore $\alpha = 0$ or
$\alpha = 1$ or $\alpha = 2$ or $\alpha = 3$)

$$E_{n,0}^{(4)} = 1 + \frac{1}{4!} + \frac{1}{8!} + \ldots + \frac{1}{(4n)!} =$$

$$= \frac{1}{4}\left(e + \frac{1}{e} + 2\cos 1\right) + o(1)$$

$$E_{n,1}^{(4)} = \frac{1}{1!} + \frac{1}{5!} + \frac{1}{9!} + \ldots + \frac{1}{(4n+1)!} =$$

$$= \frac{1}{4}\left(e - \frac{1}{e} + 2\sin 1\right) + o(1)$$

$$E_{n,2}^{(4)} = \frac{1}{2!} + \frac{1}{6!} + \frac{1}{10!} + \ldots + \frac{1}{(4n+2)!} =$$

$$= \frac{1}{4}\left(e + \frac{1}{e} - 2\cos 1\right) + o(1)$$

$$E_{n,3}^{(4)} = \frac{1}{3!} + \frac{1}{7!} + \frac{1}{11!} + \ldots + \frac{1}{(4n+3)!} =$$

$$= \frac{1}{4}\left(e - \frac{1}{e} - 2\sin 1\right) + o(1)$$

Of course, all the values of this case can be expressed in ch1 and sh1.

Remark. This work was presented at the International Conference on Complex Analysis and Related Topics, "The IXth Romanian Finnish Seminar", August 27 – 31, 2001, Braşov, Romania.

References

[1] A.Vernescu, Asymptotic Representations for Certain Remarkable Sums (abstract). International Conference on Complex Analysis and Related Topics, "The VIIIth Romanian – Finnish Seminar, August 23 – 27, 1999, Iassy, Romania.

[2] A.Vernescu, Asymptotic Representations for Certain Remarkable Harmonic Sums, Bull. Math. Soc. Math. Roumanie, 42 (90), 2 (1999), 159-169.

[3] A.Vernescu, On the Asymptotic Representations of the Regular Lacunary Finite Sums Associated to a Given Series (abstract), International Conference on Complex Analysis and Related Topics, The IX [th] Romanian – Finnish Seminar, August 27 – 31, 2001, Braşov, Romania, 48-49.

INSTRUCTION FOR AUTHORS
ANALS OF VALAHIA UNIVERSITY OF TARGOVISTE (14 pt Bold)

FIRST AUTHOR[1], SECOND AUTHOR[2], AND THIRD AUTHOR[3] (12 PT) (no titles please)
[1]First Organization, First Address (11 pt)
[2]Second Organization, Second Address (11 pt)

Abstract: This document is an example of a contribution to be submitted for the Anals of Valahia University of Targoviste. This is the abstract in font size: 12 pt with the heading in bold. Please use the Times New Roman font. The title is in size 14 pt Bold (all capital letters), the names of the authors are in size 12 pt and the name of the organization and its address are in size 11 pt. The abstract is write as one column text, single-space, font size 12, italic. The rest of the text is in single-space, typed in a two column layout and font size 12 pt. **Please do not number the pages**.

1. Introduction (Headings –12 pt bold)

Deadline for contributions: 30.03.2003.
Authors are kindly requested to adhere to the formatting instructions for font size and layout.

2. How to submit your document

Please send your contribution as an e-mail attachment to Lect. dr. Simona Apostol (apostol@valahia.ro), using Microsoft Word (Office 97 or higher for PCs) or on disc to be deposit at room 106 B2. Authors should indicate the subject matter (i.e. Physics, Chemistry , Mathematicsetc.) of their paper in their emails along with their contact address, daytime phone number if available. Authors will be notified by email if theircontribution is accepted or if it required changes.

3. How to prepare your paper

In MS Word, under the *File* menu, choose *Page setup* and set the *Top*, *Bottom*, *Left & Right Margins* as 2 cm, the *Gutter* as 0 cm, and the *Header* and *Footer* to 1.2 cm and choose *Apply to: Whole Document*. Then select the "*Paper Size*" tab and set the *Paper Size: A4* and *Orientation: Portrait*. To setup the two-column format, select *Columns* under the *Format* menu. Here set number of columns to 2 and check the *Equal column width* box on the lower left corner. Then set the *Column Width* to 8 cm and *Spacing* to 1 cm and choose *Apply to: This point forward*. It is also requested that the contributions should include

an abstract, an introduction, conclusions and relevant references in addition to the paper itself.

4. Figures and Tables

Figures and tables must fit into one column (8 cm). Wider figures or tables may be placed as single columns but only as an exception.
 Figure and table titles must be typed in bold and should appear below the figures and above the tables.

5. Equations

Equations must also fit into one column (8 cm). If wider, could be placed as single column

6. References

References should be numbered in the text in the order they are cited [1]. Multiple consecutive references may be abbreviated as [2–5]. The following style must be used for all contributions:
[1] Author-X (last/family name), A. B. (first & middle initials), *Title of the book*, Publisher, City of publication, Year, Page reference.
[2] Author-Y, C. D., and Author-Z, E. F., *Name of the Journal / Proceedings*, **83** (volume), 1526 (first page), 1998 (year).

Other

Thank you for adhering to these instructions.